SKB TECHNICAL REPORT 87-29

Alteration of isolating properties of dense smectite clay in repository environment as exemplified by seven pre-quarternary clays

Roland Pusch, Lennart Börgesson, Mikael Erlström
Swedish Geological Co, Lund

December 1987

ALTERATION OF ISOLATING PROPERTIES OF DENSE SMECTITE
CLAY IN REPOSITORY ENVIRONMENT AS EXAMPLIFIED BY SEVEN
PRE-QUARTERNARY CLAYS

Roland Pusch
Lennart Börgesson
Mikael Erlström

Swedish Geological Co, Lund, 1987-12-31

ALTERATION OF ISOLATING PROPERTIES OF DENSE SMECTITE CLAY IN REPOSITORY ENVIRONMENT AS EXAMPLIFIED BY SEVEN PRE-QUATERNARY CLAYS

Roland Pusch

Lennart Börgesson

Mikael Erlström

Swedish Geological Co, Lund

CONTENTS

SUMMARY

Seven pre-Quaternary clays with a smectite content ranging between zero and about 25 % were taken as possible reaction products resulting from chemical alteration of dense sodium bentonite. They were characterized with respect to the mineral composition and microstructural constitution and tested with reference to their hydraulic conductivity, swelling ability and creep properties.

It was found that since they were all less permeable than a typical large granitic rock mass they would serve as flow barriers in a repository. Thus, even rather extreme chemical attack is not expected to eliminate the most important barrier function of Na bentonite in repository environment. However, slight mechanical disturbance of a heterogeneously altered smectite clay buffer or seal, may be critical. Thus, the investigated, less smectitic clays experienced a rather dramatic increase in hydraulic conductivity on expansion and remolding. This is explained by the inability of a microstructurally discontinuous smectite component - particularly in the Ca-form - to swell and fill voids. The minimum content of Na smectite to preserve the self-healing capacity is estimated at 15-25 %.

Slight or moderate cementation was indicated by two of the clays by the creep tests. At a smectite content of 15-25 % it is probable that self-healing will take place after a mechanically induced breakage of the cementing bonds.

The tests gave a good basis for future development of rational, routine tests as well as for a relevant characterization of buffer material candidates.

1　SCOPE OF STUDY

Na bentonite buffer materials are expected to be largely intact in KBS 3 repository environment for several hundred thousand years. The impact of more severe conditions, such as higher temperatures than 90° C and various improbable but theoretically possible physical and chemical effects, can be illustrated by comparing the physical properties of dense Na bentonite with those of a range of clays that can be taken as representatives of possible alteration products. The present study forms a compilation of material data of such, more or less smectite-poor clays and therefore serves to illustrate changes in the isolating function of Na bentonite that undergoes various types of transformation. The report can also be taken as a basis for selecting suitable candidate materials for various isolating purposes.

A condensed description of major deteriorating processes in repository environment is first given, on which the selection of a number of representative natural soils for testing was based. The report then specifies the test program and the respective techniques that were applied, as well as the available geological soil data. The results of the experimental study are finally presented and discussed.

2　ALTERATION PROCESSES AND PRODUCTS

2.1　CHANGES INDUCED BY TEMPERATURE AND CHEMICAL AGENTS

It has been foreseen that canister envelopes of montmorillonite-rich clay, and backfills in tunnels and shafts consisting of mixtures of clay and ballast materials, will be chemically altered under the environmental conditions that prevail in repositories. The major factors that affect the integrity of the materials and lead to an unwanted reduction of the content of montmorillonite are:

* Temperature
* Groundwater chemistry
* Softening by a drop in bulk density
* Radiation

Temperature

Heating to more than about 100° C under hydrothermal conditions and subsequent exposure to potassium-bearing groundwater are known to have two major effects on the montmorillonite crystal lattice as expressed by the following generalized chemical reaction:

$$Montmorillonite + Al^{3+} + K^+ \rightarrow Illite^* + Si^{4+} \qquad (1)$$
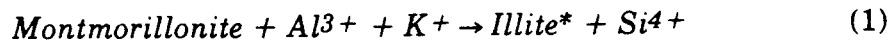
Firstly, a charge change is produced by the replacement of tetrahedral silica by aluminum, which may originate from octahedral lattice positions or external sources. This charge deficiency is a necessary prerequisite for the formation of illite. Secondly, the associated liberation of silica may cause precipitation of silica compounds, acting as cementing agents and reducing the ability of the smectite particles to swell. Once the lattice charge has been reduced, the uptake of potassium and alteration to illite is a matter of groundwater composition and time (1,2). Complete conversion to illite practically eliminates the swelling potential, while the precipitation of silica compounds yields brittle behavior by which open fractures may be generated through temperature-induced or tectonical stresses. Another major effect of these two processes is that large assemblages of discrete montmorillonite flakes become permanently aggregated together to form thicker illite particles, by which the granulometry of the clay is significantly changed. This is manifested by a reduction in clay content, i.e. the fraction of minus 2 μm particles. In turn, this reduces the cation exchange capacity and the Atterberg liquid limit and, above all, it increases the content of interconnected pore passages.

As examplified by many natural bentonite beds and deeply located sediments that were formed in Ordovician time or later, the conversion from smectite to illite is usually not complete, the degree of alteration being expressed by the percentage of expandable minerals as interpreted from XRD tests. The character of the altertion is that certain randomly or regularly occurring non-swelling units (illite) are formed in the smectite stacks. This process creates what is called mixed layer minerals. Kinetic reaction models indicate that the percentage of illite produced -

----

*   The term illite is applied here since it has been used for several of the
     discussed clays in various literature references. The term hydrous mica or
     hydromica would be preferred

by heating to 150° C during 1000 years will be about 80 %, while at 90° C, which would be the maximum temperature in a KBS 3 repository, only about 5 % illite would be formed in the same period (1). Since the temperature in such a repository is in the range of 40-60° C for another few thousand years, the total amount of illite is expected to become 10-20 %. It should be added here that it is not yet clear whether the processes that yield illite are actually Arrhenius-type reactions. The matter is focussed on in a current SKB research project.

Chemical alteration of the discussed type may also be related to pressure although no general relationships have been derived from autoclave tests or field data. The depths considered for final disposal are in the range of 0.5-3 km, to which the present discussion applies. This means that the water pressure may be in the range of 5-30 MPa, while the grain-to-grain pressure is represented by the swelling pressure which is in approximately the same range.

Groundwater chemistry

The type and concentration of dissolved cations determine whether the initially dominant sodium ion will be exchanged and thereby alter the physical properties of the clay, while pH is a determinant of the solubility of the clay minerals. As to ion exchange of monovalent cations, smectites have an affinity that is successively dropping in the following order:

	Cs >	Rb >	K >	Na >	Li
Atom radius, Å	1.6	1.49	1.33	0.98	0.78
Radius of hydrated atom, Å	5.05	5.09	5.32	7.90	10.03

According to Sposito (3) this selectivity is the result of inner-sphere complex formation, i.e. monovalent cations settled into "siloxane"* ditrigonal cavities. Na and Li may in fact be very weakly hydrated and even free to move in interlamellar water complexes that may actually grow directly on the basal planes of the montmorillonite flakes (4).

----

* plane of oxygen atoms bounding tetrahedral silica sheets

Considering also common bivalent ions the general order is:

$$H^+ > Ca^{2+} > Mg^{2+} > K^+ > Na^+ > Li^+$$
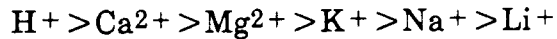
It is generally assumed that the much higher affinity for calcium than for sodium yields calcium saturation even when the concentration of this ion is considerably lower than that of sodium. Still, it appears that sodium is largely retained in the exchange positions even at a Na/Ca concentration ratio of the porewater of only 2:1, as demonstrated by the Stripa Buffer Mass Test. The Stripa water typically has a Ca content of about 19 ppm, while the other major cations have the following representative concentrations: Na 37 ppm, Mg 0.5 ppm, K 0.4 ppm (pH 9.1).

The most probable base exchange process that can be predicted under repository conditions is a partial or complete replacement of the initially dominant Na ions by Ca. This may be due to altered hydrological conditions in the repository area or to the presence of concrete constructions in the close vicinity of the clay barriers. In the KBS 3 case there is also a possibility for replacement of sodium by copper that is released from the waste containers, and, at a very late stage, a subsequent replacement of copper by radionuclides.

The uptake of bivalent ions may be an inner-sphere complex formation as in the case of saturation with monovalent ions, but it is more likely to be related to the formation of outer-sphere complexes in the form of hydrated ions off the siloxanes, or as complexes with surface hydroxyl groups (3). The physical properties of montmorillonite with calcium, copper, or magnesium in exchange positions are expected to be similar.

While exchange of adsorbed cations reversibly alters the mineral surface properties and the physico/chemical interaction between particles, pH irreversibly affects the constitution of the mineral lattices. We see from Fig 1 that a drop in pH below about 4.5 and an increase beyond about 10, produce disintegration of the clay lattices. However, in considering repositories at large depth in granite or gneiss there are only a few special cases in which the groundwater can attain pH-values off the range of 6-9. Except for the special case of concrete in contact with barrier clay materials, it requires direct and fast hydraulic communication between the repository and the ground surface where rather extreme water chemistry conditions must be assumed to prevail. Such short-circuits can be formed by tectonical movements that create steep and very deep continuous fractures or

porous shear zones. Their permeability must be high because the permeated rock would have a strong buffering capacity at long residence times.
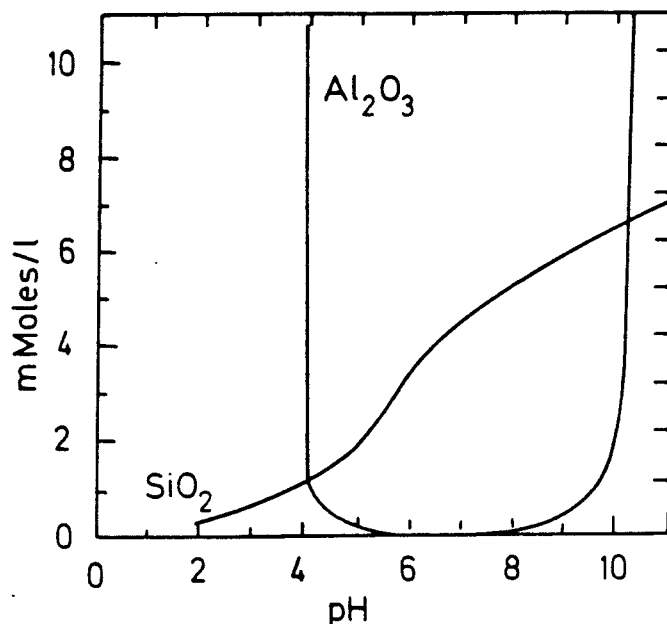
Fig 1.   Solubility of silica and aluminum as a function of pH

On the conditions mentioned, a drop in pH to a critical value at the repository level may be caused by the formation of large swamps at the ground surface. The ultimate crystalline reaction products of Na montmorillonite would then be kaolinite or dickite and possibly illite depending on the acidity, potassium content and temperature. If the amounts of dissolved iron and silica are sufficiently high, chlorite and sodium feldspars may even form. Amorphous matter consisting of silica, aluminum, magnesium and iron may also result depending on the pH situation and the ion sources, i.e. the ambient rock. Fig 2 shows a phase diagram that gives an example of possible mineral constellations as a function of the Na^+/H^+ concentration ratio.

A condition of critically high pH at repository levels may result from inflow of groundwater that is rich in dissolved calcium carbonate. It may originate from a shallow sea rich in calcium-bearing organisms as in the Forsmark area, about 150 km northeast of Stockholm.Here limestone fragments or precipitations have been found at more than 100 m depth in crystalline rock (6).
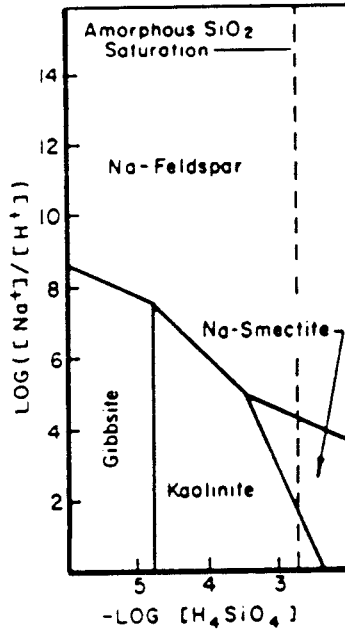
Fig 2   Stability relationship diagram for common low-temperature minerals calculated for the activity of Na+/H+ against silica activity at 25° C, 0.1 MPa. (After Garrels & Christ)

Such a condition may also result from the nearness of concrete structures. If excess $Ca(OH)_2$ from the cement is dissolved, reactions of the following type are expected:

$$Ca(OH)_2 + Al_4Si_8O_{20}(OH)_2 \rightarrow 2CaAl_2Si_4O_{12} \cdot 6H_2O \qquad (2)$$
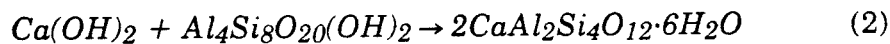
the reaction product being the zeolite chabazite. Depending on the total amount of reactants, other zeolites like $CaAl_2Si_3O_{10} \cdot 3H_2O$ (scolecite) and $CaAl_2Si_2O_8 \cdot 4H_2O$ (gismondite) may be formed. Considering the presence of Na in the bentonite, $NaAlSi_2O_6$ H_2O (analcime) is also a probable reaction product. It should be noticed that attack by high pH may also lead to $Al(OH)_4$, $Mg(OH)_2$, and $SiO(OH)_3$ in crystalline form (5). It is, in fact, even possible that only amorphous substances and gel complexes are formed in the reaction zone and that no new minerals appear. This can be concluded from various investigations of the surface character of clay minerals in natural sediments.

Density changes

Most of the alteration products in all the discussed processes have lattice densities that differ from that of Na montmorillonite. In the case of drilled deposition holes or tunnels, which form fixed boundaries of the clay, lattice contraction will cause less effective or incomplete mechanical interaction between the rock and the clay, and development of pore systems or syneresis-type fissures of long extension. This is expected when smectite minerals are altered to illite. Expansion of mineral lattices, on the other hand, means that the pore space is reduced and that recrystallization will be at least partly hindered or delayed. The formation of kaolinite and dickite as well as of zeolites, which all have lattice densities below 2.60 t/m³, is associated with lattice expansion. Hence, the porosity will decrease provided that all the involved components stay within the reaction zone. The contact pressure at the clay/rock interface will then also increase.

Cation exchange processes have a similar effect. Thus, exchange from sodium to calcium or copper produces contraction of expanded montmorillonite clay and this yields a significant increase in pore size and interconnectivity at bulk densities lower than about 2 t/m³. At higher densities the influence is not very significant, however. A large increase in concentration of dissolved sodium, as will be the case if the repository area is flooded and percolated by ocean water, has a similar effect.

A drop in bulk density and increase in porosity can also be produced by changes in total volume. Thus, in the KBS 3 case, the expansion upwards of the interface between the highly compacted Na bentonite block system and the compressible overburden will yield a drop in bulk density of the uppermost part of the bentonite at first, and later - possibly - also of the lower part. Reduction in density may also take place by loss of bentonite expanding into fractures which intersect deposition holes or tunnels and which may be widened because of changes in the rock stresses. This latter effect is not significant in fracture-poor deposition holes with waste containers but it may be of some importance in tunnels and shafts in fractured rock with clay plugs consisting of highly compacted Na bentonite.

Radiation

Two radiation effects on clay minerals are known, one being the exposure to ionizing radiation from sorbed radionuclides, the other being exposure to

radiation from external sources (2). Morphologic effects, i.e. porosity changes, pitting and fragmentation of particles have been identified on strong alpha radiation from clay-sorbed radionuclides and sol-gel transformation has been observed indicating that pH and the ion composition of the porewater were altered. The damage is probably similar to that obtained by strong γ-radiation from external sources, i.e. partial mechanical breakdown of mineral crystals and disintegration of aggregates. Such alterations have not been found to yield crystallographic changes in smectite clays even at very high radiation doses and long exposure times. Since the only safe conclusion from radiation experiments is that the treatments actually improve the barrier properties of irradiated clay by dispersing it and increasing its specific surface area, the matter will not be discussed further in this report. It should be pointed out, however, that long-term effects of radiation and radiolysis are currently unknown.

2.2   SELECTION OF REPRESENTATIVE CLAY SOILS FOR TESTING

2.2.1   General

A number of well defined, dense clays which resemble possible alteration products of highly compacted, montmorillonite-rich Na bentonite in repository environment have been identified. They are well defined with respect to the composition and geological history and will be described in detail in a subsequent chapter. Their relation to possible alteration products of montmorillonite clay contained in repositories is briefly described first.

2.2.2   Reference clays

*   Natural Na Wyoming bentonite in the form of commercial MX-80 granular powder is used here as a representative of montmorillonite-rich clay buffer materials (I)

*   The maximum repository temperature considered in this study is 150°C. Under certain geochemical conditions it may yield an extreme alteration product of Na bentonite, namely a clay of high density that is rich in illite and with no smectite left. Since the transformation of montmorillonite to illite also implies release and precipitation of silica compounds and quartz, the net product would be a dense assemblage of

illite and quartz, provided that the pH conditions do not yield a pore water chemistry that promotes formation of other minerals. A fraction of the clay particles would be in discrete form while the rest would consitute silica-cemented aggregates, reducing the initial clay content, i.e. the fraction of clay-sized particles, to 20-40 %. A natural soil of this type is the Silurian clay in the Burgsvik area, southern Gotland (II).

* Sufficiently long heating to 120-150° C of Na bentonite may yield approximately the same mineral composition as that of the Gotland clay (II) in the same type of environment but a fair fraction of the smectite would be preserved, mainly in the form of mixed-layered illite/ smectite (IS) stacks, in this temperature interval. Silica cementation leading to a content of clay-sized particles of less than 50 % would be expected. Such a transformation is examplified by the Ordovician Kinnekulle bentonites, which contain strata that are more (III) or less (IV) illiticized.

* A temperature in the range of 120-150° C combined with a rock groundwater pH lower than 6 yields conditions that can be expected to promote formation of kaolinite minerals, feldspar and possibly chlorite on the account of the smectite, which may still be partly preserved in the Na bentonite. The content of clay-sized particles would naturally be low, i.e. about 10-20 %. A dense clay with a composition of this sort is represented by the Belgian Boom clay (V).

* Temperatures slightly exceeding 100-120° C may produce a spectrum of more or less montmorillonite-holding clayey materials under intermediate pH conditions. Ultimately, one can expect an assemblage of reaction products forming a clay with some smectites preserved and with a certain small content of mixed layer minerals and quite significant amounts of quartz and illite. Considerable cementation of minute particles by precipitating silica compounds would reduce the content of clay-sized particles to 20-40 %. A material of this composition is found in the pre-Quaternary Singö fault zone in the Forsmark area (VI).

* A temperature of 120-150° C and subsequent exposure to strong ion exchange to calcium caused by percolation of Ca-rich solutions with moderate or high pH, may yield a rather extreme alteration product,

namely a smectite-poor, strongly calcite-cemented clay with quartz
particles aggregated together to form silt-sized aggregates. The
content of clay-sized particles would be less than 20 %. A dense clay of
this composition is the Cretaceous smectitic intercalation in limestone
at Ignaberga, Skåne, Sweden (VII).

*   Moderate temperatures i.e. 90-130° C, and strong influence of ion
exchange to calcium caused by percolation of Ca-rich solutions may
yield montmorillonite and hydrous mica contents of 20-30 % each, a
low content of quartz, and a high amount of cementing calcite. A
natural clay of this type is the Cretaceous Fish clay at Stevens Klint,
Sjaelland, Denmark (VIII).

2.2.3   Comments

Only two, or possibly three or four of the reference clays (II-VIII) are actual
bentonites that have undergone heat-induced alteration, while the remaining
ones only resemble reaction products that may evolve from Na bentonite that has
undergone various chemical processes in nature.

All the clays termed II-VIII were used for comparing the physical properties with
those of MX-80 Na bentonite, which served as a standard (I). For certain purposes,
like the evaluation of how cementation affects the rheological properties, certain
other clays have also been used. They will be characterized in connection with the
description of the respective testing.

3   TEST PROGRAM

3.1   GENERAL PHILOSOPHY

The physical properties that are of major importance for obtaining good barrier
properties are the hydraulic conductivity and the swelling potential as manifested
by the swelling pressure. Data from percolation and pressure oedometer tests of
the reference clays give direct evidence of changes that result from possible
chemical alteration of the initial clay and such tests were therefore basic to the
study. By determining the hydraulic conductivity of undisturbed samples at
different expansion stages, the influence of bulk density changes could be deter-

mined for two of the relatively smectite-rich clays, and by repeating the measure-
ments after remolding and reconsolidation of two smectite-poor clays, the
influence of the spatial distribution of clay mineral constituents could be illu-
strated. The rheological properties are also considered to be of significance since
they determine the character of the long term settlement of waste canisters and of
possible rapid, tectonically induced shear. Shear tests conducted so as to yield the
creep characteristics and the shear strength were therefore included in the test
program. In the course of the study it became apparent that creep tests performed
in a standardized manner are helpful in understanding how the flow-producing
micro-components are changed with respect to their number and character by
heat-induced chemical processes, which called for expansion of the creep tests
series and for offering considerable space to the subject in this report.

The characterization of the clays comprised determination of the natural water
content and the content of clay-sized particles (<2 μm), as well as XRD identi-
fication of the mineral composition. The Atterberg liquid limit was also deter-
mined since this consistency parameter is a practical measure of the content of
hydrophilic minerals. Also, the microstructure of undisturbed samples was
investigated by applying transmission electron microscopy, and in a few cases, by
light microscopy. In connection with the evaluation of the shear box tests,
scanning microscopy was used for identifying the distribution of shear strain in
two of the clays.

The XRD tests and the quantitative evaluation of the mineral compositions were
made by the Swedish Geological Survey under the guidance of Dr Ann Marie
Brusewitz, and by the Dept of Quaternary Geology, University of Lund, in
cooperation with the junior author.

The transmission electron microscopy was directed by the senior author and
conducted at the Dept of Histology, University of Lund, applying a well estab-
lished acrylate embedding technique (1). The scanning microscopy was made by
the company EMW, Maryland, USA, using a preparation technique that produces
minimum disturbance (7).

3.2 PHYSICAL TESTS

3.2.1 Hydraulic conductivity

Samples were trimmed from larger chunks to fit the swelling pressure oedometer (Fig 3). In order to eliminate leakage along the interface between the sample holder and the 1-2 cm thick samples, the latter were trimmed slightly conical so that very fine MX-80 powder could be filled and compacted in the slot, which was thereby effectively sealed off. The piston was then inserted and the sample slightly prestressed by turning the nuts. The filters were saturated with water and the sample left to reach mechanical and chemical equilibrium for about a week before hydraulic heads were applied. The hydraulic gradient was in the range of 20-30 in most of the tests, the percolation being pursued for at least 1 week, through which steady state flow was ascertained.
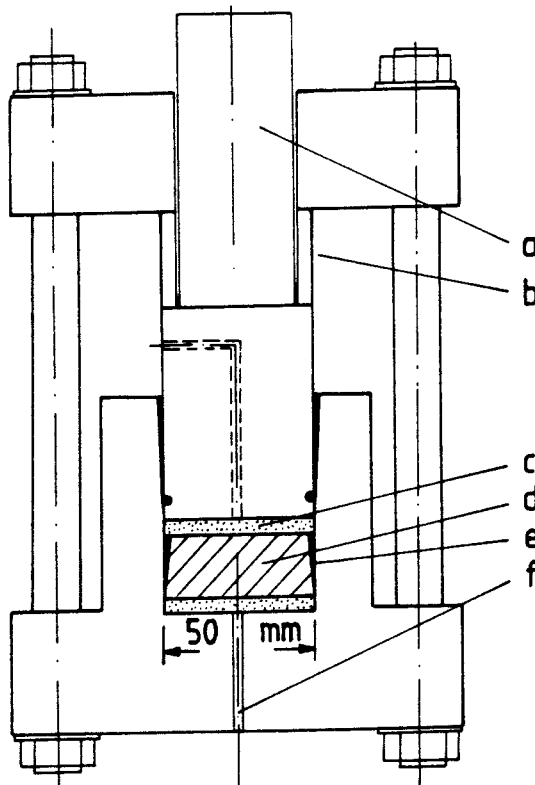

Fig 3.   Oedometer for measurement of hydraulic conductivity and swelling pressure. a) Free piston for loading the specimen to nearly zero stress conditions in the ring, thereby balancing the swelling pressure. b) is the strain gauge glued to the ring, c) filter stone of stainless steel, d) bentonite specimen, e) infilled, compacted Na bentonite powder, f) lower water inlet

Artificial Forsmark water was used in all the tests. It was composed so as to be very similar to true water that had been sampled in connection with the rock excavation for the SFR repository at Forsmark. Chlorides of sodium, calcium, magnesium and potassium were mixed to a total salt content of 11820 ppm, with the follow ionic strengths: Na^+ 2530 ppm, Ca^{2+} 950 ppm, Mg^{2+} 21.7 ppm, and K^+ 5.4 ppm. The choice of this type of water had three reasons. Firstly, at the time when the test series was planned it had become evident that brackish or salt water must be expected at depth in crystalline rock. Secondly, practically all the clays had been formed in strongly brackish or salt water. Thirdly, the use of brackish water would yield a somewhat higher hydraulic conductivity than distilled water or Allard water, and would therefore yield conservative values.

3.2.2   Swelling pressure

The swelling pressure was determined in the usual way, i.e. a carefully recorded force was applied on the piston, the reading being taken when the ring with the strain gauge (Fig 3) became almost stress-free. Measurements were made immediately after the end of the percolation test.

3.2.3   Rheological properties

3.2.3.1   Technique

At the planning stage of the investigation considerable effort was put in finding a relatively simple technique for determining characteristic rheological properties of the dense clays in their natural state. Triaxial tests could not be chosen on the ground that most of the clays were stratified with only a limited part being representative of the clay component and also because some of the samples exerted much higher swelling pressures than could be balanced by the cell pressure. Shear tests using $\phi50$ mm samples could not be used for the most smectite-rich samples because the available machine did not have enough load capacity to balance the swelling pressure.

These disadvantages were eliminated by using shear boxes consisting of two rigid halves, the sample being trimmed to fit exactly in the box between non-corrosive filters. After insertion of the sample, a normal stress corresponding to the swelling pressure was applied and adjusted so that equilibrium was attained, and a

shear force was then applied and increased stepwise. By this, the creep strain could be measured under constant stress conditions and with the sample kept drained. Fig 4 illustrates the arrangement, the diameter of the boxes being in the range of 20-50 mm.

The load steps, which were initially set at approximately 20 % of the shear strength, were usually left on until the creep rate had dropped to less than about $10^{-8}s^{-1}$, which required about one week in most cases. The loads were increased until failure was finally achieved.

The disadvantage of this kind of testing is that the stress conditions in the sheared sample are not well defined. Thus, plastic zones are developed at the periphery in the course of the shear strain and it is not a straight-forward matter to predict their extension or to relate strain and strain rate to the stress conditions. The problem is almost classical and requires a considerable amount of research work to be solved. For the present purpose of evaluating a characteristic average shear stress to which the macroscopic strain and creep rate can be related, a simple theory has been worked out. It is briefly outlined in the subsequent text.

A practical difficulty in running creep tests of this type is that a perfect contact between the sample and the shear box components may not be established at the start of the test. The strain recorded for the first load step in the test series may therefore not be relevant.

3.2.3.2   Stress/strain distribution in sheared samples

The extension of the plastic zones and the distribution of stresses in the sheared sample was determined in a preliminary study by using 2D FEM technique (FLAC program)*. The material was taken to be ideally elastoplastic with a maximum shear stress of 0.7 MPa - obtained at a shear strain of 2 % - and a shear modulus of 30 MPa. Poisson's ratio was assumed to be 0.45 and 0.475 in separate runs. The breadth/ height ratio was taken as 1.5 and the number of elements 561.

----

*   The study was conducted by Peter Cundall, ITASCA, Marine on St Croix, Minnesota 55047, USA
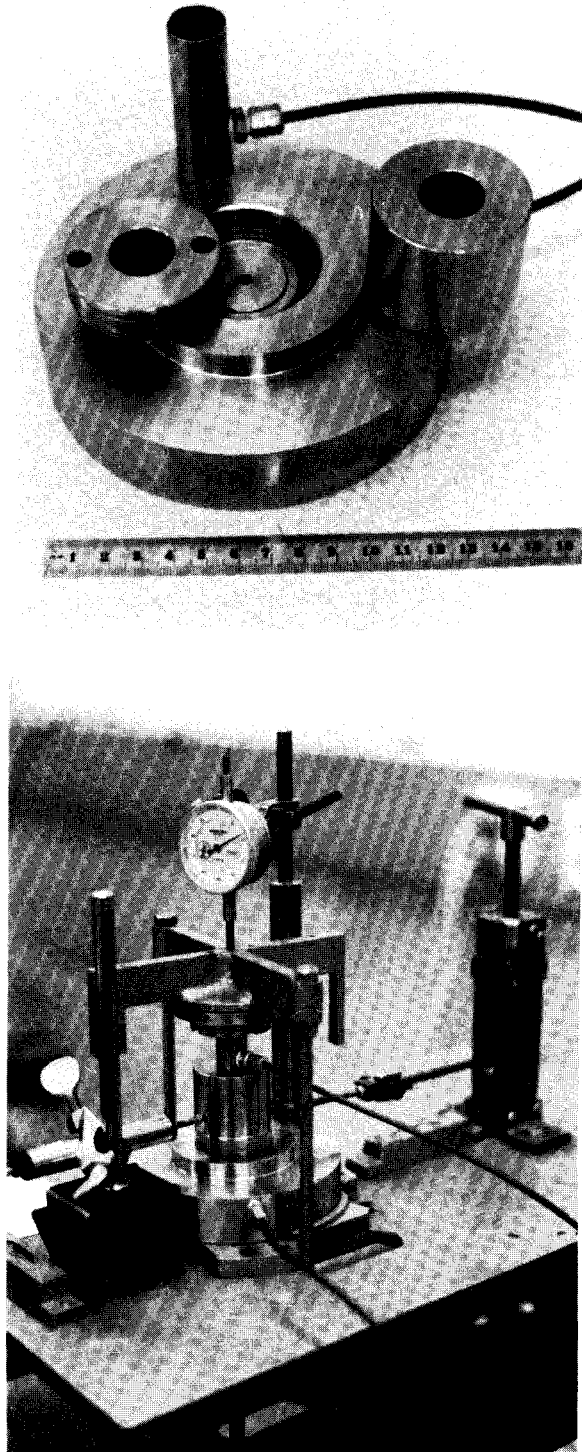
Fig 4. The shear box (upper) and the shear apparatus with electronic strain
gauge mounted horizontally for automatic creep recording. Changes of
sample height are measured by use of the mechanical gauge

The reference shear strain was defined as the relative lateral displacement of the
shear-box halves divided by the diameter, and using this definition it turned out
that at 2 % strain, the shear stress all along the midplane had reached the yield

value. Figs 5 and 6 show the principal stress patterns and the distribution of the shear stress at 0.5 % and 1 % strain, respectively. The difference between 2D and 3D stress/strain conditions is not very significant in the present context.

The successive plasticizing in the course of the shear deformation is demonstrated by the FEM study, the fraction of the total midplane area that has reached the yield state at different strain percentages (Δ/D) being summarized in Fig 7. The plasticized zone undergoes complete microstructural breakdown leading to alignment of practically all particles and to the development of one large flow zone. It contributes to the shear resistance by a constant amount equal to the yield stress, by which the total shear force must be reduced in the evaluation of the average operative shear stress τ in the intact part of the sheared sample. Taking this part to be cylindrical with a base equal to (A-A$_s$), τ will theoretically be as given by Eq. (3):

$$\tau = \frac{F - \tau_f(A - A_s)}{A_s} \tag{3}$$

where   F = shear force

τ_f = shear strength (yield stress)

A = total cross section area

A$_s$ = area of non-plasticized zone

For stresses not exceeding about 80-90 % of the shear strength, τ can be taken as the quotient F/A with sufficient accuracy. The FEM study suggests that the height of the intact, i.e. non-plasticized part of the sample can be taken to be 1/3 of its diameter.

The shear strain of the entire sample is defined as:

$$\frac{A - A_s}{A} = \frac{\Sigma\Delta}{\Delta f} \tag{4}$$

where $\Sigma\Delta$ = accumulated displacement from the first load application

Δf = total shear displacement at failure

Principal stresses
Max. Stress= 3.023E+06
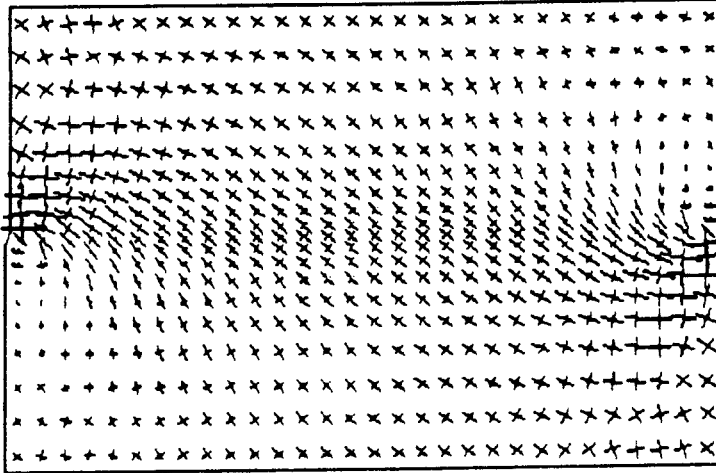
XY-stress contours
Contour Interval= 5.000E+04
F: 1.500E+05
J: 3.500E+05
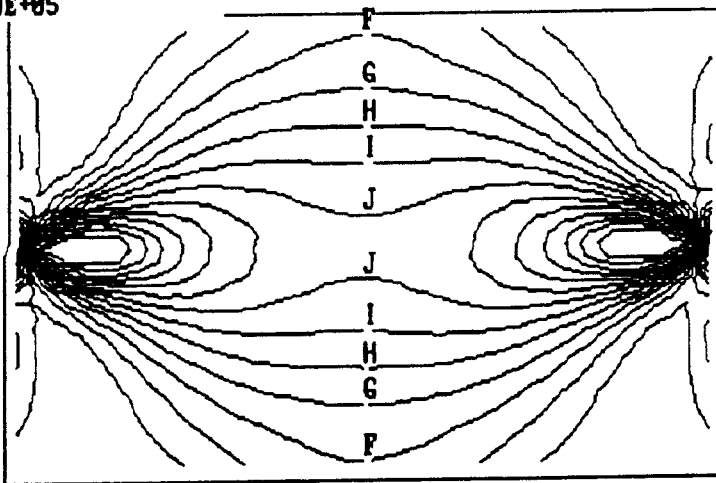
Fig 5.   0.5 % shear strain. Upper picture shows the orientation and ratio
          of the principal stresses, while the lower picture shows the shear
          stress contours: F = 0.15 MPa, G = 0.20 MPa, H = 0.25 MPa,
          I = 0.30 MPa, J = 0.35 MPa (v = 0.475)

Principal stresses
Max. Stress= 3.167E+06
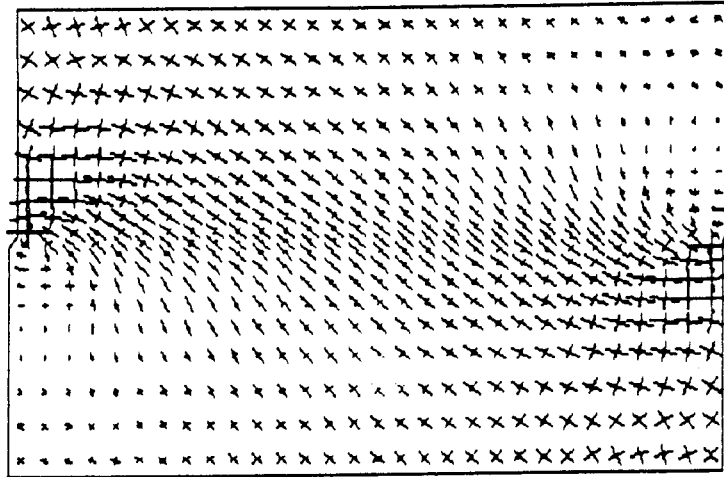
XY-stress contours
Contour interval= 5.000E+04
 F: 5.000E+04
 J: 2.500E+05
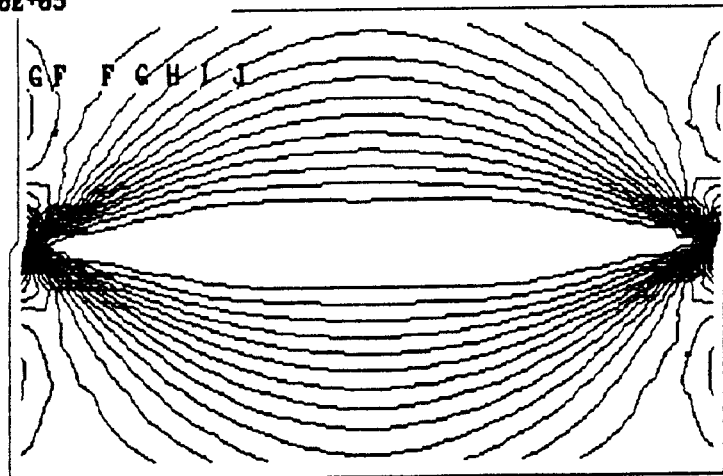
Fig 6.   1.0 % shear strain. Upper picture shows the orientation and ratio
of the principal stresses, while the lower picture shows the stress
contours: F = 0.05 MPa, J = 0.25 MPa, R = 0.65 MPa (v = 0.475)
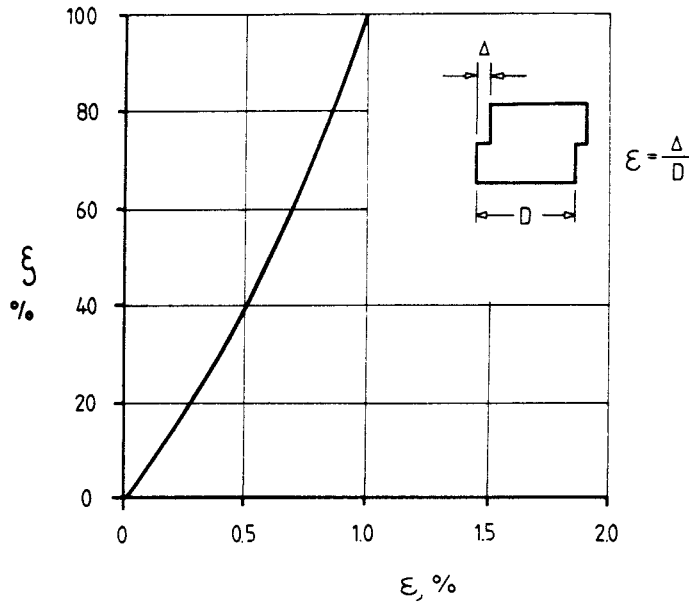
Fig 7.   Fraction of total midplane area that is in the yield state $\xi =$ A_s/A, (in %) at different strain percentages ($\varepsilon = \Delta/D$)

Applying the previously mentioned height/diameter ratio of the non-plasticized core, its angular shear strain has the form for each individual load step that is given by Eq. (5):

$$Y = \frac{3\Delta}{D_s} = \frac{3\varepsilon}{\sqrt{1 - \dfrac{\Sigma\Delta}{\Delta_f}}} \tag{5}$$

where D_s is the diameter of the non-plasticized part of the sample (Fig 8), Δ the recorded shear displacement for the respective load step and $\varepsilon = \Delta/D$. For load steps close to failure considerable uncertainties in evaluating the strain appear since $\Sigma\Delta/\Delta_f$ then approaches unity.

3.2.3.3   Microstructural evidence

The actual microstructural strain associated with shear leading to failure has been documented by applying scanning microscopy. The tests concerned the reference clay (I) i.e. Na Wyoming bentonite that was compacted in the form of air-dry powder and then saturated with brackish water under confined conditions in a 30 mm shear box to a bulk density of 1.82 t/m^3 at saturation (dry density
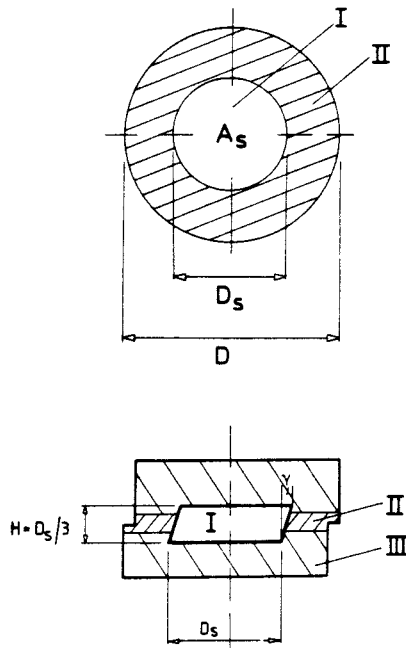
Fig 8.   Shape and size of the intact i.e. non-plasticized part (I) of the
          sample that determines the rheological properties of the sample.
          II is plasticized part while III is a passive part

$\rho_d = 1.30$ t/m^3). After about one week at rest for microstructural homogenization,
the sample was exposed to stepwise increased shear forces until failure was
developed (τ_f = 400 kPa). The total displacement Δ_f at failure was about 0.6 mm,
but the two box halves were displaced by a few millimeters before the shear could
be stopped and the sample extracted. It was left to rest under undrained condi-
tions for several hours and then removed from the shear-box and freeze-dried as a
first preparation step in the microstructural investigation. After mechanical
fracturing to obtain a section perpendicular to the mid plane of the shear box, the
exposed surface was cleaned by several tape peelings whereafter gold sputtering
was made as the last preparation stage.

The electron microscopy, which comprised about 100 SEM exposures, revealed
that the central 0.5 mm wide zone containing the theoretical shear plane, showed
the highest degree of particle orientation due to the large post-failure strain. The
quantification of this microstructural feature simply refers to the measured frac-
tion of the total area of each micrograph that showed at least 10 µm long zones of
aligned particles. It is expressed as the orientation factor (D), which varies from 0
% for completely random particle orientation to 100 % for perfect alignment of all
particles. D typically ranges between 10 and 20 % for undisturbed Na bentonite

prepared in the described way, the orientation being inherited from the particle alignment in the virgin bentonit grains (cf. Fig 17).

Fig 9a demonstrates that almost 40 % of the central "shear" zone, extending to ±0.25 mm from the theoretical shear plane, is represented by a D-value of 40-80 %. For the clay extending to 1.0 mm from this shear plane the histogram in Fig 9b shows a distribution pattern of the D-factor that is similar to that of the adjacent 1 mm wide zone (Fig 9c) and not too different from that of the clay located 2-4 mm off the theoretical shear plane (Fig 9d). This suggests that the shear strain was approximately the same in the central 6-8 mm high clay zone, which appears to be in reasonable agreement with the FEM-derived stress distribution pattern at intermediate and high stresses. Figs 10-13 show characteristic SEM micrographs of the sheared sample.

The conclusion from this study is that a large part of the sample was activated in the course of the shearing, which is thus in accordance with the FEM analysis. The absence of a very clearly developed continuous shear zone in the center of the sample suggests that considerable self-healing associated with particle regrouping took place in the course of the relaxation period.

3.2.3.4   Evaluation of creep tests

The rheological parameters of major interest are the creep strain and strain rate at successively increased shear stresses. At low and intermediate shear stresses the creep rate is known to be retarded under constant deviatoric conditions, the general creep law being of the form (6):

$$\dot{\gamma} \propto \tau^{\alpha} \cdot T^{\beta} \cdot t^{-m} \tag{6}$$

where $\dot{\gamma}$ = angular strain rate
α = stress exponent exceeding unity
β = temperature exponent exceeding unity
m = time exponent

Experience tells that m < 1 predicts large strain and risk of failure, while m > 1 leads to finite strain at t→∞. For shear stresses lying between 1/3 and 2/3 of the shear strength, i.e. the stress leading to rapid failure in conventional shear tests, m is usually about unity, while lower shear stresses yield higher m-values.
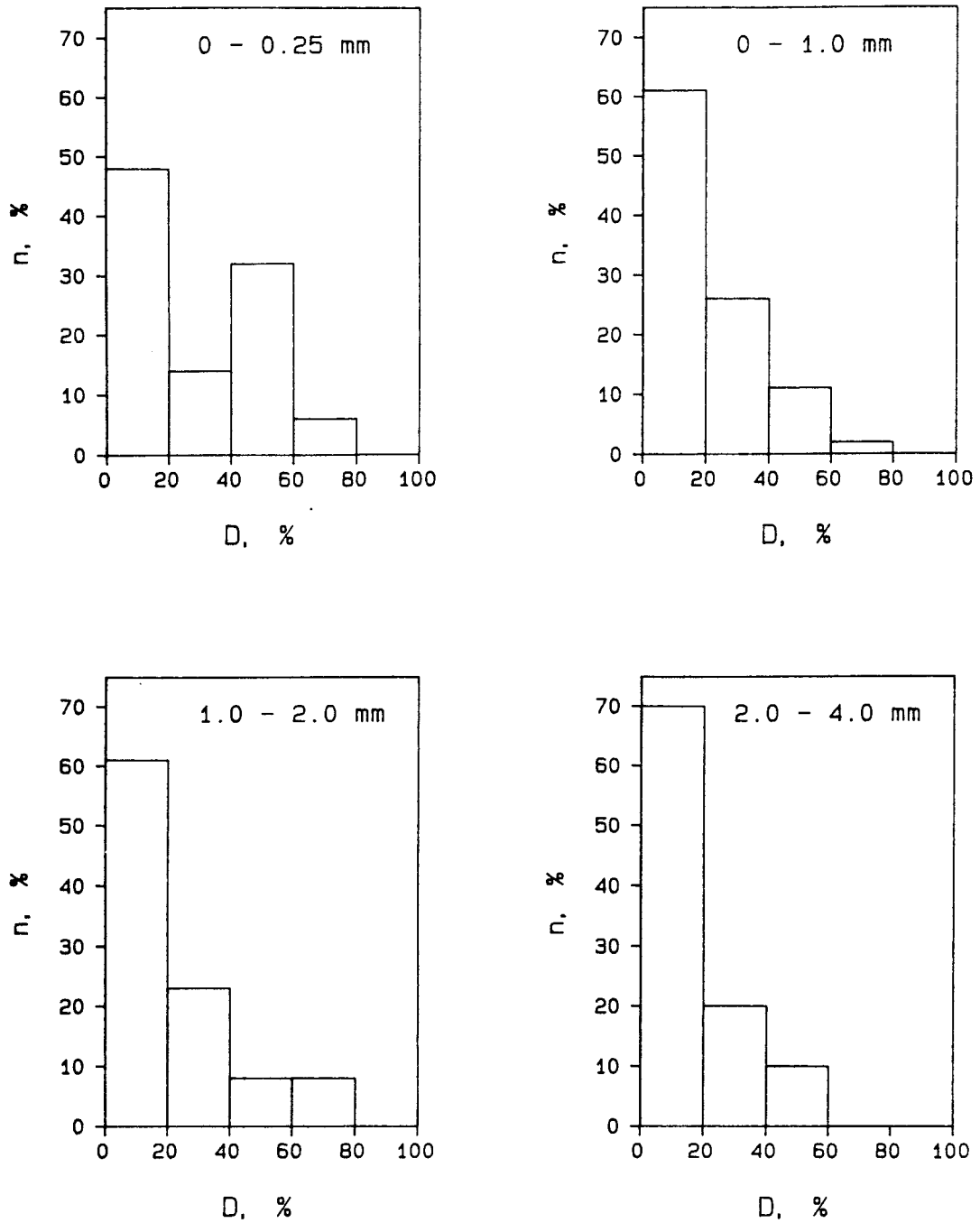
Fig 9.   Histograms showing the distribution of the orientation factor D
for various parts of the sheared MX-80 sample

Applying a statistical model that embodies changes in the number and heights of thermally activable energy barriers to slip, Pusch & Feltham (9) have shown, on purely theoretical grounds, that m = 1 provided that the successive slip does not lead to such large accumulation of microstructural defects that failure ultimately takes place. The critical stress that yields creep failure depends on the average strain rate as well as on the accumulated strain. Experience with many creep curves offers evidence that for a certain, usually long time interval, the plot of strain versus time fits Eq. (6) for m = 1.
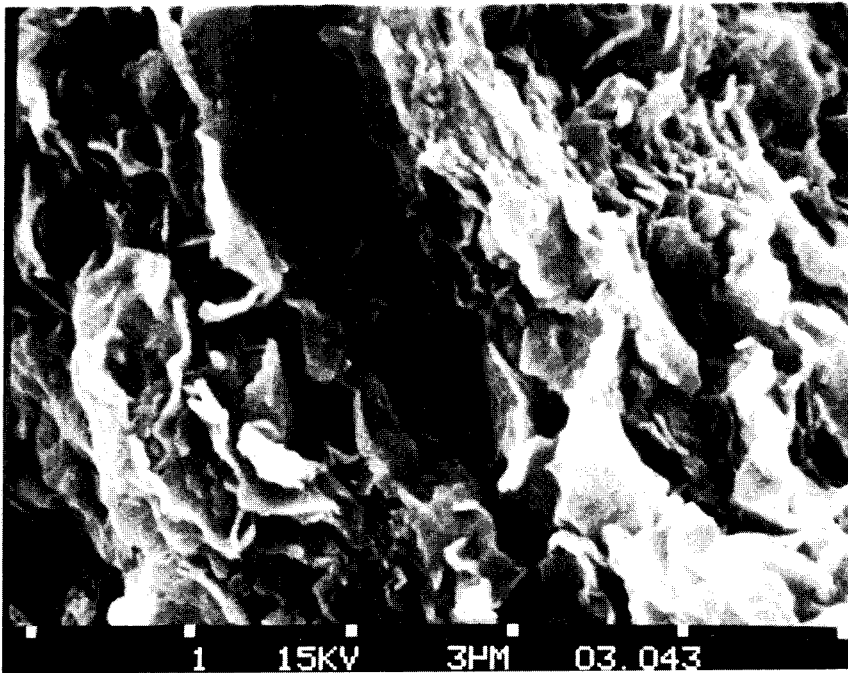
Fig 10.   Typical alignment of particles in the midplane of the sheared
           sample. The oriented zone extends over many tens of micrometers
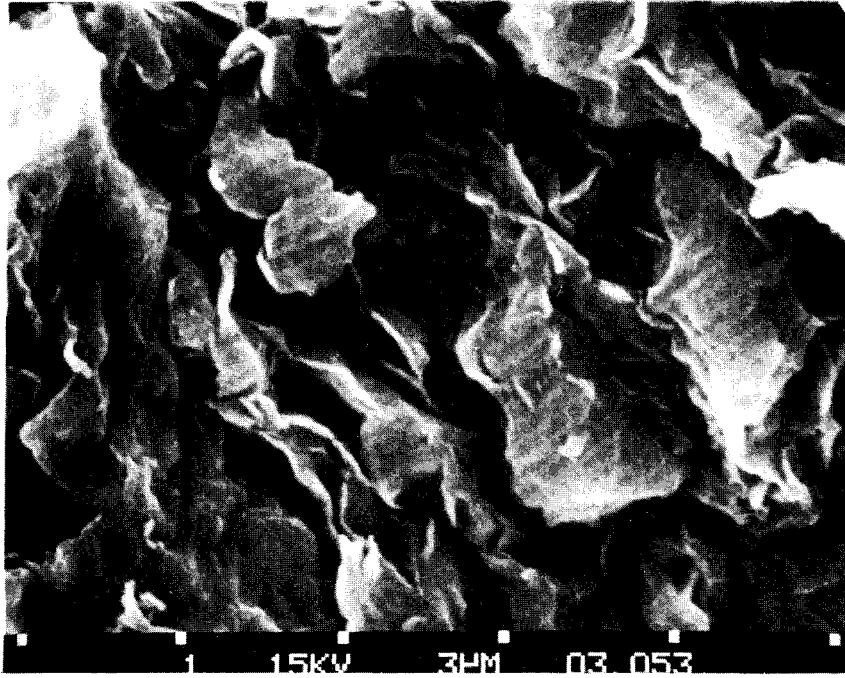
Fig 11.   Slip zone at 0.3 mm distance from the midplane oriented almost
           perpendicularly to the plane of the paper. The lower left shows the
           edge of a dense bentonite grain with montmorillonite flakes
           oriented parallel to the plane of the paper
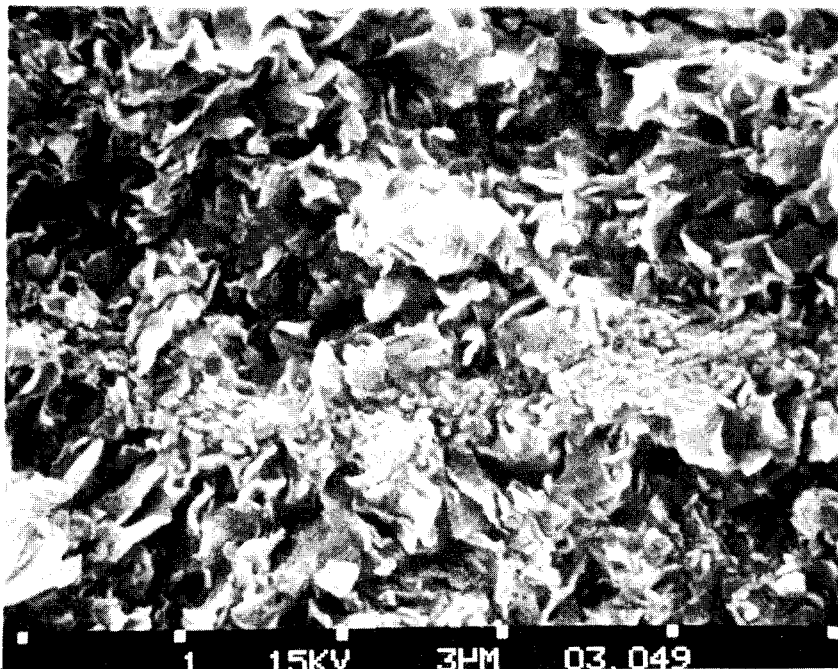
Fig 12.   Local slip band in relatively random particle matrix at 0.3 mm
           distance from midplane
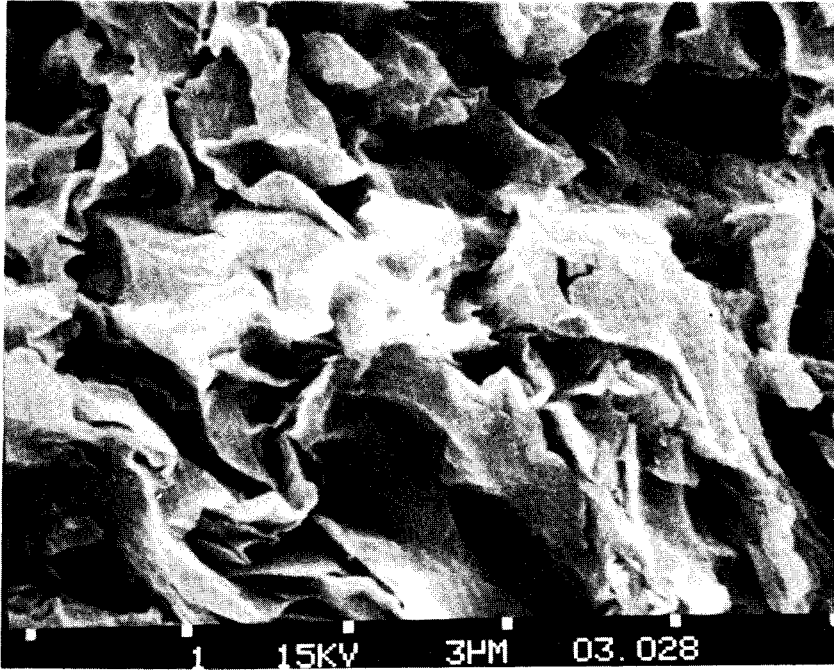
Fig 13.   Slight, local particle orientation at 3 mm distance from the
           midplane

For m = 1 the expression in Eq. 6 is identical with the log time creep law, the
general form of which is:

$$\dot{\gamma} \propto \tau^{a} \cdot T^{\beta} \frac{1}{t+t_{o}} \tag{7}$$

and

$$\gamma \propto \tau^{a} T^{\beta} \log (t+t_{o}) \tag{8}$$

where t_{o} is a constant (cf Fig 14). For constant temperature conditions Eq. (8) can
be put in the form:

$$\gamma = B \ln (t+t_{o}) + A \tag{9}$$

The explicit form of Eq. (9) will be used here with A, B and t_{o} being taken as
characteristic parameters. B is of primary interest since it reflects the stress
dependence, while t_{o} is a measure of the microstructural distortion that is caused

at each load application. Theoretically, t_o should increase with the applied stress for virgin clays, except when cementation contributes to the shear resistance. In cemented clays the creep rate retardation is very strong as long as the cementation is intact while initiation of cement bond breakage at a sufficiently high stress yields a drop in creep rate that is initially strong but which is less significant at later stages. This results in negative t_o:s (10). This matter will be elaborated on in the last chapter.

The characteristic behavior of cemented clay is illustrated by a creep test of Quaternary quick silty clay from Molde, Norway (Fig 15). Oedometer tests have demonstrated that this soft clay, which has a bulk density of 1.9 t/m^3 ($\rho_d = 1.43$ t/m^3) and a water content of about 30 %, is collapsible with a significantly cemented microstructure and an undrained shear strength of 0.35 MPa. Its clay content is about 43 %. The creep testing was conducted under drained conditions and a higher normal pressure, i.e. 0.3 MPa, than the natural overburden pressure, which is 0.085 MPa. Two load steps were applied and it is clear from the upper diagram that both yielded creep curves that obey the log $(t + t_o)$ relationship. The low load gave a τ-value of about 50 % of the shear stress at creep failure, the time/strain curve being very smooth, while the high load gave jerky and rapid creep, indicating fast flow after breakdown of the cementing bonds. The creep parameter values are given in Table 1, from which we see that t_o is negative for the low stress, which is represented by the curve with upward concave shape in the initial creep period in the lower diagram of Fig 15. The high stress creep curve exhibits the usual upward convex shape of non-cemented clays.

The sample was kindly put to the authors' disposal by Prof Nilmar Janbu, Dep of Soil Mechanics, University of Trondhjem, Norway.

Table 1   Creep parameters of cemented
Norwegian clay

Shear stress τ, MPa	A*	B*	t_o s
0.071	171	12.5	-35
0.100	-569	113.5	1076

* The values in the table must be multiplied
by 10^{-4} to yield the actual figures

Creep tests of the type conducted in the present study mainly serve to illustrate how structure-sensitive the clays are. Conclusions were drawn mainly as to 1) how continuously the creep strain was developed at each individual load step and 2) whether there were creep rate anomalies that indicate breakage of cementing bonds. As indicated by the rather comprehensive discussion in the last chapter, a number of new aspects on the influence of chemical changes and microstructural heterogeneity on the creep properties have evolved from the study and it is foreseen that creep testing will turn out to be of considerable value in future characterization of clay-based buffer materials.
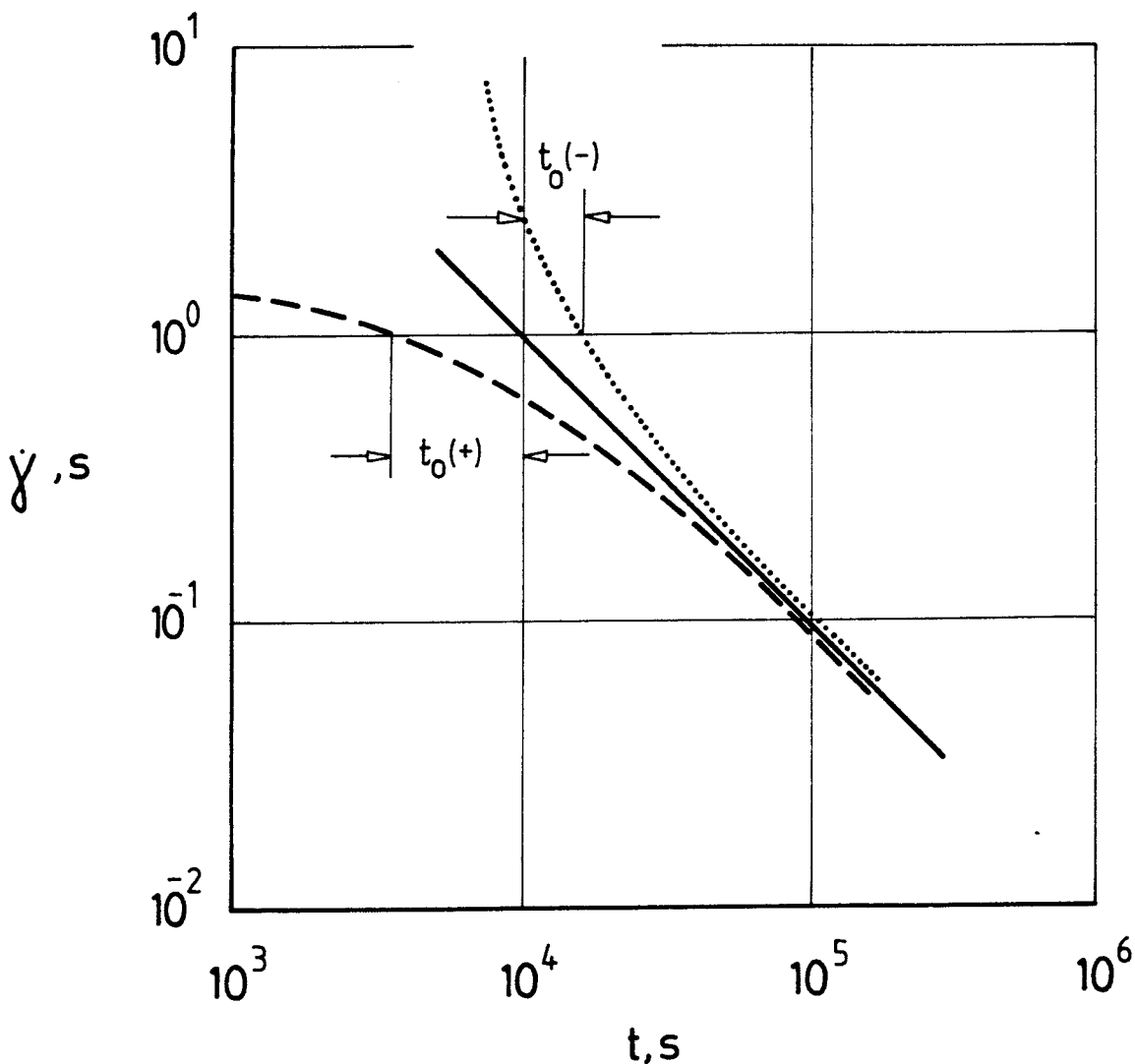
Fig 14.   Creep curves according to Eq. (7), the full line corresponding to $t_0 = 0$. Broken line represents positive t_0:s while t_0 is negative for the dotted one
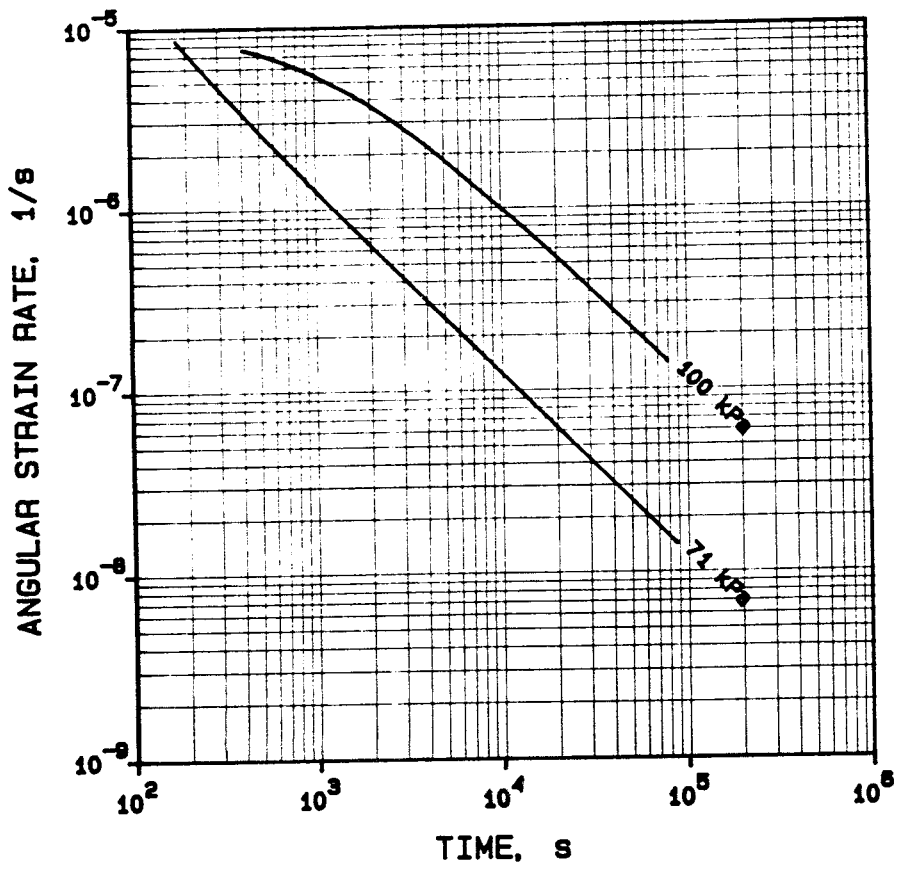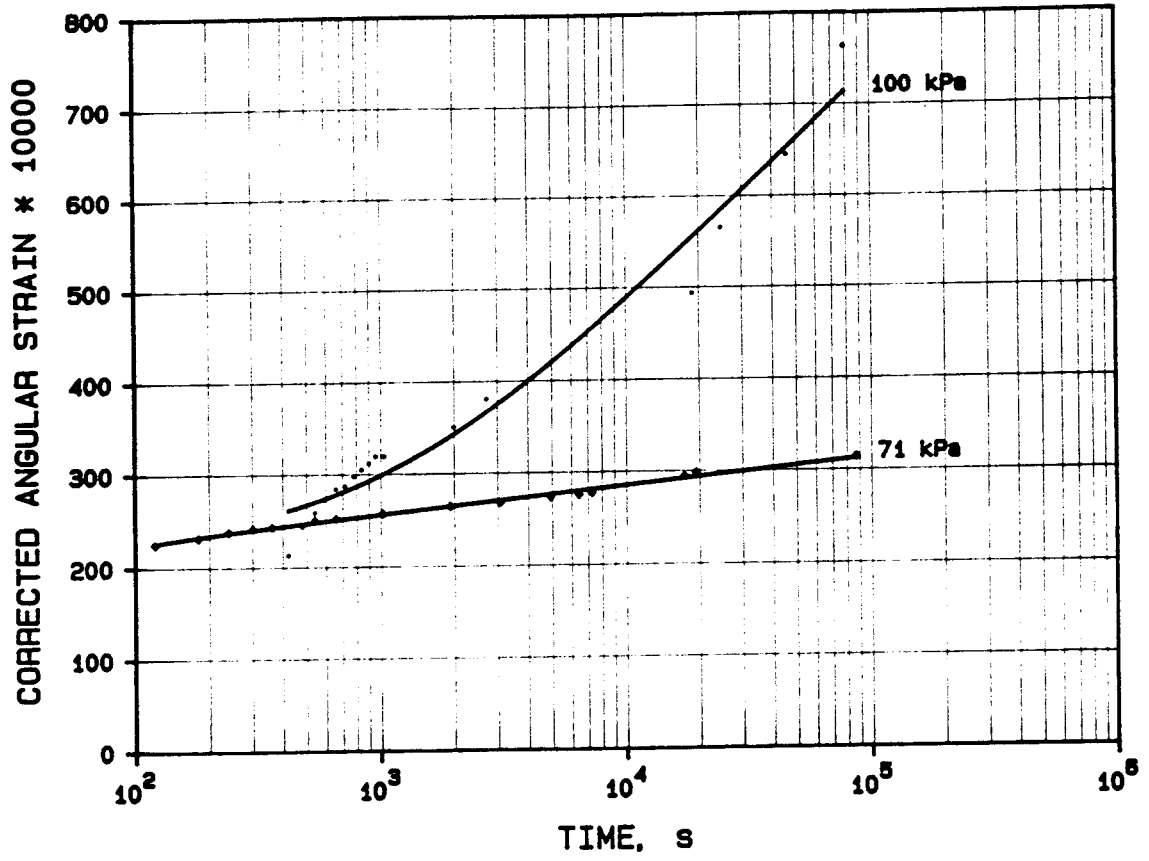
Fig 15.   Creep strain versus time (upper), and strain rate versus time
(lower) of cemented Norwegian clay from Molde

4 TEST RESULTS

4.1 INTRODUCTION

For the sake of clarity each reference clay will be presented separately in this chapter. The origin, composition and physical state will be described first, while test data are compiled in the later part of each presentation.

4.2 MX-80 Na BENTONITE CLAY (I)

4.2.1 Origin, composition and physical state

4.2.1.1 Origin

The clay material originates from bentonite deposits in Wyoming and South Dakota where it forms beds with a thickness of up to several meters. After excavation, the slaty material is dried, ground, and stockpiled under conditions that yield a water content of the air-dry clay powder of about 10-12 %. The MX-80 material produced by the American Colloid Co was chosen for the study.

4.2.1.2 Composition

The clay content, i.e. the content of particles with a Stoke diameter less than 2 µm, is 80-90 %. Fig 16 shows a typical X-ray diffractogram with a (001) peak displacement from 12.9 Å at RH ~50% to 17.4 Å upon ethylene glycol treatment, indicating that Na montmorillonite is the dominating clay mineral component. Silt is the dominant remaining fraction which mainly contains quartz and feldspars as well as some micas, sulphides and oxides. The chemical composition is given by Table 2. It is estimated that smectite forms 65 % of the total solid mass.

Spectrometric analyses have shown that the natural porewater of this clay contains 70 mg Na, 30 mg Ca and 15 mg Mg per liter porewater, which suggests that a significant amount of bivalent cations, i.e. about 10-30 %, may be in interlamellar positions.

While the most accurate characterization of the clay is through XRD and chemical analyses, the Atterberg liquid limit is a handy way of estimating the surface properties of the clay material. For MX-80 it amounts to 400-550 % depending on the origin and homogeneity of the raw material.
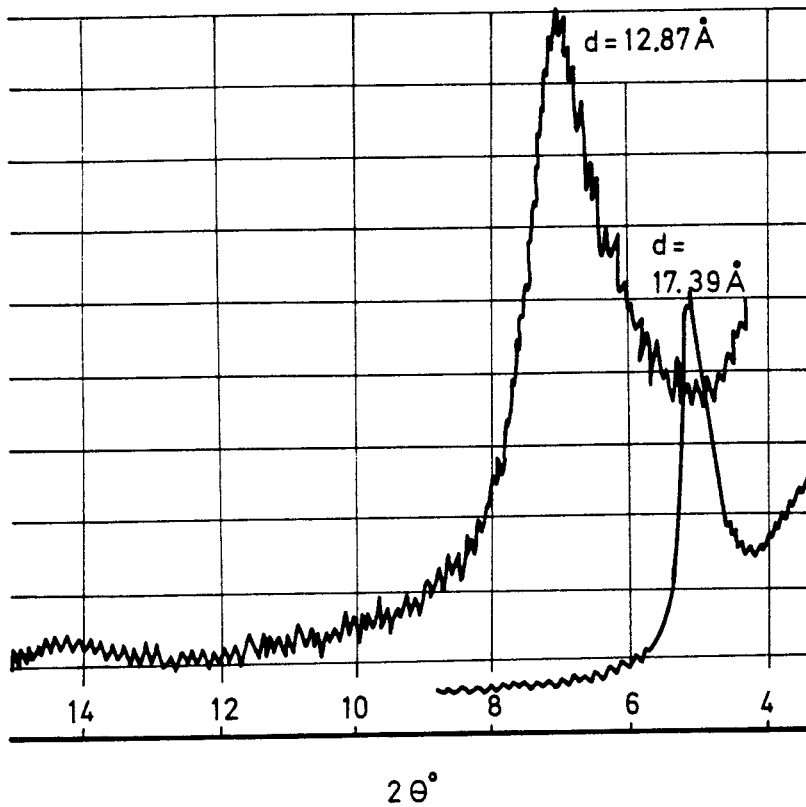
Fig 16. X-ray diffractogram of MX-80 powder. 2θ° is given by the horizontal scale. 12.87 Å is the 001 spacing of air-dry clay which is expanded to 17.39 Å by ethylene glycol treatment (lower curve)

4.2.1.3 Physical state

The properties of MX-80 clay that are currently referred to in the SKB research work are characteristic of the clay product that is formed when the clay powder is left to hydrate and homogenize in a confined space so that complete water saturation and internal particle equilibrium positions are achieved before actual testing is commenced. For dry densities exceeding about 1.2 t/m^3 this yields an apparently homogeneous physical state but electron microscopy has revealed that the microstructure is in fact heterogeneous in a way that largely governs the physical properties of this kind of artificially produced clay. Thus, the dense bentonite powder grains form a densely fitting, continuous network with pores which become occupied by a montmorillonite clay gel emanating from the dense grains (Fig 17). This gel, which has a density that varies depending on the pore size and porewater chemistry, is responsible for the hydraulic conductivity and the major part of the ion diffusion capacity (11).

Table 2 Representative chemical analysis of MX-80 bentonite
(Asea- Atom)

	%
SiO	63.0
Al_2O_3	16.1
Fe_2O_3	3.0
CaO	1.1
MgO	1.6
Na_2O	2.2
K_2O	0.48
Li_2O	<0.01
MnO	0.03
TiO_2	0.10
F	0.10
Cl	<0.01
S	0.12-0.23
Cu	<0.01
Zn	0.01
Cr	<0.01
Ni	<0.01
AsO_4	0.018
No_3	none
PO_4	0.060
S in sulphides	0.12
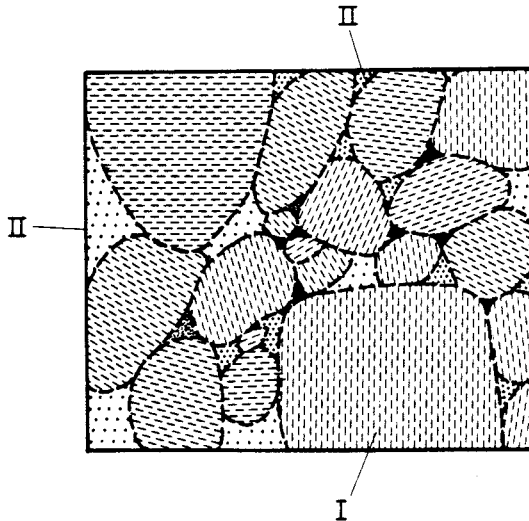
Fig 17.   Generalized microstructure of matured MX-80 clay. I represent
           expanded bentonite grains, while II refers to montmorillonite gels
           formed in the pores between the grains

4.2.2   Physical properties

4.2.2.1   Hydraulic conductivity

The hydraulic conductivity of MX-80 clay has been extensively investigated, the
values compiled in Table 3 being representative for the percolation of distilled and
very slightly brackish water.

Table 3.   Hydraulic conductivity k in m/s at different bulk
           densities of Na bentonite

ρ_m t/m³	ρ_d* t/m³	k, m/s	
		Room temp very low gradients	70°C, gradient 10^4 to 10^3
2.10	1.75	1.5×10^{-14}	1.5×10^{-13}
2.00	1.59	2×10^{-14}	2×10^{-13}
1.90	1.43	3×10^{-14}	5×10^{-13}
1.80	1.27	5×10^{-14}	8×10^{-13}
1.70	1.11	8×10^{-14}	10^{-12}

* Dry density

4.2.2.2 Swelling pressure

Characteristic values of the swelling pressure of MX-80 bentonite are given in
Table 4. For clay saturated with ocean water or weakly brackish water, the
swelling pressure is approximately the same when the bulk density exceeds about
2.0 t/m³, while at lower bulk densities the porewater chemistry is a determinant
of the swelling pressure.

Table 4.　　Swelling pressure p_s in MPa versus bulk density of
Na bentonite at room temperature

ρ_m t/m³	ρ_d t/m³	p_s, MPa 20°C	Remark
2.15	1.83	35	Weakly brackish to saline
2.10	1.75	25	"
2.05	1.67	12	"
2.00	1.59	8	"
1.95	1.51	4	"
1.80	1.27	0.5-1	Weakly brackish water
1.70	1.11	0.2-0.5	"

4.2.2.3 Rheology

The rheological properties of dense MX-80 were investigated in creep tests of clay
samples with a bulk density of 2.1 t/m³ ($\rho_d = 1.75$ t/m³). By preparing two almost
identical samples, one with the standard Forsmark water and the other with
distilled water, the influence of a moderate increase in porewater salinity-from
fresh water to brackish conditions was illustrated. The diagrams in Fig 18
illustrate the rheological properties of the sample with distilled water and from
them we conclude that the creep strain versus time approaches a pure log t
behavior for the applied load steps, which all gave shear stresses of "intermediate"
magnitude. The normal stress was equal to the swelling pressure 15.3 MPa
throughout the test. Failure occurred at a shear stress of 2.4 MPa. The diagrams
in Fig 19 show the corresponding behavior of MX-80 clay with Forsmark water at
the same bulk density. This sample had a normal pressure of 15.0 MPa, i.e. practi-

cally the same as the clay with distilled water, but failure took place at a somewhat higher shear stress, namely 2.9 MPa. The log t creep law applies well also to this version as concluded from the straight line relationship in the strain/time plot. As for the clay saturated with distilled water, the curves in the diagram displaying the strain rate as a function of time show regular ordering and a smooth shape. It is immediately seen, however, that the salter clay exhibits a lower creep rate at each comparable stress level, indicating a stronger and less deformable particle network. This is quantitatively indicated by the lower B-values of this clay for the respective stress levels (cf. Table 5).

From a microstructural point of view the higher salt content would logically yield a more aggregated pattern and therefore a higher stiffness. This would yield less viscous and more elastic and brittle behavior of the clay. The lower viscosity of the salt clay is demonstrated by the fact that the creep rate at the shear stress 1.60 MPa is less than 50 % of the fresh-water version. The values of the parameter t_0 are higher for the salter clay, which suggests more comprehensive initial microstructural reorganization at the load applications. This points, in turn, to a less significant contribution of the pore-filling clay gel to the cohesion of the salter clay, while its internal friction, generated after initial aggregate displacements, is estimated to be higher than for the electrolyte-poor clay.

It should be emphasized that the uncertainty in defining the shear strain at failure makes the evaluation of stress and strain and therefore of the creep parameters somewhat uncertain for the highest load.

The approximate stress dependence of the creep at room temperature can be quantitatively estimated by considering the relationship between τ and B. Good agreement over the larger part of the stress ranges was obtained for $B \propto \tau^{2.7}$ for the clay saturated with distilled water as well as for the salter clay. Preliminary tests with MX-80 of lower density appear to give higher t_0:s, which is logical since the microstructural reorganizing to reach "steady" creep is then more comprehensive.

The recorded axial strain of the samples was less than 3 ‰, indicating that the creep took place under practically constant volume conditions.

Table 5. Creep parameters of MX-80 clay with 2.1 t/m^3 bulk density

Clay	Shear stress τ, MPa	A*	B*	t_0 s	Remark
Distilled water (shear strength 2.4 MPa)	1.07	-13.8	3.7	1075	
	1.34	-22.7	6.7	612	
	1.60	-48.7	11.2	453	
	1.87	-111.6	22.4	468	
Forsmark water (shear strength 2.9 MPa)	1.07	-20.8	3.8	5168	
	1.60	-20.7	4.7	1615	
	2.14	-114.1	17.8	1641	
	2.41	-262.5	36.2	2492	Stress exceeding "Intermediate" range
	2.67	-	915	10500	

* The values in the table must be multiplied by 10^{-4} to yield the actual figures

4.3 GOTLAND CLAY (II)

4.3.1 Origin, composition and physical state

4.3.1.1 Origin

Samples were extracted from the bluish clay layers of the clay/siltstone sequence of the Burgsvik sandstone formation at Kättelviken, Gotland, Sweden. It was deposited in salt water in Silurian time and is assumed to consist of weathering products brought to the shallow sea by aqueous transportation. Alternatively, it may originate from bentonite deposits. The samples were taken from a previously investigated clay layer with the identification number 1012 (12). The appearance of the Kättelviken exposure is shown in Fig 20.

Earlier oedometer tests have shown that the preexisting maximum pressure caused by post-Silurian deposits or by the Pleistocene ice cover was about 10 MPa. The present overburden is only 0.1-0.15 MPa.
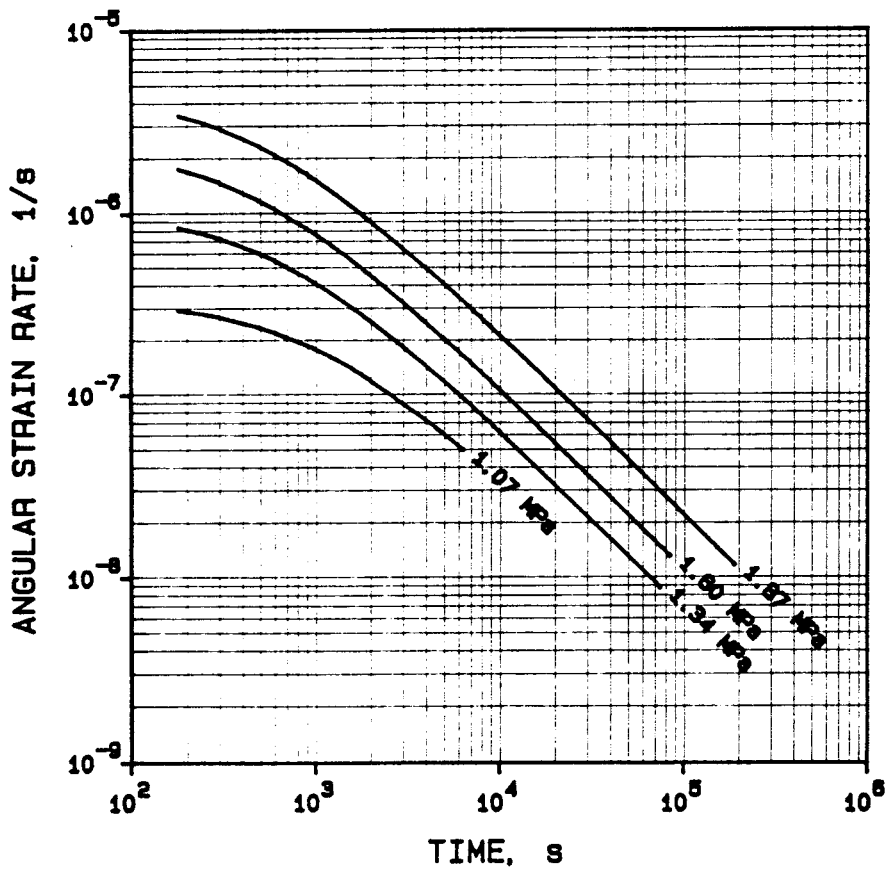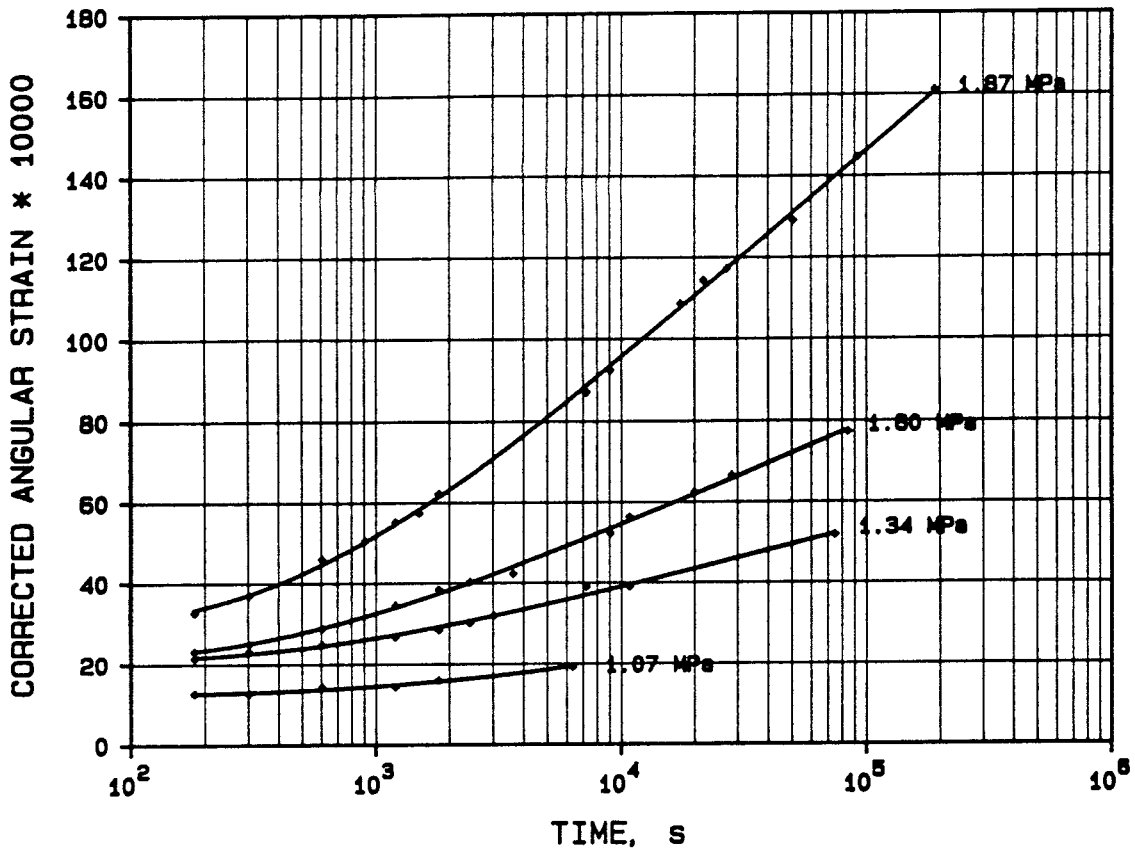
Fig 18.   Creep strain versus time (upper), and strain rate versus time
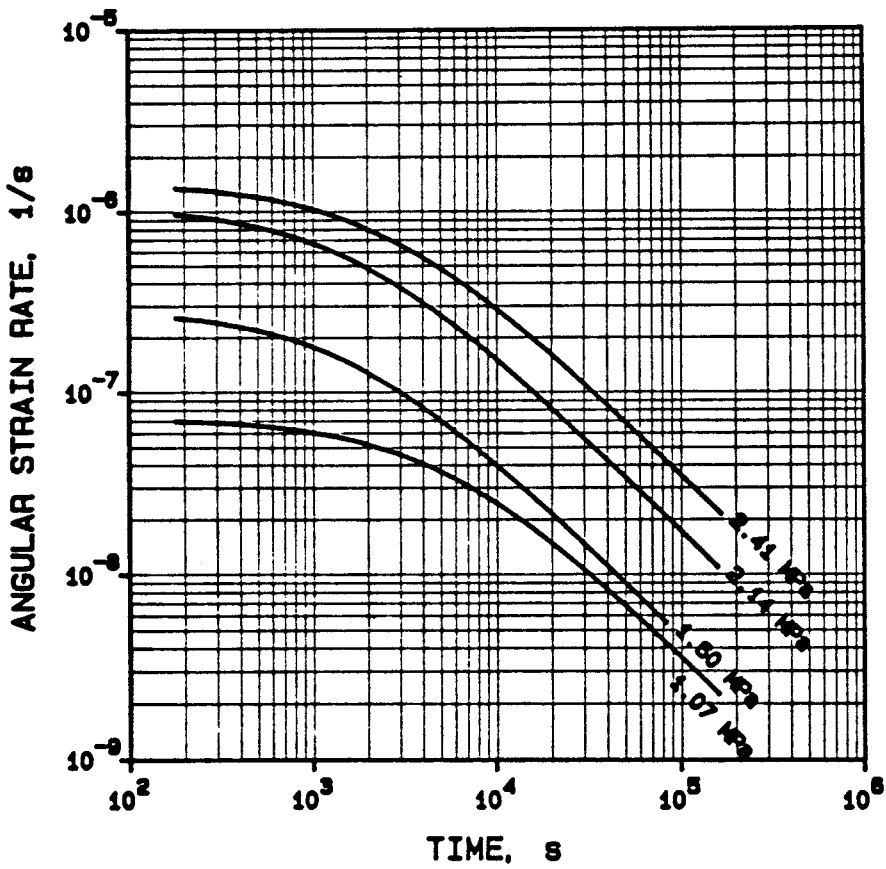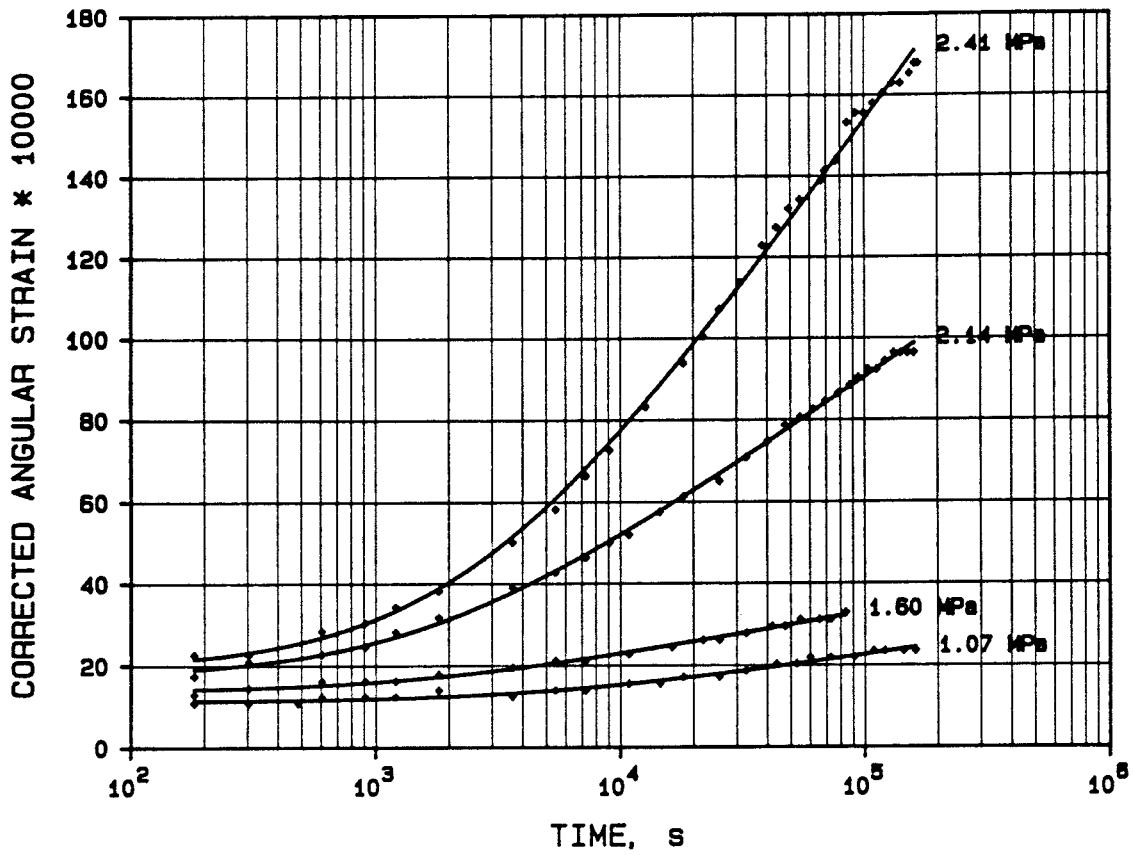(lower) of MX-80 clay saturated with distilled water

Fig 19.   Creep strain versus time (upper), and strain rate versus time
           (lower) of MX-80 clay saturated with Forsmark water
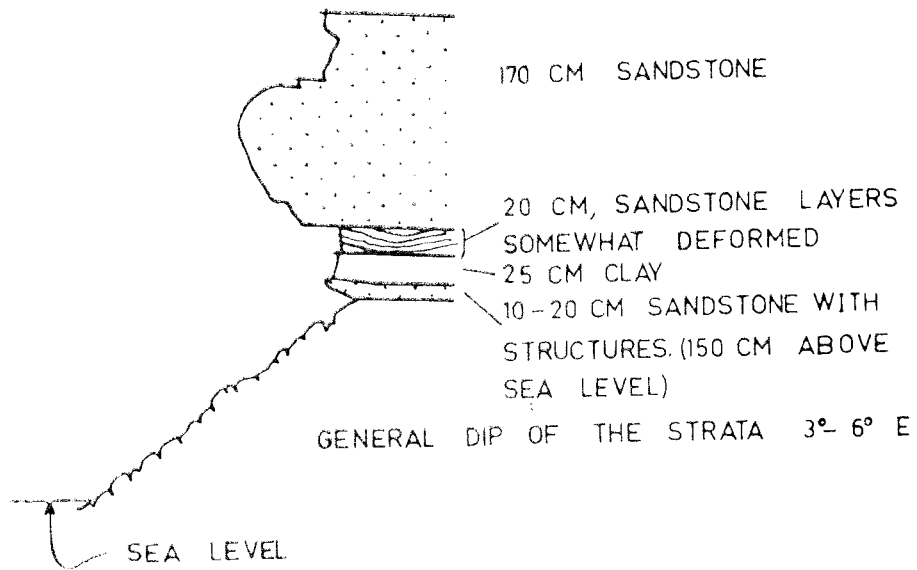
Fig 20.   View of the Silurian siltstone/clay sequence underlying a 2.5 m
sandstone covered by oolite

4.3.1.2 Composition and physical state

The clay content and bulk density were found to be 28 % and 2.11 t/m^3 ($\rho_d = 1.76$ t/m^3), respectively, while the average water content was 21 %. Chunks of this silty clay, which contains very thin calcite-cemented siltstone seams, have a plastic character and disperse rather easily when rubbed in water. Spontaneous dispersion in water is slow and incomplete, however, which indicates that the material is slightly cemented. According to earlier investigations, the microstructural pattern of the clay gel component is very open despite the heavy preconsolidation, and this may be explained by an arrangement of the silt grains so as to form a continuous self-supporting network with the clay contained in the pores (13). The typical transmission electron micrograph in Fig 21 shows significant shear strain and a high frequency of clay domains, which are typical microstructural features of heavily compacted clays. They yield a significant tortuosity of the narrow continuous pore passages and therefore a low hydraulic conductivity.

The liquid limit of the clay was found to be 44 %, which, considering the relatively high clay content, suggests that smectites are not present. This is also verified by XRD analyses indicating that the clay fraction has the following approximate composition: Illite (40 %), quartz (20 %), chlorite (15 %), calcite (10 %) and feldspars (10 %), (cf. Fig 22). The silt and sand fractions mainly consist of quartz and mica minerals with calcite and feldspars as accessory minerals. Volcanic glass has not been detected but some quartz grains are found to be very angular, which may suggest a bentonite origin of the clay material.

The main soil physical data of the clay are given in Table 6. It shows two sets of values, referring to the initial undisturbed condition as well as to a remolded, reconsolidated state. By conducting percolation and swelling tests on both types it was assumed that the influence on these physical properties of natural microstructural features, like particle orientation and non-uniform clay distribution, would be revealed.

4.3.2 Physical properties

4.3.2.1 Hydraulic conductivity

The average hydraulic conductivity of the undisturbed sample was found to be 1.5×10^{-11} m/s in tests where the percolation was perpendicular to the plane of

Fig 21.   TEM micrograph of ultramicrotomed Silurian clay from Gotland.
          The arrow indicates the statistically certified general particle
          orientation
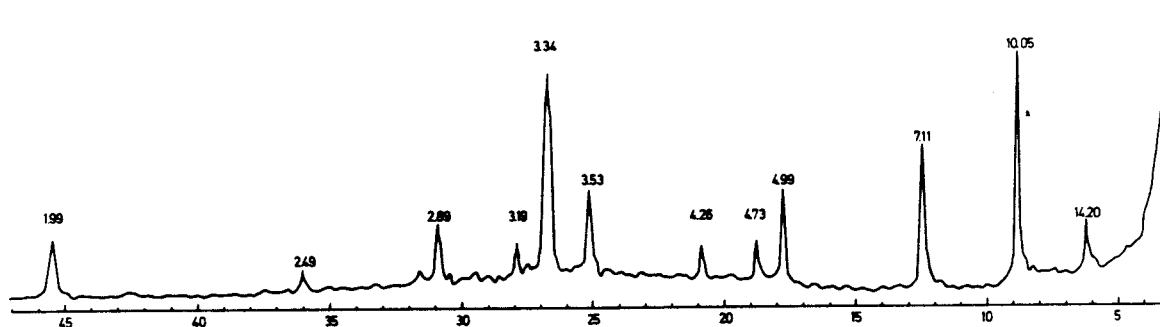
Fig 22. XRD diagram of the clay fraction of Silurian clay from Gotland

Table 6. Main data of the Silurian clay from Gotland

Condition	Bulk density t/m3	Dry density t/m3	Water content %	Remark
Undisturbed	2.11	1.76	21	-
Remolded	2.20	1.91	15	Reconsolidated

particle orientation. The tests had a duration of about 1 week, with gradients ranging from 10^2 to 10^3.

A remolded, homogenized sample was prepared from undisturbed clay material by drying and light grinding, with subsequent compaction of the soil powder in the oedometer to a density that was intended to be the same as that of the undisturbed sample. It was then saturated with Forsmark water and percolated as in the case of the undisturbed clay. The hydraulic conductivity of the remolded clay was found to be higher by about one order of magnitude, i.e. to 1.6×10^{-10} m/s, despite the slightly higher bulk density, the difference probably being due to a better microstructural continuity and higher tortuosity of the undisturbed clay. An additional reason for the higher permeability of the remolded clay is the inability of the illite/chlorite clay gel to expand and fill up voids between clay and silt aggregates. Such void filling is known to be significant when the clay minerals consist of smectite (cf. Fig 17).

4.3.2.2   Swelling pressure

The swelling pressure of the undisturbed sample was found to be 0.5 MPa, while almost no pressure could be recorded when the remolded material was tested. While the applied technique of determining the swelling pressure is suitable for non-cemented smectite clays it may not yield totally relevant values of slightly cemented, undisturbed clays of the presently discussed type. The reason for this is that the swelling pressure due to the physico/chemical expansion potential is counteracted by the cementing bonds which at least partly prevent the expansion. Thus, the slight compression that is involved in the standard pressure recording procedure may yield a pressure value which mainly relates to the compression resistance of the stiff, cemented soil. The evaluated swelling pressure of the undisturbed Silurian sample is therefore not very reliable, as demonstrated also by the fact that the equally dense remolded sample, in which numerous cementation bonds must have been broken in the preparation stage, exhibited practically no swelling pressure at all.

4.3.2.3   Rheology

Three types of tests were performed using Forsmark water and differently prepared clay materials. The main investigation concerned undisturbed clay that was sheared parallel to the bedding plane, the shear movement being arrested when large strain had developed preceding failure. The second study involved continued loading after a period of relaxation, which was assumed to yield a change in creep behavior due to changes in the energy barrier spectrum. The third study concerned a remolded, homogenized and reconsolidated material obtained in the same way as the sample used for the conductivity testing. The intention was to check whether the creep behavior of the disintegrated material, with no cementing bonds left, was different from that of the virgin clay.

The diagrams in Fig 23 show the character of the rheological properties of the undisturbed, natural sample, the shearing taking place at a normal pressure of 120 kPa, which is the overburden pressure in nature. It is observed that the plotting of creep strain versus time verifies that the creep is of the log t type for all the load steps. The upward concave shape of the initial part of the creep curves for the three intermediate stress levels in the lower diagram illustrates the aforementioned typical feature of fast retardation of the creep strain of cemented soils. We see from Table 7 that this shape is characterized by negative t_0 values. The

different curve shape for the highest load, yielding a high positive t_o value, suggests that the large majority of the cementing bonds had been broken and that much microstructural reorganization took place before the creep rate finally began to retard. The first load step in Test phase I probably gave inconsistent values due to an initially slightly incomplete sample/box contact.

Table 7. Creep parameters of Gotland clay with 2.1 t/m³ bulk density

Test phase	Clay	τ, kPa	A*	B*	t_o
I	Undisturbed	29	2.1	2.5	131
	$\rho = 2.11$ t/m³	45	29.9	2.8	-100
		61	87.9	2.8	-33
		76	24.7	16.1	-107
		92	-4507	459.1	24464
II	Continued test after	29	-71.8	6.7	152660
	1 week relaxation	61	13.1	1.5	232
	under constant	76	32.1	6.0	5980
	normal pressure	92	2.8	3.6	1
		111	-61.8	15.9	211

* The values in the table must be multiplied by 10^{-4} to yield the actual figures

Fig 24, which refers to the second test phase after 1 week of relaxation, demonstrates that the log t creep law was approximately valid also in this state, supporting the assumption that this law has a very wide applicability. We conclude from the very small strain at all stress levels, except the highest one, that the preceding stress/ strain history and the relaxation period has yielded a strong over-consolidation effect. This is in agreement with Pusch & Feltham's stochastic creep model according to which a successive shift towards higher energy barriers takes place in the course of the creep at low and moderate shear stresses. Macroscopic failure was obtained when the shear stress was finally increased to 127 kPa.

The third test phase, in which the remolded and reconsolidated material was tested, gave completely different results. At loading, the creep, which initially obeyed the log t law, was insignificant for the first half hour but it then increased rapidly, the increase being associated with a compression of about 60 µm. Retardation occurred after about one hour, following the log t creep law (Fig 25). The sample failed at a shear stress of 75 kPa, i.e. considerably less than the shear strength of the virgin clay which had a lower density. This supports the conclusion that cementation contributed to the shear resistance of the virgin clay.

From the sets of B-values in the first two test phases it is possible to estimate the approximate stress dependence of the creep. For the virgin clay state in the first phase we find that τ and B are related as given by the expression $B \propto \tau^{1.8}$ up to 76 kPa, thus showing less stress-dependence than the MX-80 clay. This load step caused a considerable increase in strain rate and thus a higher stress exponent, probably because of comprehensive breakage of cementing bonds. For the pre-stressed, relaxed specimen there is no obvious relationship between stress and strain, except for the logical increase in strain at the highest load.

The recorded axial strain of the samples in phases I and II was less than 20 µm, i.e. 1 ‰, indicating that the creep took place under constant volume conditons.
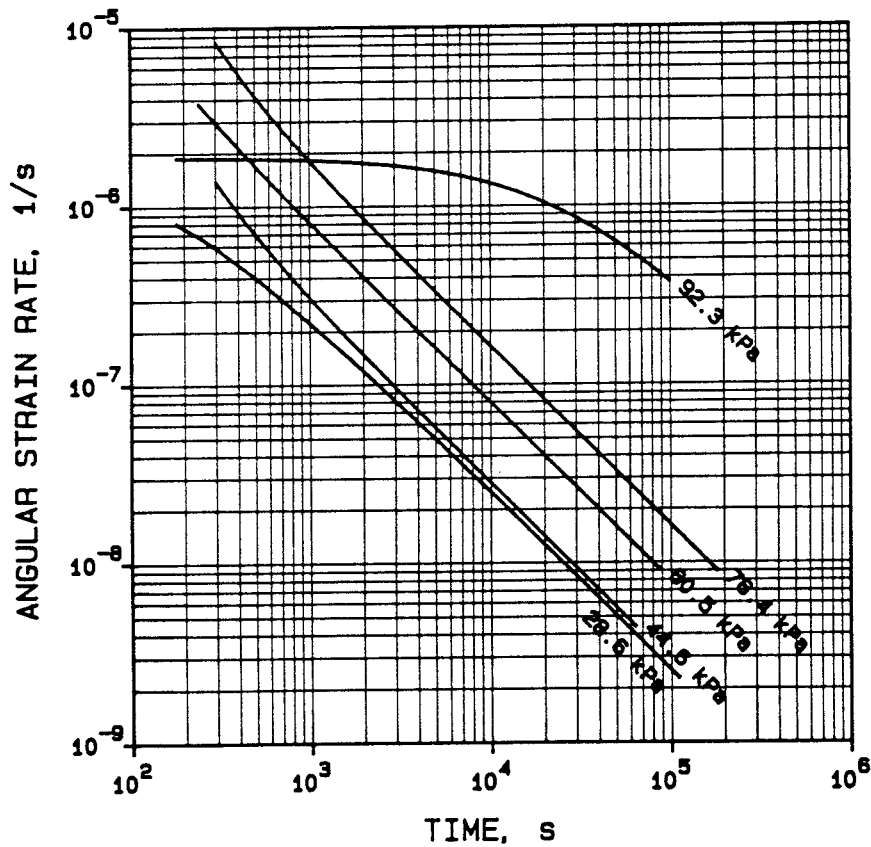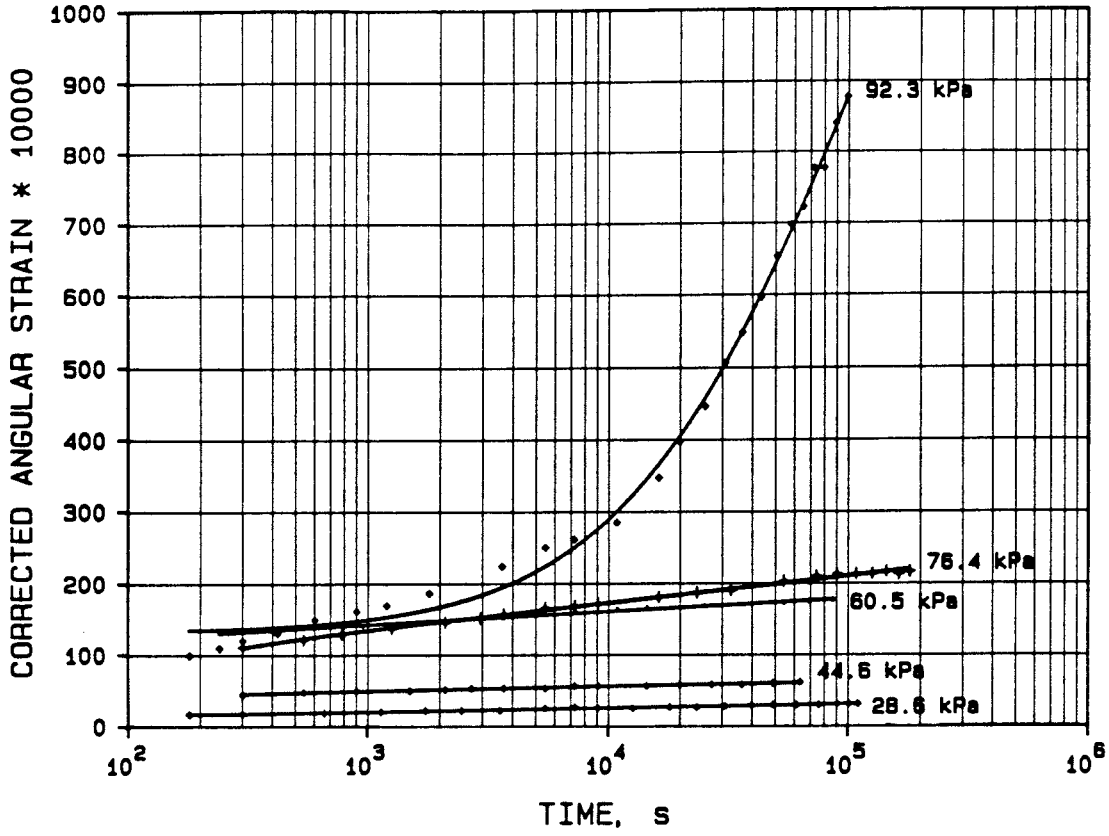
Fig 23.   Creep strain versus time (upper), and strain rate versus time
(lower) of the undisturbed Gotland clay (II)
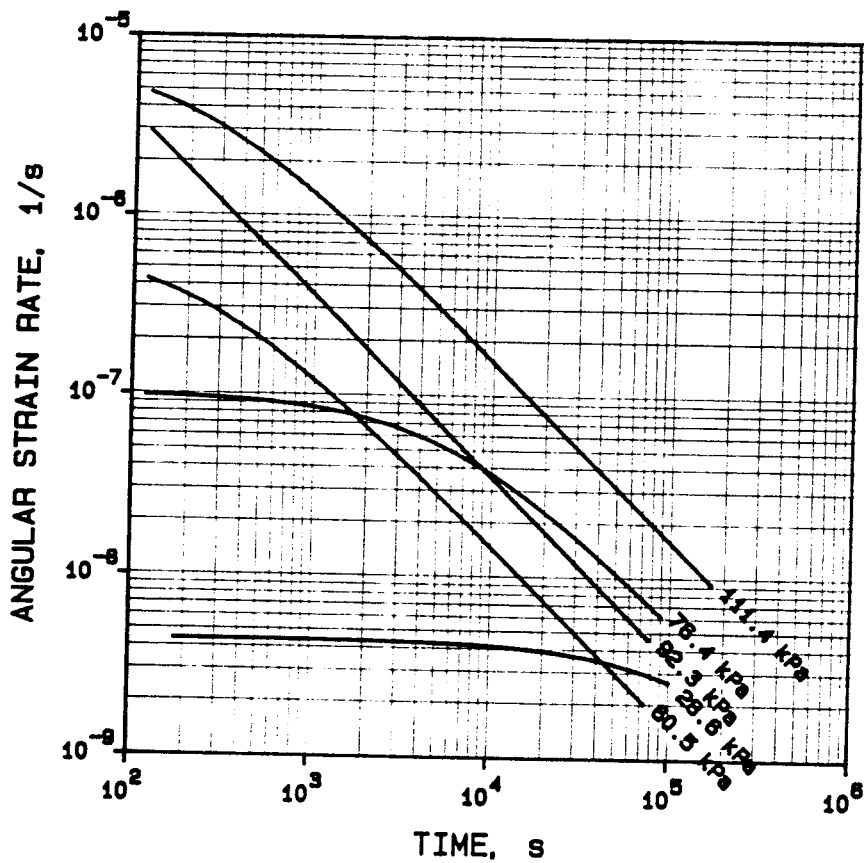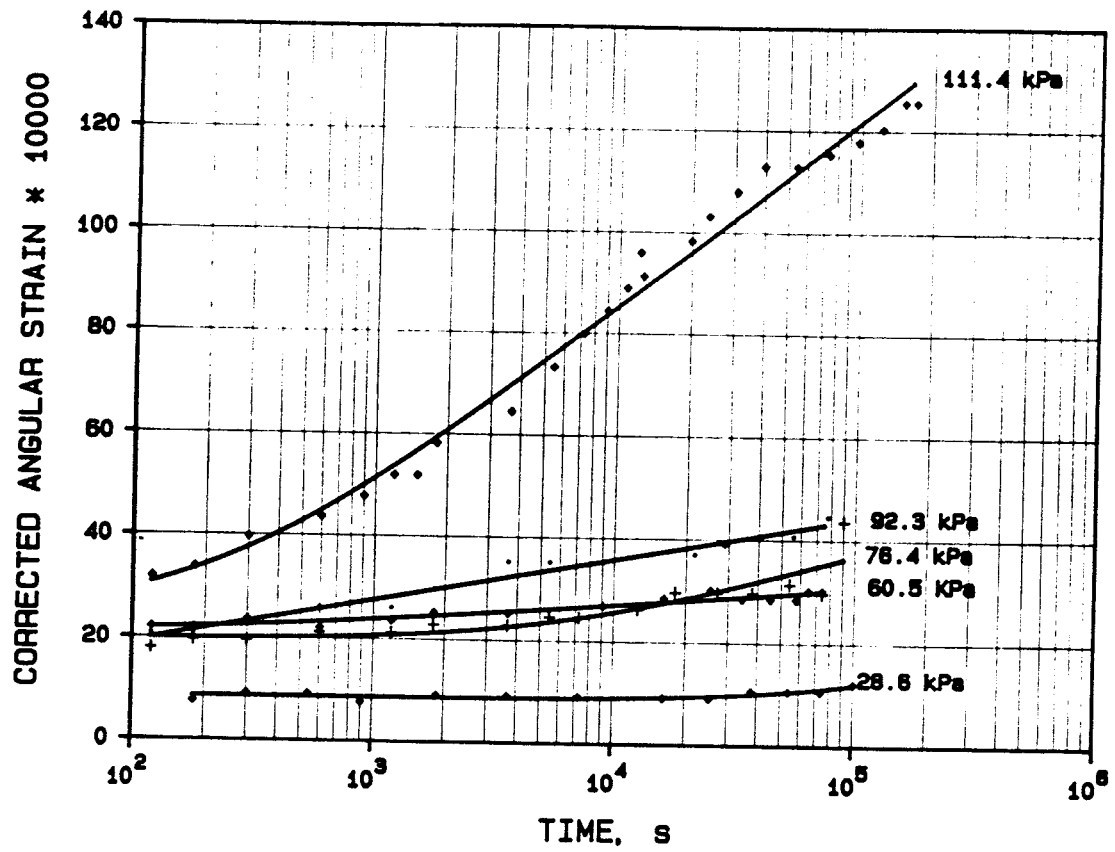
Fig 24.   Creep strain versus time (upper), and strain rate versus time
(lower) of the prestressed and relaxed Gotland clay (II)

CLAY : GOTLAND DISP   ANGLE : 19.8 DEGR   Date of test: 06/02/1987
STEP NUMBER : 2   SAMPLE TEMP : 20 DEGR C
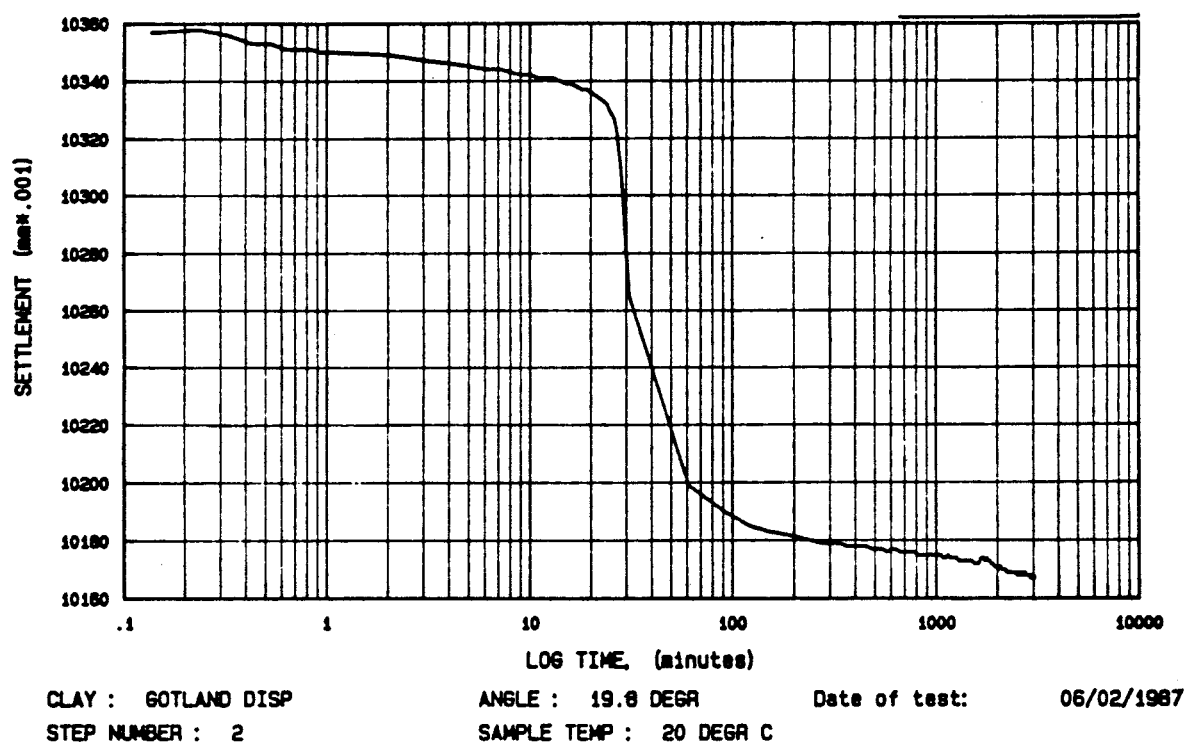
Fig 25.   Typical creep behavior of dispersed, reconsolidated Gotland clay.
           Shear stress 45 kPa, normal pressure 120 kPa

4.4   KINNEKULLE CLAYS (III and IV)

4.4.1   Origin, composition and physical state

4.4.1.1   Origin

The Ordovician bentonite at Kinnekulle has been extensively investigated, i.a. in
conjunction with the current SKB and NAGRA research. The 2 m thick bed from
which samples were taken is a member of a sequence of limestone, shaly mud-
stone and bentonite strata, which is overlain by mudstones, graptolithic shales
and basalt (Fig 26). Conodont analyses and back-calculation of the heat flow
caused by the intrusion of basalt in post-Ordovician time suggest that the bento-
nite has been exposed to a temperature of 110-160°C for about 1000 years (7). The
previous maximum overburden due to possible Devonian sediments, and to the
Pleistocene ice-sheet, caused a preconsolidation pressure of at least 20 MPa. The
present overburden is only about 100 kPa.

4.4.1.2   Composition

The main bentonite bed has a clay content of 35-40 %. Careful analyses of the mineral composition and element distribution have shown that montmorillonite, illite and mixed layer minerals are dominant. The upper part of the main bentonite bed has been found to be richer in illite than the central part (7, 13) and this has been ascribed to heat-induced beidellitization of the montmorillonite and thermally aided diffusion of dissolved potassium from overlying shales. The present investigation concerned a relatively montmorillonite-rich sample termed III from the central part of the bed (K8), and a less montmorillonitic sample, IV, from its upper part (K12). Montmorillonite, illite, and mixed layer minerals were found to form about 45 % of the clay fraction in sample K12 and 60 % in sample K8, accessory minerals being micas (15 and 5 %, respectively), quartz (10 %), and feldspars (10 %). In sample K12, chlorite (10 %) and kaolinite (5 %) were also present, indicating a difference in source material of the upper and central part of the main bed. Using recent literature data (14) the illite/smectite (I/S) ratio is about 0.65 for sample K8 and about 0.45 for the one termed K12. On these grounds the fraction of smectitic components of the <u>total</u> solid mass can be estimated at about 25 % for sample K8 and 15 % for sample K 12.

Representative XRD diagrams are shown in Fig 27. While the upper boundary zone as well as adjacent thinner layers show a high background/wide-peak pattern indicating substantial biotite/chlorite/ mixed-layer representation, samples from the central part of the main bed exhibit a more uniform composition characterized by 10 Å and 14.7-15.5 Å reflections at air-drying, and a 17.1-17.9 Å range on glycolation. This suggests that Ca is the dominant adsorbed cation in the larger part of the thick bed (11). Considering the fact that montmorillonite formed only 15-25 % of the total mineral content, the Atterberg liquid limit, which was found to be approximately constant throughout the entire bed and averaged at 75 %, is surprisingly high. It suggests that sodium forms a significant part of the adsorbed cations [cf. (10)].

4.4.1.3   Physical state

Significant resistance to dispersion of the bentonite has been reported in the literature (7, 14, 15). It is most certainly attributed to slight cementation, probably by precipitation of heat-released silica, as concluded from a comprehensive microstructural investigation that showed very small nodules at the edges of

Position of samples	Litho-Strati-graphic Symbols	Litho-Stratigraphic Description
		Soil
		Debris
	≡	Grey, reddish clay shale
	≡	Grey limestone
	≡	Grey shale, clay intercalations
	≡	Grey limestone, clay intercalations
		Clay
		Grey limestone
5.50 (K13)		Clay
5.70 (K12)	≡ ≡	Dark-grey shale
5.90 (K11)		
6.10 (K10)		
6.45 (K9)		
6.65 (K8)		
6.85 (K7)		
7.10 (K6)		
Contact 7.30 (K5)		
clay/limest 7.36 (K4)		Grey limestone
7.95 (K3)		Clay Grey limestone
8.30 (K2)		Clay
		Grey limestone
9.20 (K1)		Clay
		Grey limestone

Stratigraphic Columnar Section, RP 1
(standard Legend Royal Dutch Shell group
of companies).
Figures in front of sample code denote
depth in meter below ground surface.

Fig 26. Core profile at the Mossen bentonite quarry

dense stacks of montmorillonite flakes. Calcite precipitation, which forms macroscopic fillings of fissures and continuous pores, may also contribute to the cementation effect, which is expected to yield brittle properties in addition to the slaking resistance. Macroscopically, the bentonite has a shaly character, indicating a preferred particle orientation, which is also verified by the representative micrographs in Fig 28.
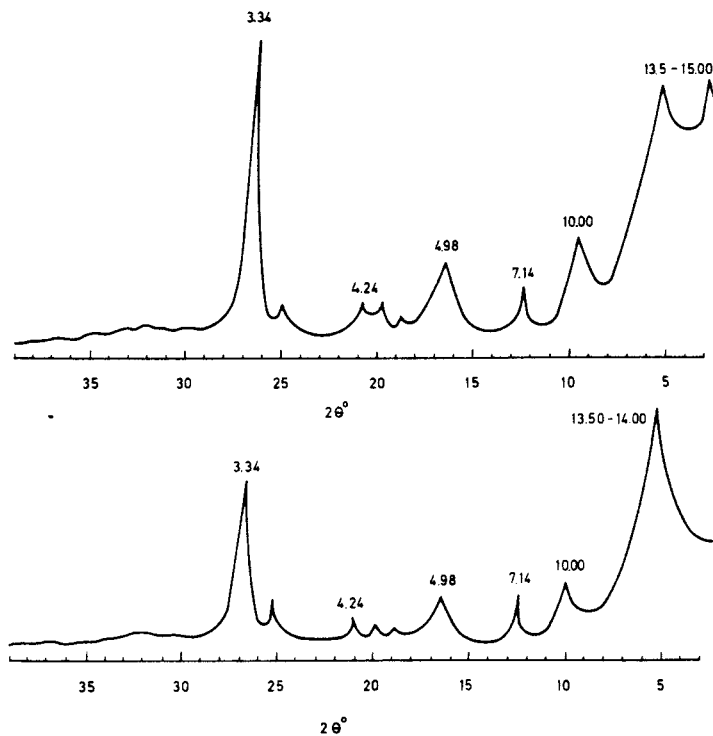
Fig 27. XRD diagrams of sample from the upper part of the main bentonite bed at Mössen, Kinnekulle (upper diagram) and of the central part after (14)

General soil physical data of the investigated clay are compiled in Table 8. The undisturbed samples were compressed (K8) or expanded (K12) from a dense state, the testing being made after about one week of rest to reach equilibrium. The samples had dried somewhat from their original state, the typical natural water content of the bentonite bed being in the range of 27-35 % for the smectite-rich part, and 22-23 % for the more illitic, upper part. Experience shows that a smectite-rich clay consolidated under a pressure to which the Kinnekulle series is likely to have been subjected, reaches equilibrium at a water content of 20 % at maximum. The higher present content demonstrates that the clay has absorbed groundwater and swelled to reach equilibrium with the overburden pressure 100 kPa.

Table 8. Main data of the clays from Mossen, Kinnekulle

Clay type	Condition	Bulk density t/m³	Dry density t/m³	Water content %
III (K8)	Undisturbed	2.05	1.66	23
	Compressed by 1 mm	2.09	1.74	19
	Compressed by 2 mm	2.15	1.83	16
IV (K12)	Undisturbed	2.25	1.98	13
	Expanded by 1 mm	2.17	1.85	16
	Expanded by 2 mm	2.10	1.75	19

4.4.2   Physical properties

4.4.2.1   Hydraulic conductivity

The hydraulic conductivity of the bentonite samples is given in Table 9 as a function of density. Percolation took place perpendicular to the general stratification for about 1 week under a hydraulic gradient of 10^2 to 10^3.

We find from Table 9 that the conductivity of the sample that was richer in illite was 40-50 times more permeable than the equally dense, more smectitic one. This difference is explained by the fact that the permeability is largely controlled by the tendency of clays to disperse and form aggregates, the most surface-active mineral montmorillonite forming the most homogeneous and least pervious particle system.

4.4.2.2   Swelling pressure

The swelling pressure of the bentonite samples is given in Table 10 as a function of density, the pressure being recorded perpendicular to the general stratification. As in the case of the conductivity testing we find a clear difference between the two samples, the pressures being significantly higher for the more smectite-rich clay. We see that the swelling pressure of the undisturbed montmorillonite-rich
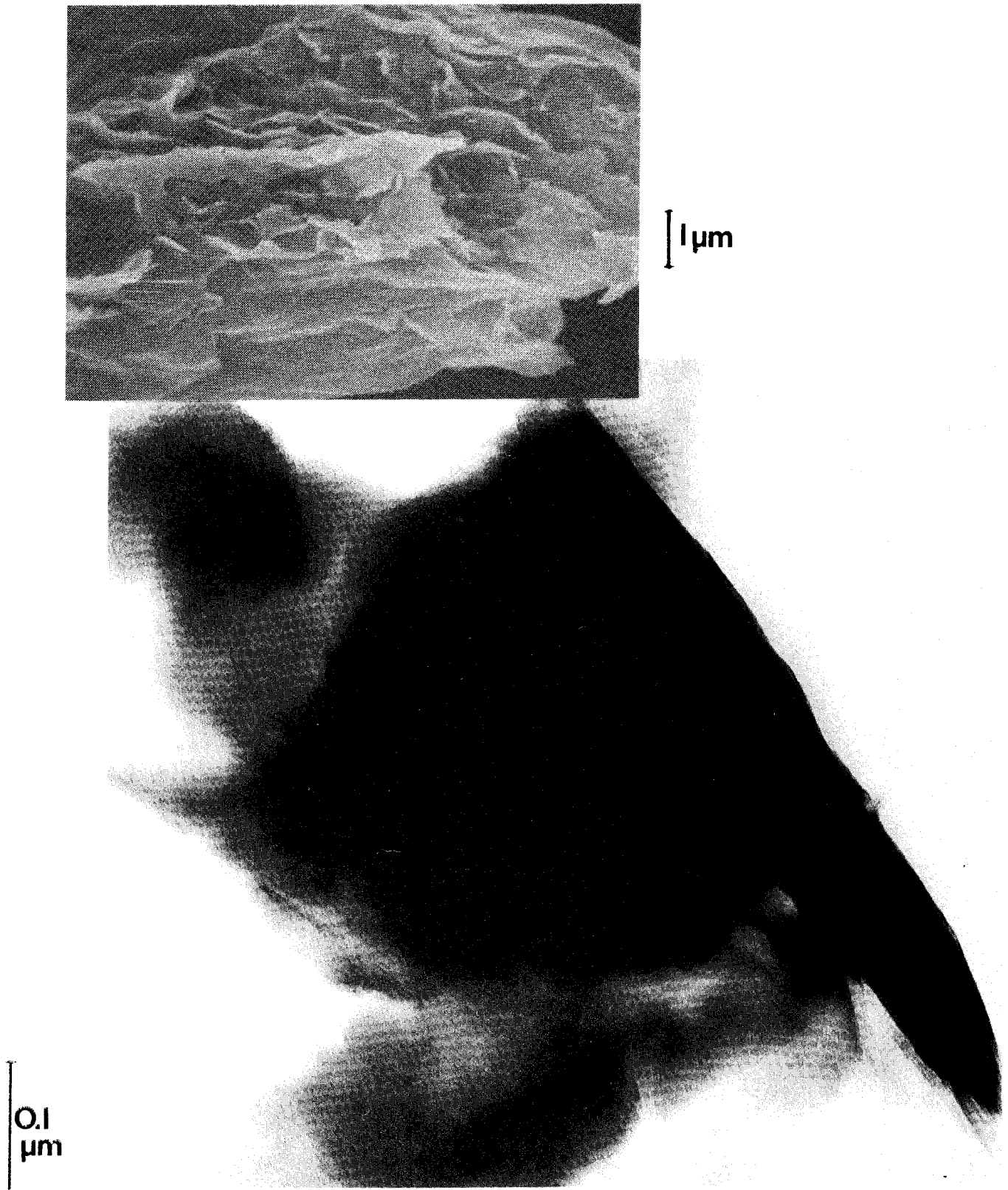
Fig 28.   Characteristic micrographs of the Kinnekulle bentonite. Upper:
           typical SEM micrograph of the main bed showing a clear tendency of
           particle orientation. Lower: TEM micrograph of ultramicrotomed
           sample showing an unexpanded dense, stack of flakes to the right
           associated with expanded aggregates

Table 9. Hydraulic conductivity of the Kinnekulle bentonite samples

Clay type	Condition	Bulk density t/m3	Dry density t/m3	Water content t/m3	Hydraulic cond m/s
III (K8)	Undisturbed	2.05	1.67	23	5×10^{-13}
	Compressed	2.09	1.73	19	10^{-13}
	Compressed	2.15	1.83	16	10^{-13}
IV (K12)	Undisturbed	2.25	1.98	13	3×10^{-12}
	Expanded	2.17	1.86	16	4×10^{-12}
	Expanded	2.10	1.75	19	5×10^{-12}

sample is substantially higher than the overburden pressure, which is at least
partly explained by the fact that the samples had dried somewhat. This had
caused some consolidation and increase in dry density and therefore higher
swelling pressures than those acting in nature. As illustrated by the creep tests
and the aforementioned lack of spontaneous dispersion in water of natural speci-
mens, it is probable that cementation also resisted expansion in the natural beds.
Cementation is also assumed to have affected the recorded swelling pressures in
the same way as for the Silurian clay (cf. Chapter 4.3.2.2) and especially the
values of Sample K12, i.e. the least smectitic one, are strongly overrated.

4.4.2.3 Rheology

Fig 29 shows the general character of the rheological behavior of the most smec-
titic bentonite sample from the central part of the thick bed. The upper diagram
shows that log t-type creep characterized all the curves except for that of the
highest load. We see that discontinuous, rather large strain was developed at the
second load step, yielding the shear stress 64.5 kPa, and this can be explained by
microstructural breakdown in the form of fractured cementation bonds. The fact
that the material sustained this and a few additional loads without fully develop-
ed macroscopic failure indicates that only part of the strength-producing compo-
nents had been mobilized. Thus, it is probable that the strain at higher stresses

Table 10. Swelling pressures of the Kinnekulle bentonite samples

Clay type	Condition	Bulk density t/m³	Dry density t/m³	Water content t/m3	Swelling pressure MPa
III (K8)	Undisturbed	2.05	1.67	23	3.8
	Compressed	2.09	1.73	19	15.0
	Compressed	2.15	1.83	16	43.0
IV (K12)	Undisturbed	2.25	1.98	13	26.0
	Expanded	2.17	1.86	16	14.5
	Expanded	2.10	1.75	19	3.8

caused mechanical breakdown of cemented clay aggregates by which montmorillonite flakes and stacks of flakes were released and set free to expand and create new bonds in a "self-healing" process.

The tests, which were conducted at a normal pressure of 300 kPa using a sample that had been consolidated under this pressure for several weeks, gave a shear strength value of 100 kPa. The bulk density of the sample was 1.85 t/m³.

The creep parameters are given in Table 11. We see from the lower diagram in Fig 29 that the second load application gave large immediate displacement and a negative t_0-value indicating that cementation bonds initially governed the creep behavior. Higher loads again gave jerky creep and positive t_0:s increasing with the applied stress, which suggests that the cementation had been broken down.

The influence of shear stresses on the creep can be roughly interpreted from the relationship between τ and B. We find that for the four first load steps, $B \propto \tau^{3.2}$, which indicates a stronger stress-dependence than of the previously discussed clays.

A total compressive strain of about 70 µm, i.e. 3.5 ‰, took place at loading up to = 56 kPa, while an additional compression by about 6 ‰ occurred in the higher

Table 11. Creep parameters of Kinnekulle clay (K8)

Shear stress τ,kPa	A*	B*	t_0 s
56	-2.1	2.8	654
65	116	5.8	-154
79	-22	5.4	112
87	-67	11.6	2118
95	-8936	657	869000

* The values in the table must be multiplied by 10^{-4} to yield the actual figures

load test series. It is concluded that the creep took place under almost constant volume conditions at the individual load steps.
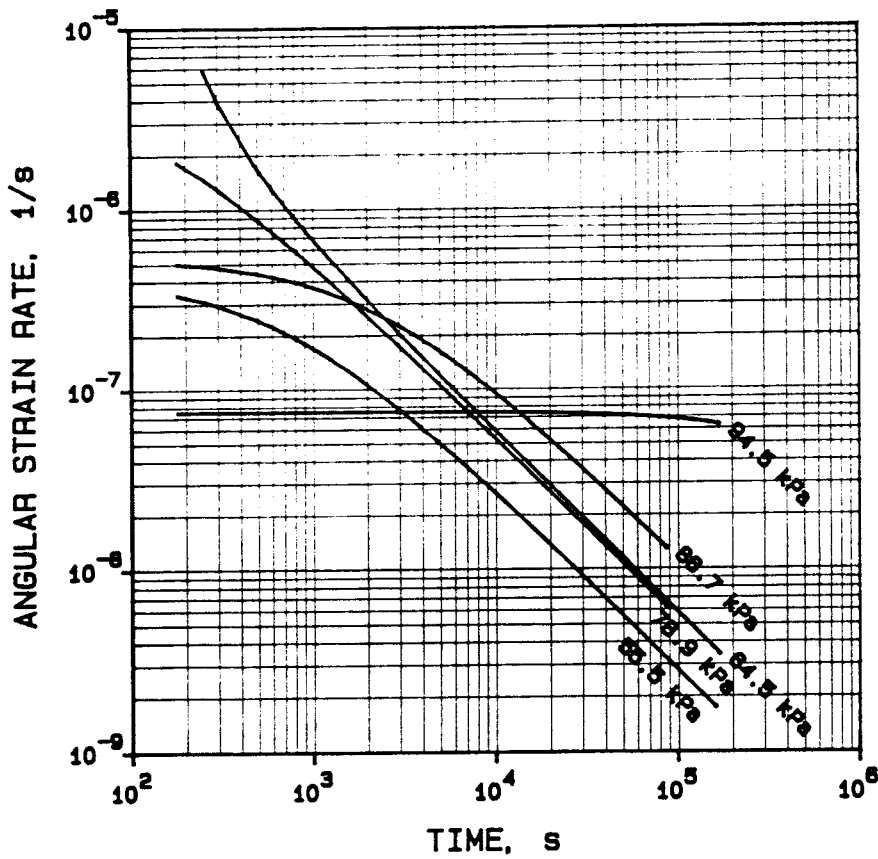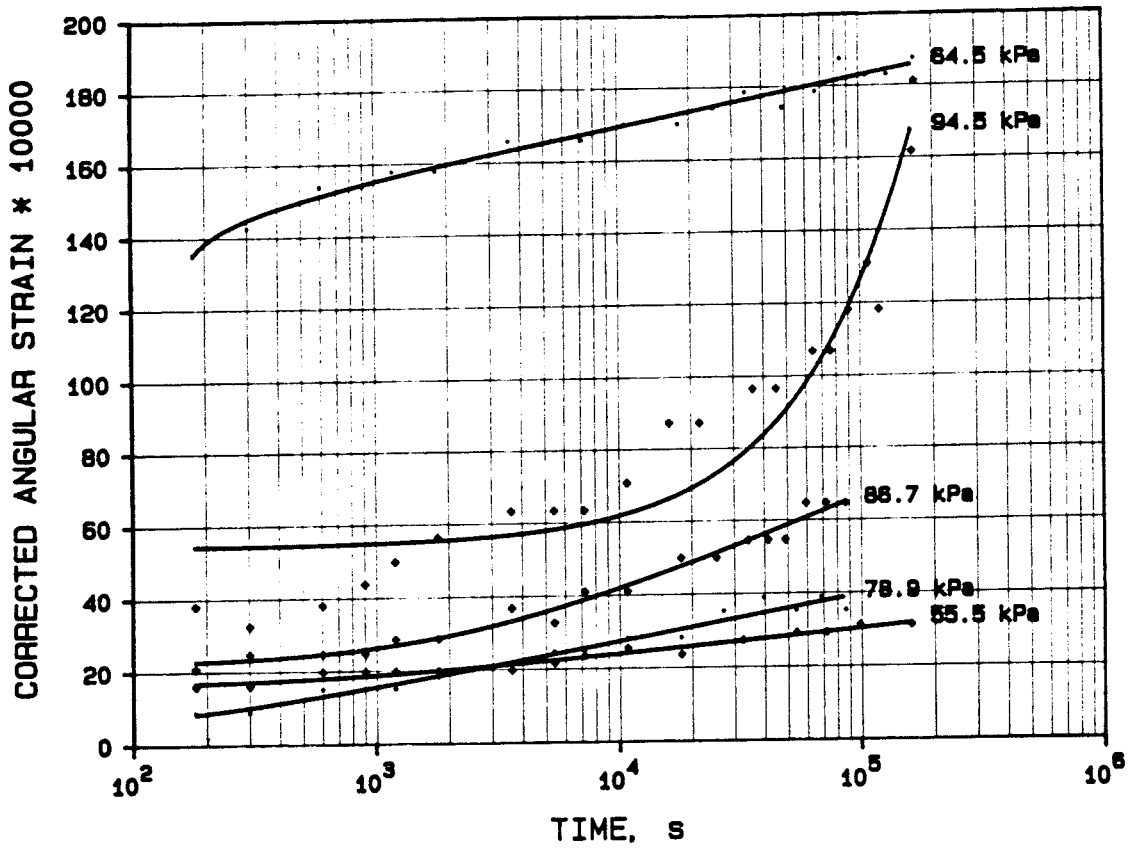
Fig 29.   Creep strain versus time (upper), and strain rate versus time (lower)
of the Kinnekulle clay (IV)

4.5   BOOM CLAY (V)

4.5.1   Origin, composition and physical state

4.5.1.1   Origin

The sedimentary Boom clay series, which was formed in late Cretaceous and early
Tertiary time, represents a homogeneous facies. It is approximately horizontally
layered and lacks tectonic dislocations or significant variations in composition. At
the Mol site it is overlain by about 100 m sandy sediments.

The source material was weathered rock of various origin from which silt/clay
detritus was river-transported to the large trough that extended in NW/SE
direction from the North Sea to Liege. The vertical preconsolidation pressure of
the presumably normally consolidated samples that were used in this study, was
about 2.7 MPa.

4.5.1.2   Composition

The material exposed at the front of the short test drift at 200 m depth at Mol
appeared as a homogeneous, very dense grey mass when the senior author visited
the site in early 1985. Undisturbed samples from this area were subsequently
taken by CEN and kindly put to our disposal. It was assumed that the mode of
formation and the compaction that the sediment must have experienced under the
heavy overburden, had caused stratification and strong anisotropy that needed to
be considered in the selection of samples for testing. The laboratory study there-
fore started with a general textural analysis based on optical microscopy.

The clay content of representative 100 g samples was found to be about 55 %
according to hydrometer analyses. Since the Atterberg liquid limit was found to
be about 60 % it was assumed that the clay contains a certain but not very high
amount of smectitic minerals and this was also verified by the XRD diffracto-
metry (Fig 30). Air-dry specimens were found to yield a broad but very strong
reflection at about 14 Å, which was displaced to 17.3 Å on ethylene glycol treat-
ment, indicating that Na is the major adsorbed cation. The quantitative mineral
composition is estimated to be as follows: mixed-layer minerals (35 %), illite (30
%), kaolinite (25 %), quartz (5 %). Smectites are estimated to form about 10 % of
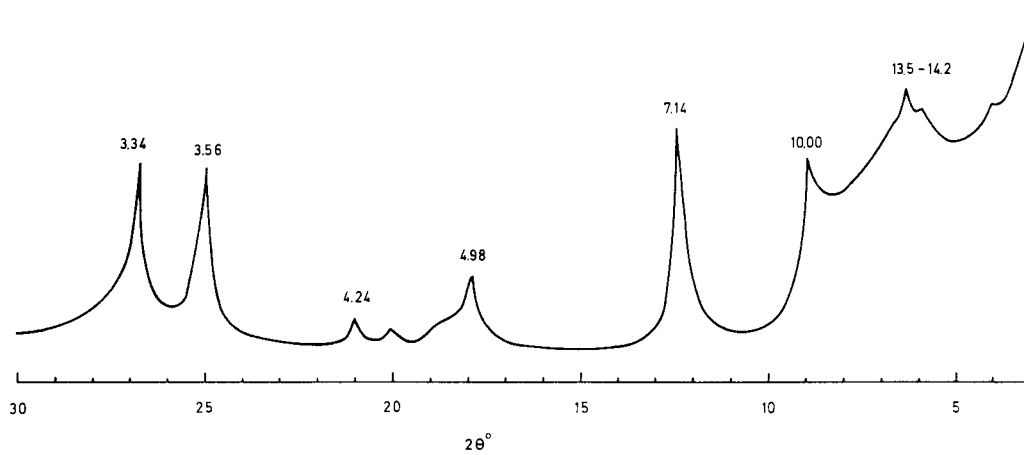the total solid mass.

Fig 30. XRD diagram of the clay fraction of Boom clay

4.5.1.3   Physical state

Samples of Boom clay from 200 m depth have a bulk density of 2.05 t/m^3 (dry density 1.60 t/m^3) and a water content of about 25 %. The general structural character of the Boom clay was investigated in a separate study in order to get a view of the distribution of minerals, clay-sized particles and other features of importance for the selection of relevant samples and for the interpretation of the test results. For this purpose arbitrarily taken samples were soaked with and embedded in acrylate plastic after replacement of the porewater by ethyl alcohol treatment. 30 µm sections were prepared and series of overlapping micrographs taken over a length of about 1 mm, the inspection and photographing being made in polarized light perpendicularly to the bedding plane. This study clearly demonstrated that the clay is very heterogeneous, with thin seams and lenses of fine silt (Fig 31).

Electron microscopy of ultramicrotomed, acrylate-embedded samples clearly showed the very dense microstructural character of clay-rich portions. As demonstrated by Figs 32 and 33, shear stresses induced by the strong compression in the course of consolidation in nature produced the typical domain features that were also typical of the Silurian clay from Gotland. Fig 32 clearly demonstrates the preferred, horizontal orientation of the majority of the particles. No crystalline or amorphous precipitates can be seen, which suggests that the material is not strongly cemented and therefore not brittle. The impression from ocular inspec-
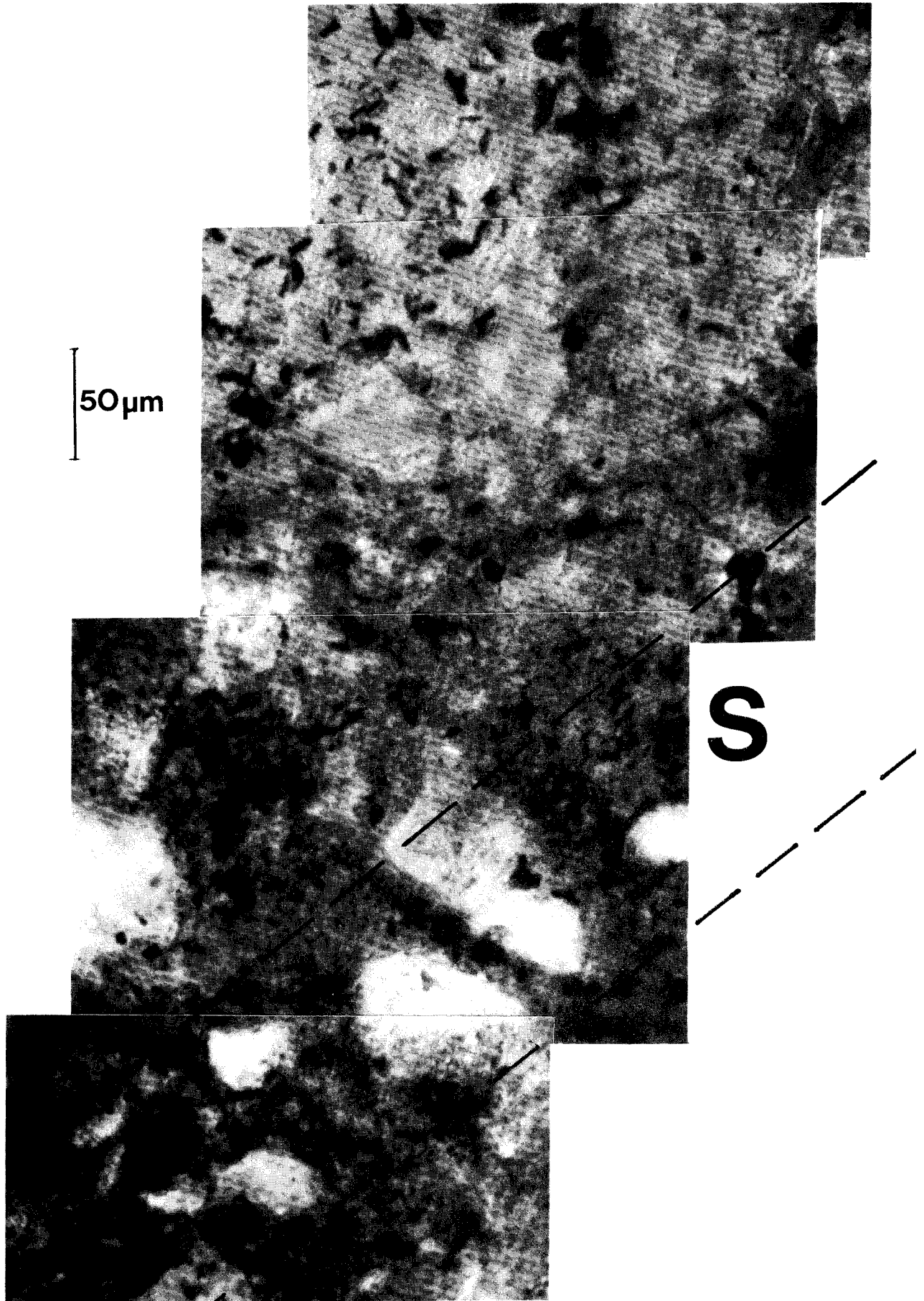
Fig 31. Set of overlapping optical micrographs of 30 μm section of acrylate-embedded Boom clay showing typical variatins in compositions. S-zone denotes silt layer

tion of the test drift at 200 m depth also indicated a tough and cohesive behavior of the clay in the development of large creep strain under high shear stresses that took place at that stage.

The samples tested with respect to perviousness, swelling properties and rheological behavior, were kept in N_2 environment and thus effectively isolated from oxidation until testing took place.

4.5.2 Physical properties

4.5.2.1 Hydraulic conductivity

Typical values of the hydraulic conductivity obtained in laboratory tests with percolation perpendicular to the bedding plane are in the range of 7×10^{-12} - 5×10^{-11} m/s, averaging at 10^{-11} m/s.

4.5.2.2 Swelling pressure

The swelling pressure of Boom clay was expected to be lower than that of the Kinnekulle clays but significant higher than the very low value of the smectite-free Gotland clay. It turned out, however, that the Boom clay only gave a swelling pressure of 500 kPa, i.e. the same value as the Gotland clay despite its considerable content of expanding clay minerals. It is concluded that the low pressure was due to the heterogeneous microstructure with non-uniform distribution of the smectite component.

4.5.2.3 Rheology

The creep tests, which were conducted under an effective normal pressure of 2.7 MPa, yielded the relationships in Fig 34 log t-type creep took place at the lowest load while the creep behavior at higher loads was slightly irregular, suggesting considerable microstructural distortion and particle damage. Failure took place at a shear stress of 930 kPa. We see from the lower diagram that the initial part of all three curves have an upward convex shape, indicating that cementation is insignificant. The evaluated creep parameters gave the set of values that is given in Table 12.

Fig 32.   TEM micrograph of ultramicrotomed Boom clay showing strong
particle orientation parallel to the bedding plane

Fig 33.   TEM micrograph of ultramicrotomed Boom clay showing strong
domain formation due to shear stresses induced by the consolidation

Table 12.   Creep parameters of Boom clay with 2.05
             t/m³ bulk density

Shear stress kPa	A*	B*	t_o s
480	-15.8	4.1	194
670	-2.2	13.8	465
800	-59.6	17.5	54

*   The values must be multiplid by 10^{-4} to yield the
    actual figures

The influence of shear stress on the creep is roughly illustrated by the relation-
ship between τ and B, which is approximately the same as for the Kinnekulle
clays. The relationship was found to be of the type $B \propto \tau^{2.9}$.

The total recorded axial strain was less than 0.3 ‰, indicating that the creep took
place under constant volume conditions.

4.6   FORSMARK CLAY (VI)

4.6.1   Origin, composition and physical state

4.6.1.1   Origin

An often cited argument that is in favor of the use of smectite clays as barriers in
repositories is that smectite-holding weathered zones in crystalline rock appear to
be chemically stable and have their isolating properties preserved for very long
period of times. Such a material was included in the study in the form of un-
disturbed blocks collected from clay-weathered rock of the Singö fault zone at
Forsmark. The exact location is the section termed 5/269 of the northern access
tunnel to the SFR repository, the depth below ground surface being about 30 m.

The obvious schistose character of the clay indicates large shear strain after the
clay weathering process, which may have taken place in connection with tectonic
processes in Silurian, Jurassic or Tertiary time in connection with percolation of
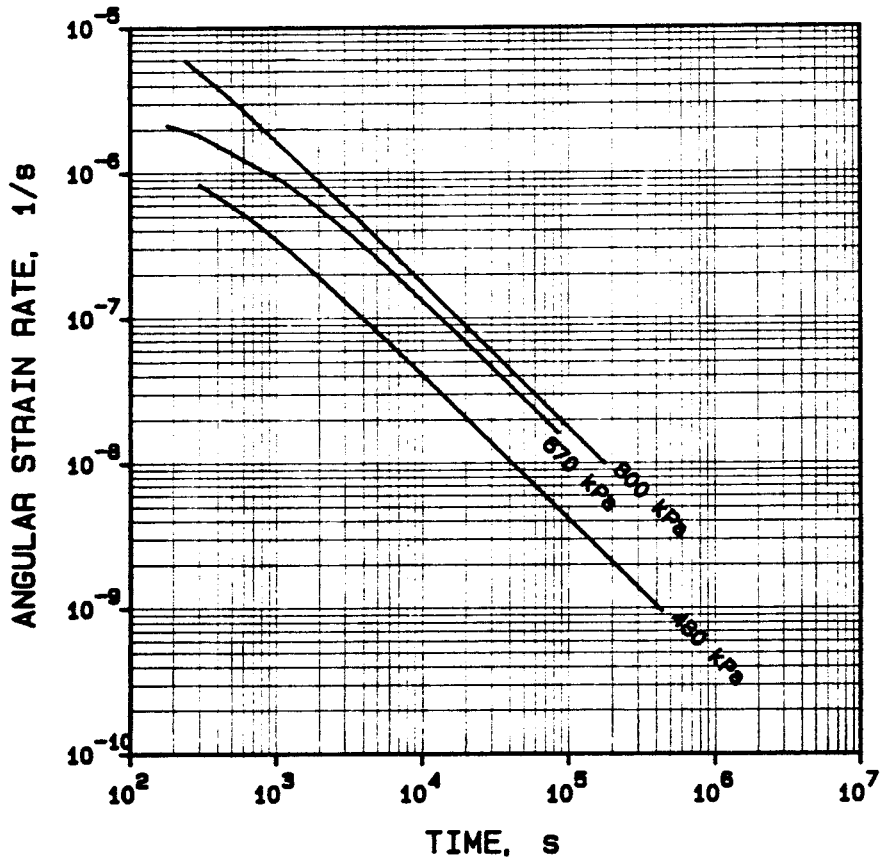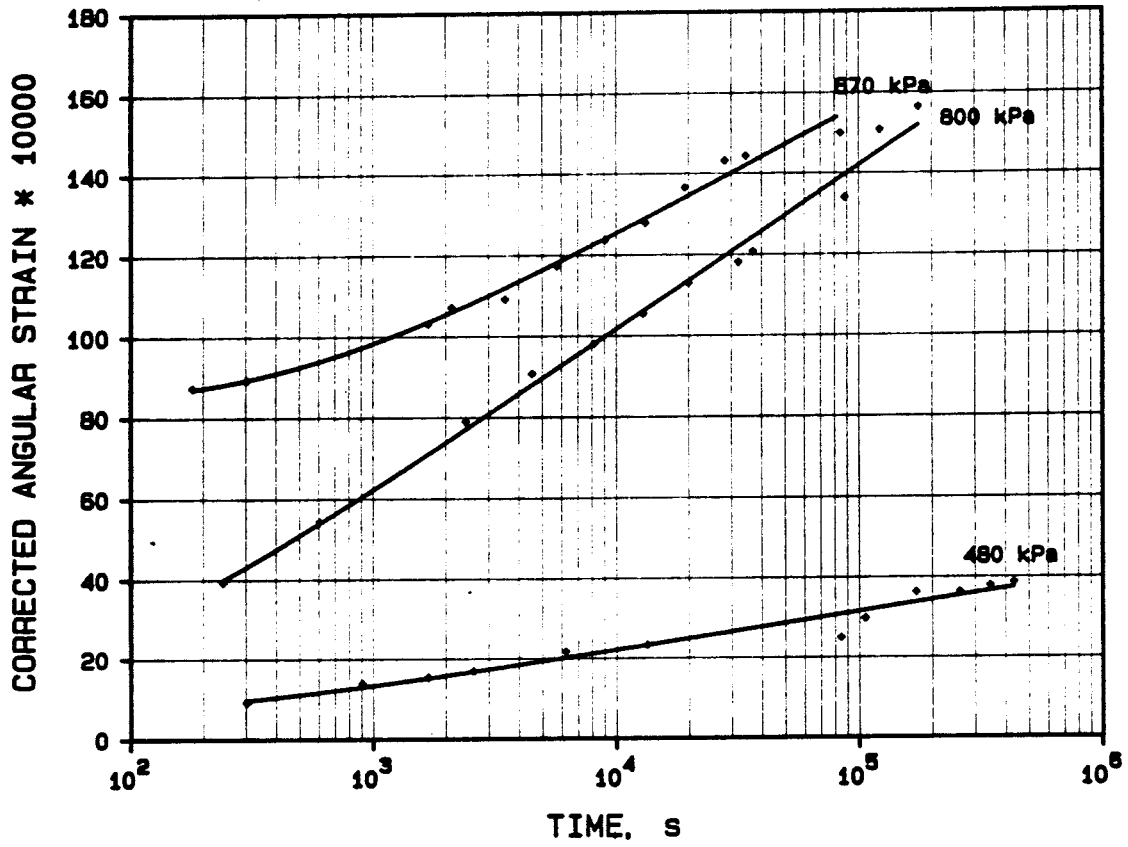
Fig 34.   Creep strain versus time (upper), and strain rate versus time (lower) of Boom clay (V)

the Singö fault zone by hydrothermal solutions. The age of the clay material in its present form is probably at least a few tens of million years.

4.6.1.2 Composition

Larger chunks, were found to have a bulk density of 2.30 t/m3 (dry density 2.06 t/m3), and a clay content of 18 %. No larger grains than coarse silt particles were present in the tested material, which had a water content of about 16 %.

Element analyses of thin sections by use of electron probe technique (SEM microscope) showed that the fine-grained matrix consists of clearly separated regions of smectite and illite yielding chemical compositions which roughly fit these mineral types. It is remarkable that this matrix does not contain other minerals except for clay-embedded, strongly weathered quartz grains. This indicates that the weathering and alteration took place in several stages, probably first to pegmatite and later to phyllosilicates.

The liquid limit of the material was found to be 33 %, which, considering the low clay content, suggests a certain content of smectite. XRD analyses (cf. Fig 35) confirmed this and gave the following composition of the clay fraction: quartz (50 %), illite (30-35 %), chlorite (5 %), feldspars (5 %), smectite (5-10 %). Only about 2 % of the total solid mass consisted of smectite.

4.6.1.3 Physical state

The high silt content gave the non-cemented material the semi-liquid, unstable condition that is typical of such soils when exposed to water. It tended to flow from the tunnel walls to the floor as shown in Fig 36. The undisturbed samples that were used in the laboratory study were taken from an intact, large block that had fallen from the weathered zone in the course of tunnel blasting operations.

The frequent silt grains made it impossible to cut ultrathin sections for electron microscopy and the detailed organization of clay-sized particles is therefore not known. However, the zonal distribution of smectite and illite that is illustrated in the optical micrograph in Fig 37 is probably of greater practical importance. We conclude from such investigations that the smectite component is so widely dispersed that its sealing function should be insignificant. The general microstructural heterogeneity and high content of silt-sized grains are expected to yield
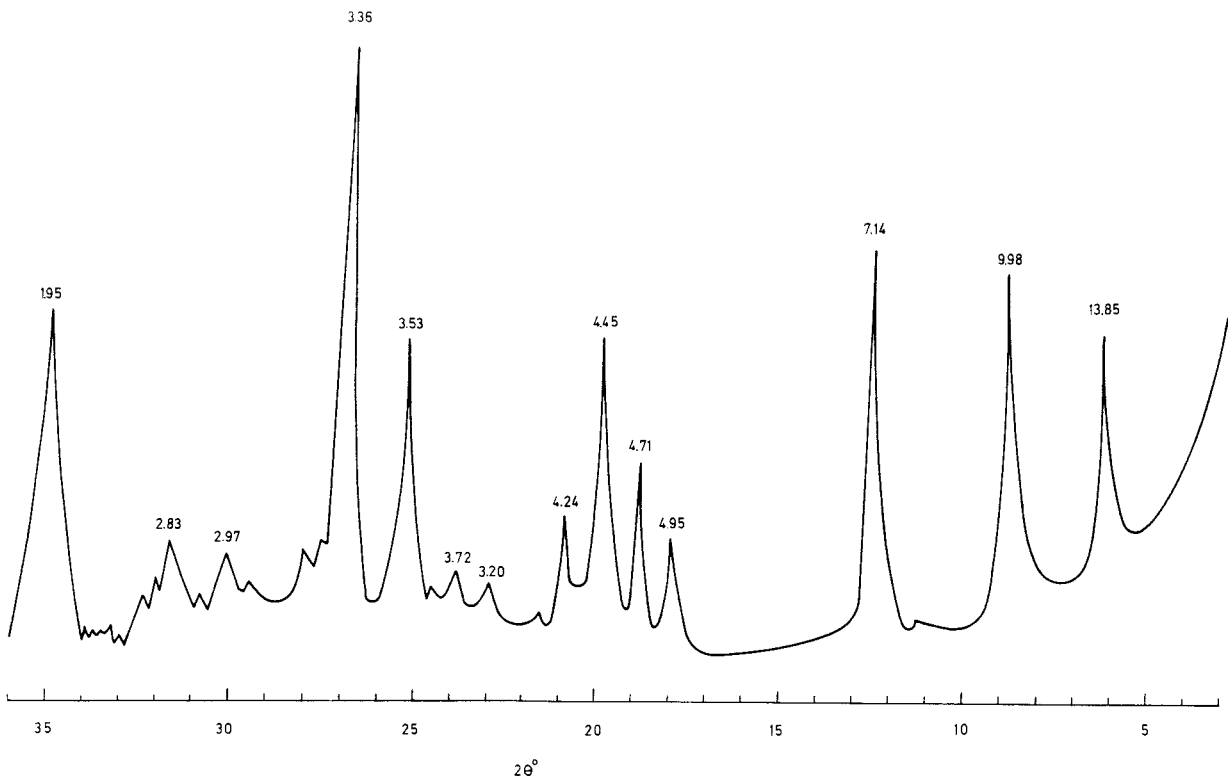
Fig 35. XRD diagram of the clay fraction of Forsmark material

an irregular, strain-dependent creep behavior especially at higher loads when particle fracturing is expected to take place.

The main soil data are shown in Table 13. It shows two sets of values, referring to the initial, undisturbed condition as well as to the remolded, reconsolidated state. The aim of arriving at the same bulk density was not reached.

Table 13. Main data of the Forsmark clay

Condition	Bulk density t/m³	Dry density t/m³	Water content %	Remark
Undisturbed	2.30	2.06	16	-
Remolded	2.05	1.68	22	Reconsolidated
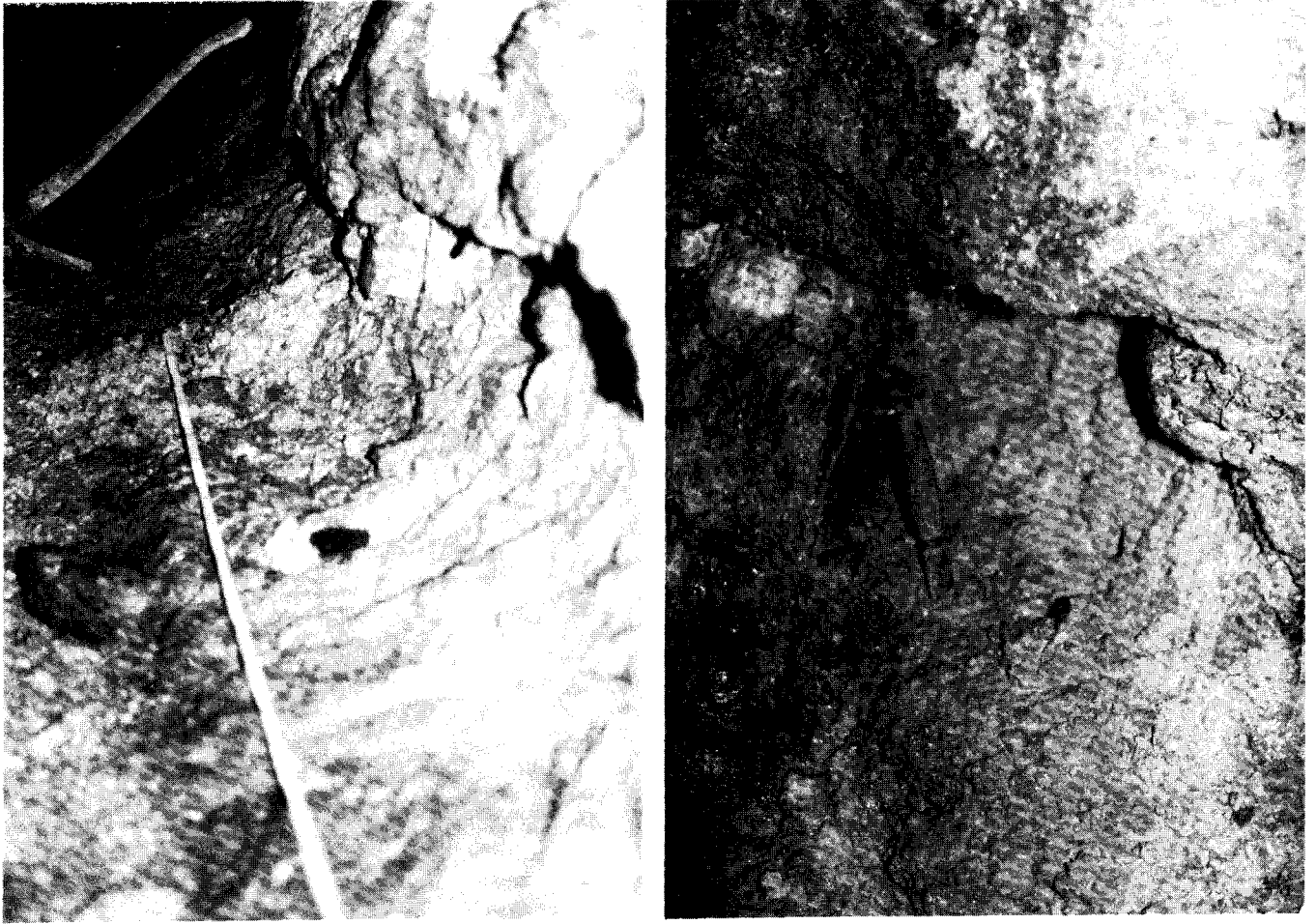
Fig 36.   Character of the Forsmark clay. Left: Material flowing from the wall forming a heap at the end of the yardstick. Right: The consistency of the fine-grained mass was very soft

4.6.2   Physical properties

4.6.2.1   Hydraulic conductivity

Percolation tests using hydraulic gradients ranging between 10 and 100, gave an average hydraulic conductivity of undisturbed clay of 1.2×10^{-10} m/s. The corresponding value of remolded, reconsolidated material was significantly higher, i.e. 10^{-9} m/s, the difference being primarily explained by the lower density of the remolded sample.

QUARTZ GRAIN   SMECTITIC   ILLITIC

CAVITIES   IC = INTRACLAST (CLAY-WEATHERED)

Fig 37.   Optical micrograph of 30 μm section of acrylate-embedded Forsmark clay with interpretation of the mineral distribution (reduced size)

4.6.2.2   Swelling pressure

The recorded swelling pressure of the undisturbed clay was 600 kPa, which is in reasonable agreement with the low smectite content. No swelling pressure could be obs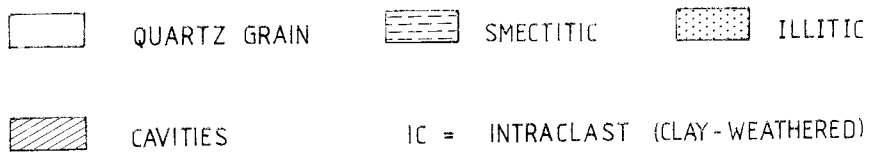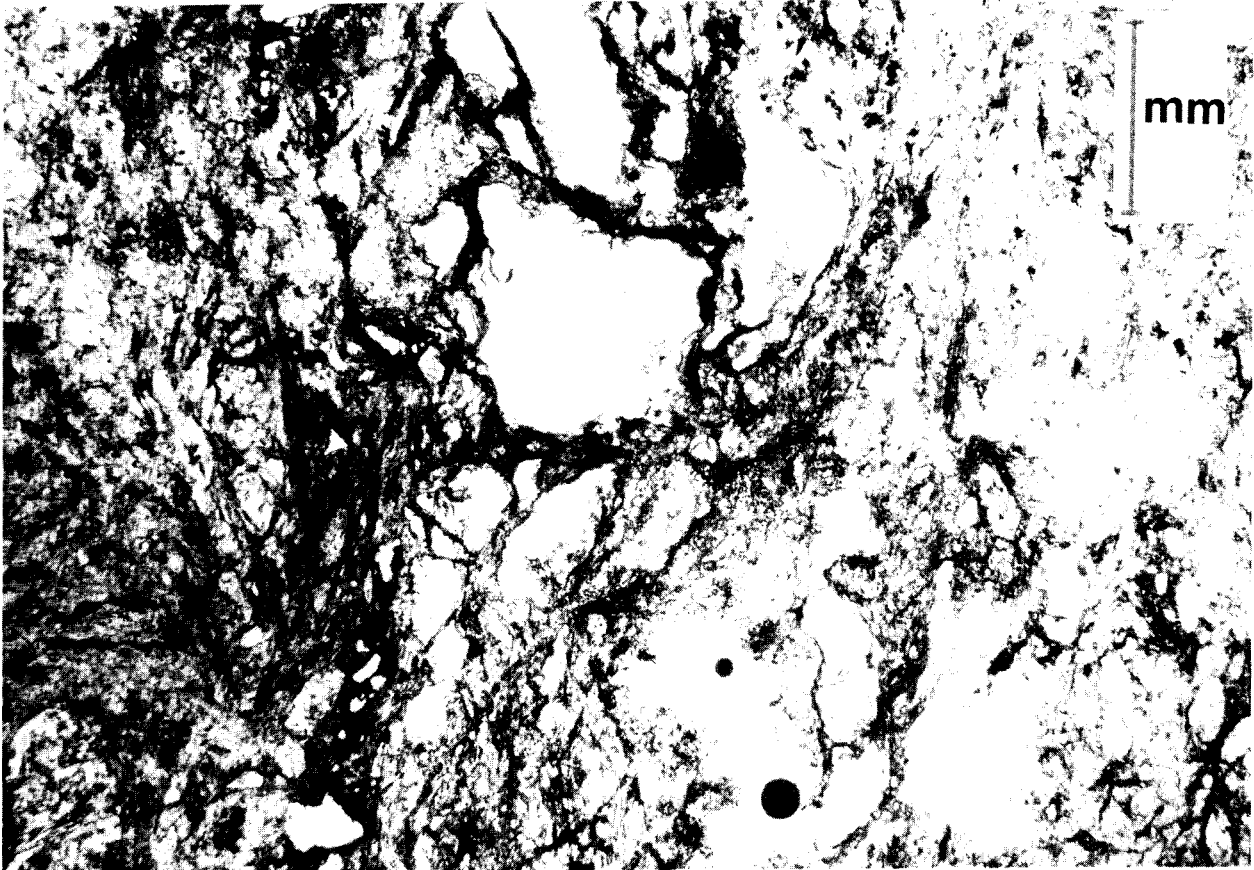erved when the remolded, reconsolidated clay was tested, and this may be explained by the effective dispersion of the clay component on mechanical agitation.

4.6.2.3   Rheology

Creep tests were conducted under an effective normal pressure of 600 kPa. It is obvious from Fig 38 that the behavior was quite different from that of the previously described clays. Thus, the instantaneous strain on load application was significant while the time-dependent deformation was very small except for the highest load. It gave an irregular, "stick/slip"-type movement in contrast to the continuous log t-type behavior of the creep at lower loads, the discontinuous character of the creep being in good agreement with what could be predicted on the basis of the microstructural analysis. Failure took place at a shear stress of 290 kPa, which is remarkably small considering the high bulk density and very dominant content of rock-forming minerals. It is highly probable that the clay component became smeared-out on the surfaces of larger mineral grains by the large shear strain thereby forming a lubricant with a shear resistance typical of clays (cf. Chapter 5.4.3.2).

4.7   IGNABERGA CLAY (VII)

4.7.1   Origin, composition and physical state

4.7.1.1   Origin

An early description of the Ignaberga Cretaceous limestone formation in which subhorizontal, thin clay seams occur, was given in 1934 by Lundegren (16). Fig 39 shows the location of the site and the appearance of typical clay strata, from which samples were taken for the present study. Lundegren concluded that the clay had been formed by downward infilling of eroded material in slots that had been formed by dissolution of carbonate material. While this may be a possible expla-nation of the origin of a few steep branches of the seam system, it cannot be true
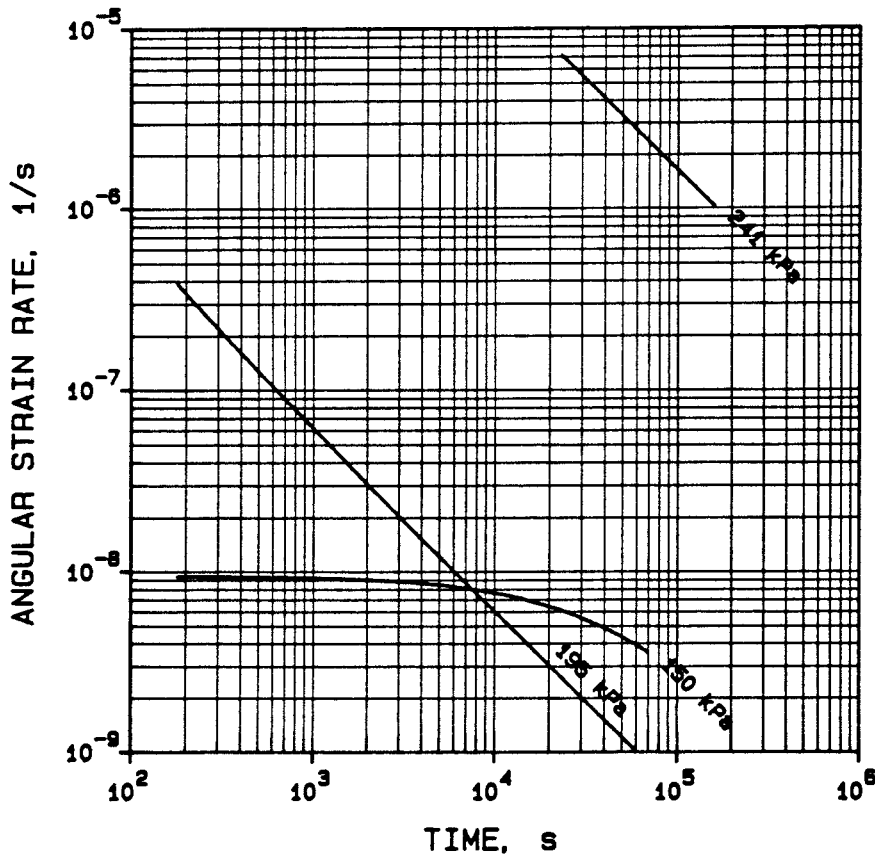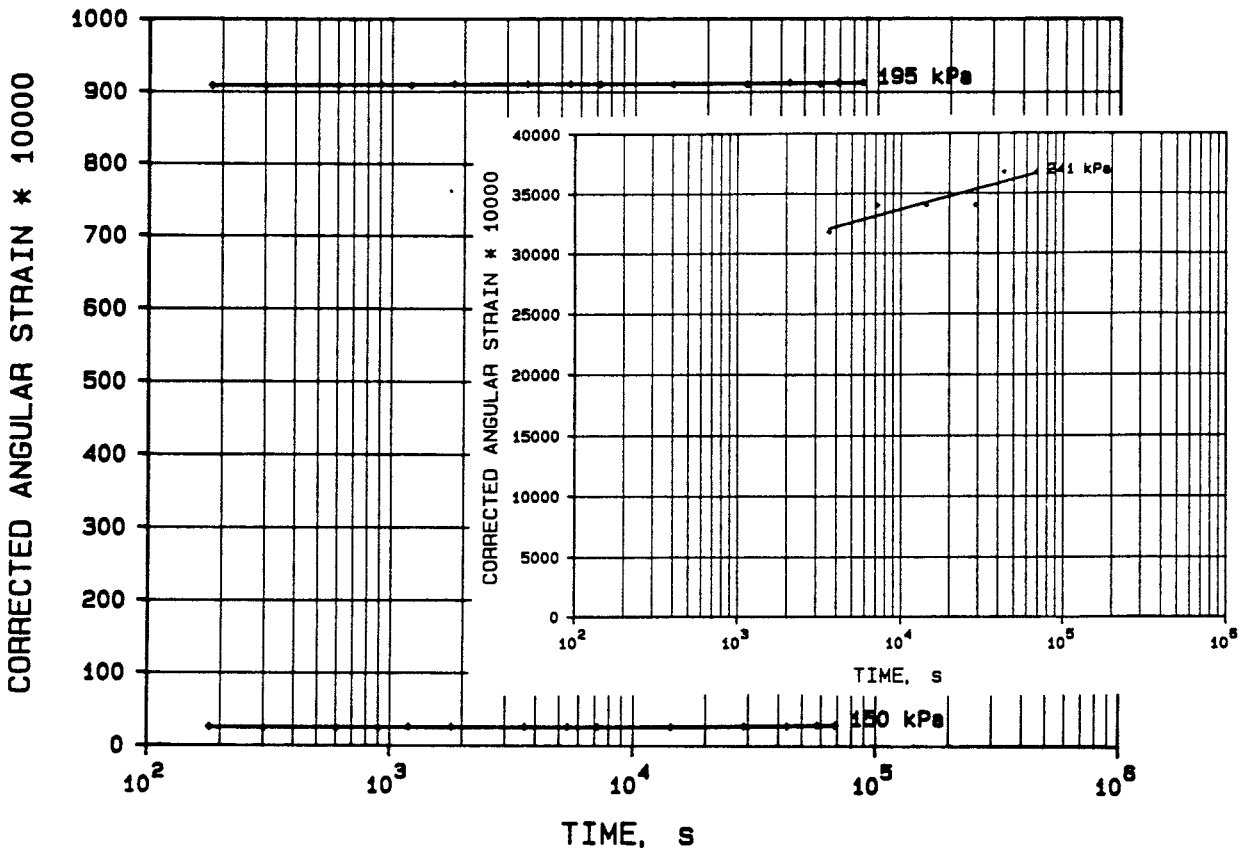
Fig 38.   Creep strain versus time of Forsmark clay for shear stresses of different magnitude

for the dominant, flat-lying 1-10 cm thick layers. A more probable mode of formation is that high water pressures and hydraulic gradients were set up below the front of a rapidly retreating glacier at the end of the latest ice age, by which shallow rock slabs were lifted, forming subhorizontal slots that were penetrated by rapidly flowing, soil-carrying water. This would bring about laminated infillings from "turbidity currents" (17).

4.7.1.2   Composition

The clay material, which is poor in expanding minerals, typically has a brittle character and its relatively low bulk density, i.e. 2.0 t/m³, indicates that consolidation in nature has taken place under moderate pressure. Its significant strength is therefore ascribed to cementation by carbonates which are natural mineral constituents of the material and which may also have been precipitated from the calcium-rich groundwater. The clay content is only 18 %, and the water content was found to be about 20 % of undisturbed samples, indicating that the sampled material was not completely water saturated.

XRD analyses showed the following composition of the clay fraction: calcite (50 %), smectite and mixed-layer minerals (30 %), illite (10 %), quartz (5 %). Grains belonging to the coarser fractions consisted almost entirely of calcite (cf. Fig 40). Smectite was concluded to form about 5 % of the total solid mass.

4.7.1.3   Physical state

It was estimated that the obvious anisotropic character of the clay was due to a heterogeneous distribution of particles of different size, and transmission electron microscopy verified that clay-rich laminae, oriented parallel to the boundaries of the clay layers were typical structural features. This suggested that determination of the hydraulic conductivity of undisturbed as well as of remolded, reconsolidated samples would illustrate the importance of the distribution of low-permeable soil components.

Fig 40 illustrates the constitution of the material. We see that the silty, calcite-dominated matrix contains thin laminae which are rich in clay-sized particles and have a rather open character.
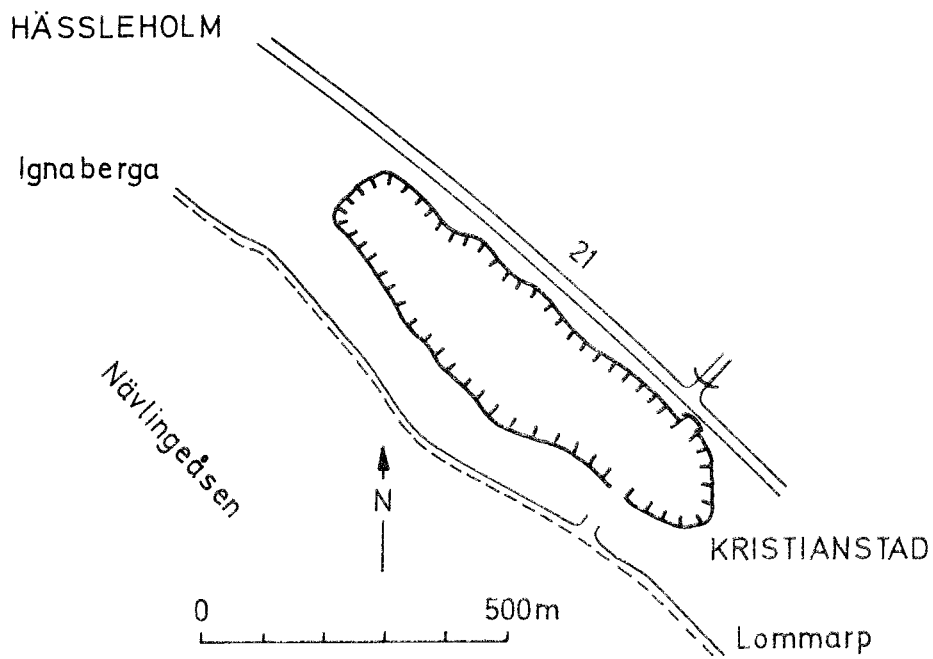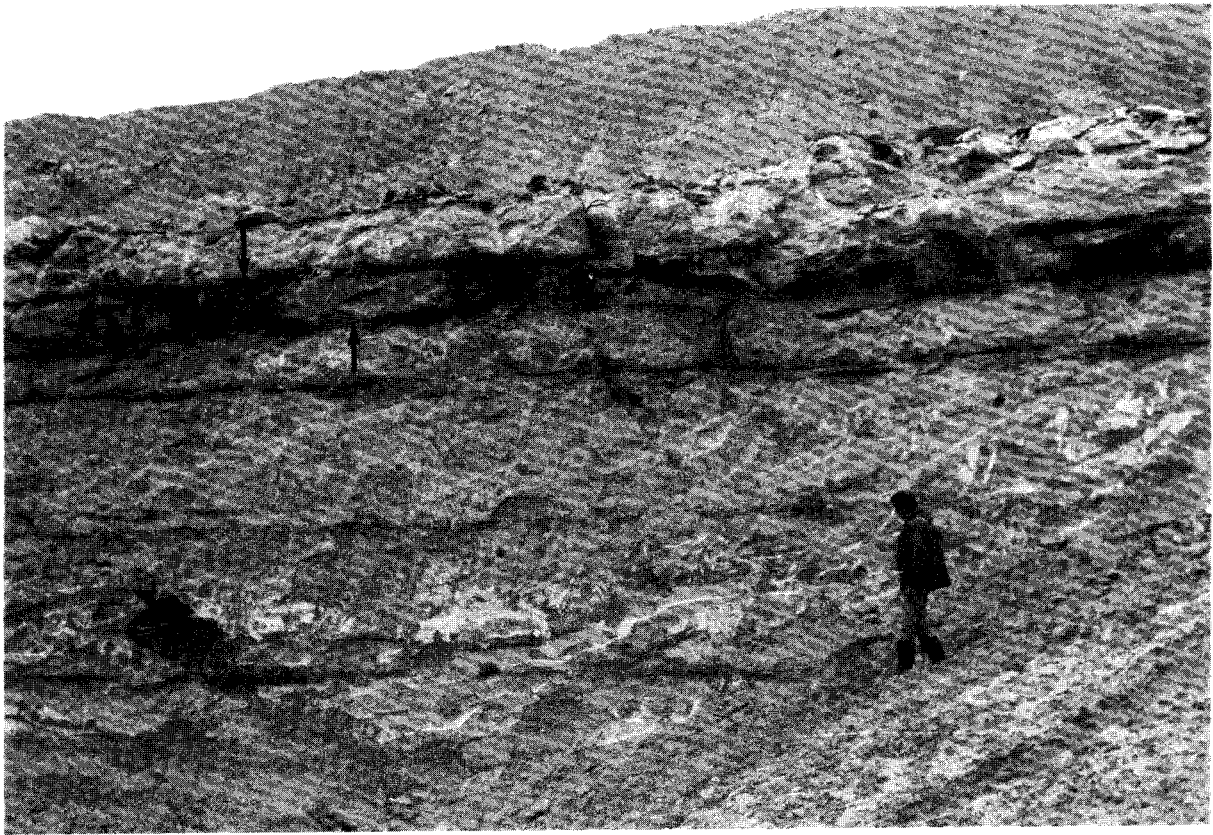
Fig 39. Steep cut in the Ignaberga quarry with typical clay seam pattern
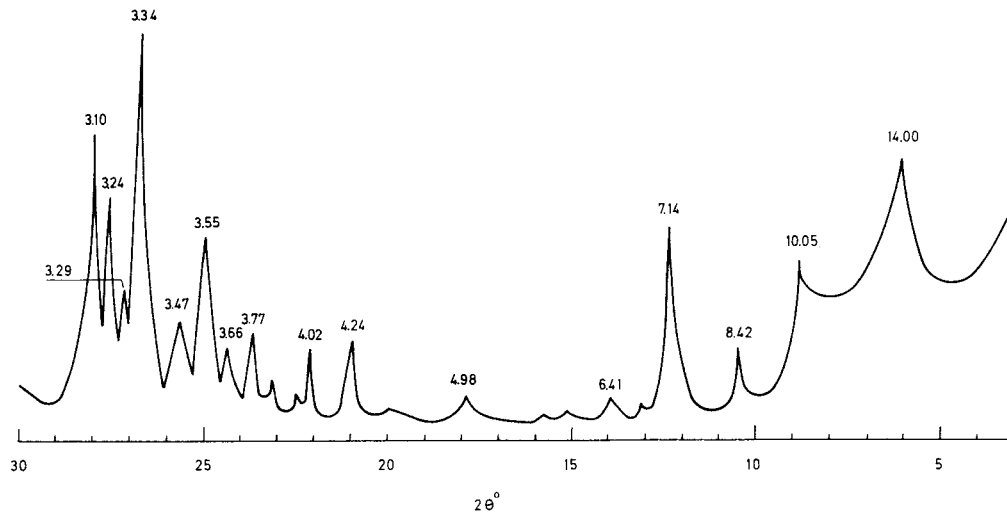
Fig 40. XRD diagram of the clay fraction of Ignaberga material

The main soil data of the clay are given in Table 14. It shows two sets of values, which refer to the initial, undisturbed condition as well as to the remolded reconsolidated state. Reconsolidation gave a slightly higher density than that of the undisturbed sample.

Table 14. Main data of the Ignaberga clay

Condition	Bulk density t/m³	Dry density t/m³	Water content %	Remark
Undisturbed	2.00	1.58	20	-
Remolded	2.10	1.75	20	Reconsolidated

4.7.2   Physical properties

4.7.2.1   Hydraulic conductivity

Tests in which percolation took place perpendicularly to the stratification and using hydraulic gradients of 10-50 gave an average hydraulic conductivity of 2×10^{-11} m/s. The corresponding value was only 10^{-8} m/s of the remolded and reconsolidated material, which indicates the strong impact of the distribution of the smectite component on bulk permeability. It is quite clear that a buffer material with such a low content of smectite is very sensitive even to slight mechanical disturbance.

4.7.2.2   Swelling pressure

The swelling pressure of undisturbed Ignaberga clay, measured perpendicularly to the stratification, was found to be 800 kPa. The value appears to be high with respect to the low smectite content, but it may again reflect the microstructural feature of thin, relatively dense and clay-rich zones. Since they form continuous laminae with a high degree of orientation in the undisturbed state, they may well cause a significant, highly anisotropic swelling pressure. At remolding, the smectite particles are expected to become uniformly distributed and randomly oriented as concluded from the tests of the Forsmark clay, and the swelling pressure should thereby be strongly reduced. This was also verified by the test results of the remolded and reconsolidated material, which exhibited no swelling pressure at all, despite its higher bulk density.

4.7.2.3   Rheology

No creep tests were conducted because of the difficulty of bringing sufficiently undisturbed material into the shear box.
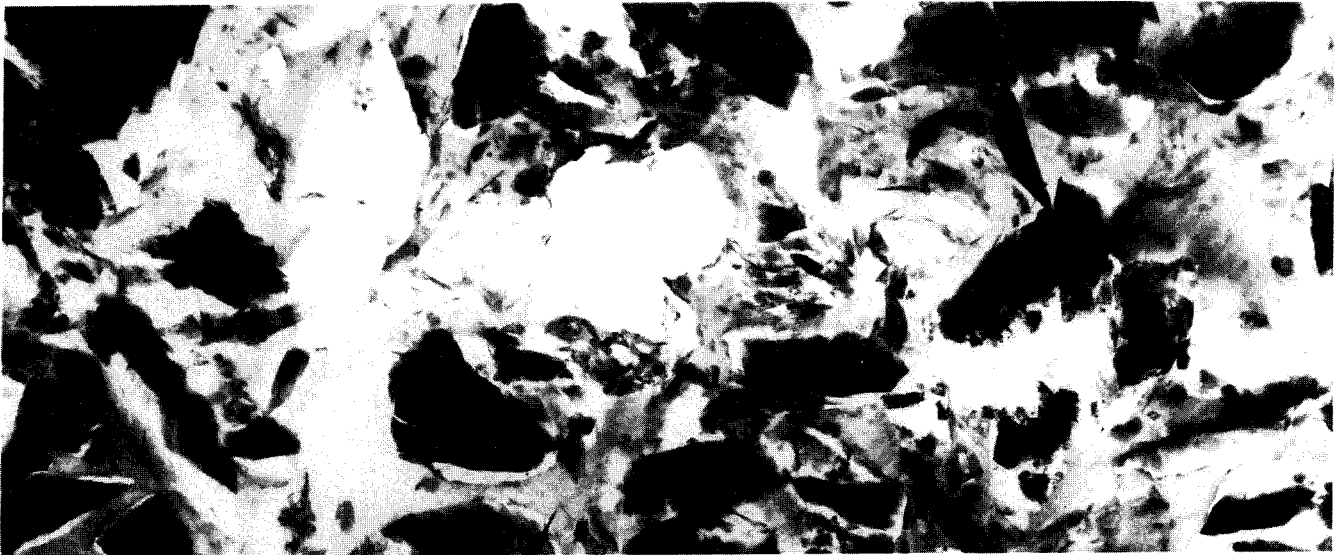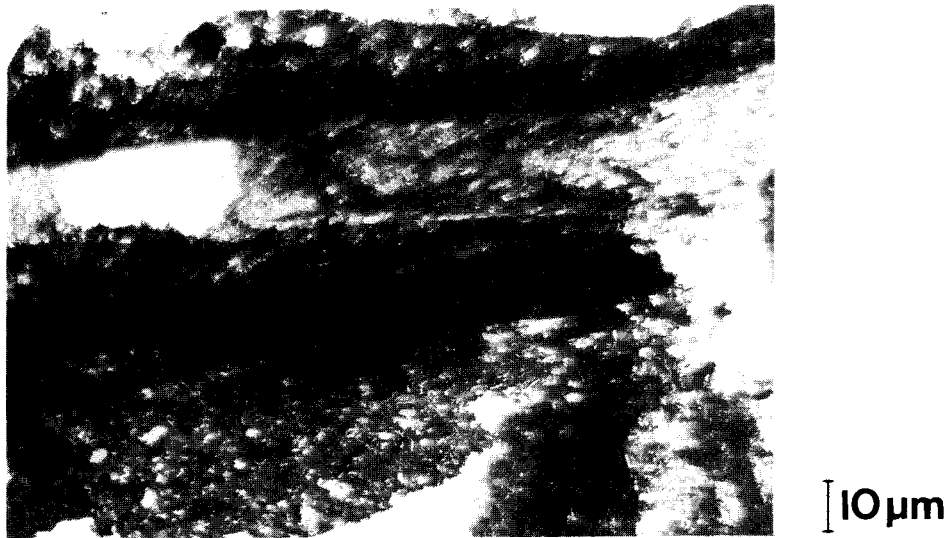
Fig 41   Microstructural features of the Ignaberga clay. Upper: Parallel
          laminae of clay-rich material in silty matrix. Lower: detailed picture
          of the particle arrangement

4.8   FISH CLAY (VIII)

4.8.1   Origin, composition and physical state

4.8.1.1   Origin

The Fish clay is a Cretaceous, thin marl bed forming the basal layer of the Danian of Stevns Klint, in Denmark (Fig 42). The site is located about 30 km south of Copenhagen.

The classical explanation of the origin of the clay, which is known to have sedimented in very shallow sea water and which forms large, oblate lenses, is that it was formed from the glass component of volcanic ash (18). Recent studies suggest, however, that some of the material composing the Fish clay is authigenic while some part is terrigeneous, possibly originating from glass dust produced by an asteroid impact (19). It is equally possible, however, that the smectites were neoformed.

Supposing an original montmorillonitic composition of the clay, later diagenetic processes, probably in connection with percolation of salt solutions, may theoretically have altered the original smectite minerals to the present montmorillonite-/illite or vermiculate/illite mixed-layer assemblage in which the ratio of expandable/nonexpandable layers is generally about 8/1. Such transformation would require partial substitution of Al for Si (beidellitization) in addition to K-uptake which is compatible with recently forwarded ideas on illitization kinetics if the involved activation energy for the substition is high and the temperature during 70 million years reaction time is taken to be 20°C (20). Permeation of hot hydrothermal solutions would have required much shorter times for such alteration.

4.8.1.2   Composition

The bulk density and water content of the strongly anisotropic, laminated clay were found to be 1.85 t/m³ and 41 %, respectively. The clay content of the investigated clay-rich samples was found to range between 60 and 75 %. Earlier investigations have shown that quartz, calcite and montmorillonite are the main minerals in this fraction, and this has been confirmed by later studies, which have indicated that also minor amounts of siderite, hematite and pyrite are present.

A rough quantitative picture of the minerals belonging to the clay fraction is: calcite (40-50 %), mixed-layers, mainly montmorillonite (40-50 %), illite (10 %), quartz (5 %), cf. Fig 43. The exchangeable cation of the smectite component is calcium. The liquid limit was found to be 80 %, which is in reasonable agreement with the conclusion that smectite constitutes about 30 % of the total solid mass and that it is in calcium form.

4.8.1.3   Physical state

The sediments in the Stevns Klint area have been covered by younger sediments of unknown thickness which were eroded in Tertiary time. The probable maximum overburden was due to the Pleistocene ice-cover, which caused a pressure of at least 10 MPa. The present effective overburden pressure is about 400 kPa, which is expected to be balanced by the swelling pressure.

A number of rock fall events have taken place in the area (cf. Fig 42), which makes it possible to estimate roughly the drained shear strength along the bedding plane. Thus, simple slope stability calculations yield the figure 150-200 kPa under the existing overburden.

Ordinary optical microscopy of 30 µm sections verified that the clay is strongly anisotropic and contains lense-like voids, which may be fissures or compressed pores that may initially have contained gas (Fig 44). Transmission electron microscopy showed that particle alignment is also a typical microstructural feature (Fig 45). The comprehensive electron microscopy showed that the microstructural pattern was very similar to that of the MX-80 reference clay although sodium is the dominant exchangeable cation of the latter.

Major soil data are given in Table 15. As in the preceding investigation the clay was tested in an undisturbed condition as well as remolded and reconsolidated.
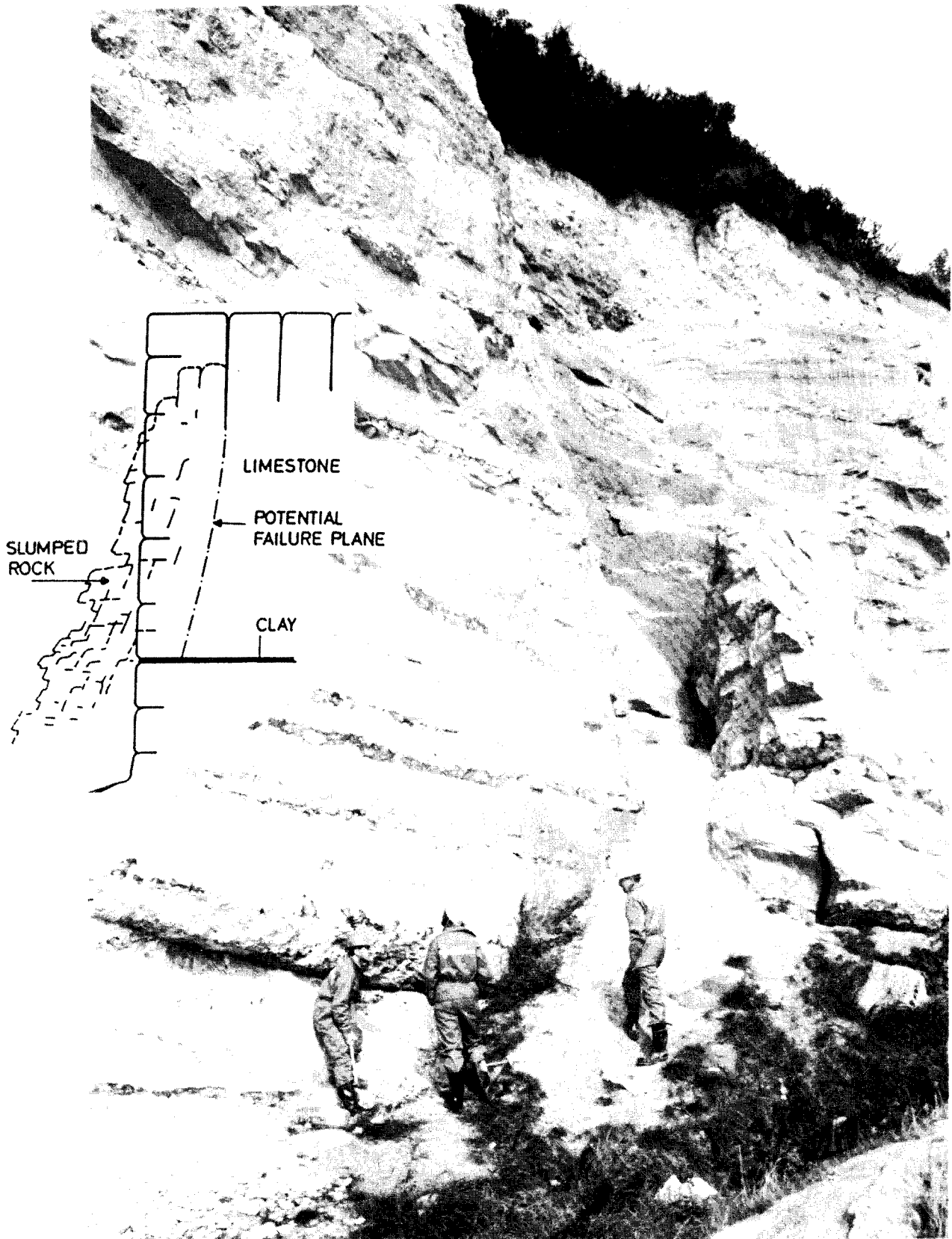
Fig 42.   Cross section of the steep cliff at Stevns Klint in south-eastern
            Själland, Denmark. The clay layer is covered by about 15 m of
            limestone. Potential slope failure due to creep in the clay is
            indicated
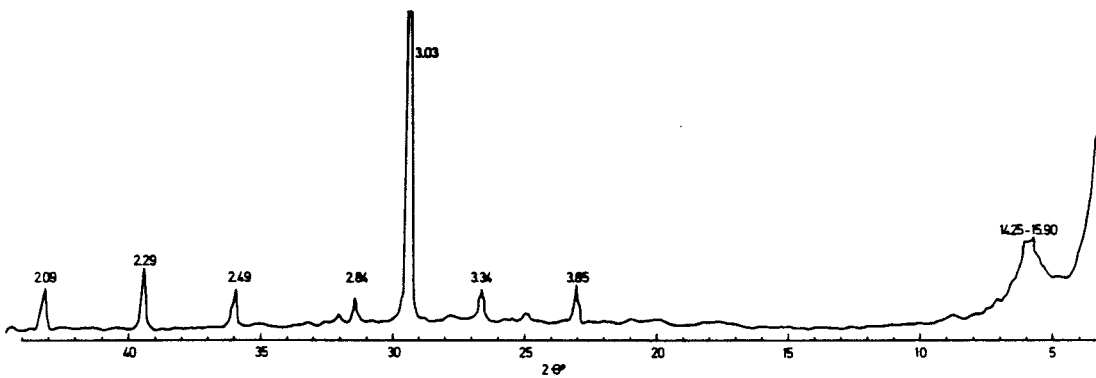
Fig 43. XRD diagram of the clay fraction of Fish clay

Table 15. Main data of the Fish clay

Condition	Bulk density t/m³	Dry density t/m³	Water content %	Remark
Undisturbed	1.85	1.35	41	-
Remolded	1.83	1.32	45	Reconsolidated

4.8.2   Physical properties

4.8.2.1   Hydraulic conductivity

Percolation tests were made of undisturbed clay as well as of samples which had been remolded and reconsolidated. The undisturbed sample was percolated perpendicularly to the stratification at hydraulic gradients ranging between 10 and 50, the average hydraulic conductivity being 1.5×10^{-12} m/s. The remolded and reconsolidated sample was approximately ten times as permeable ($k \sim 2 \times 10^{-11}$ m/s) and since the bulk densities were practically the same, the two tests offer an excellent example of the influence of microstructural order on the hydraulic conductivity.

4.8.2.2   Swelling pressure

The swelling pressure of the undisturbed clay was accurately determined in the consolidation phase of the shear box tests and found to be about 400 kPa, i.e. the same as the overburden pressure. The corresponding pressure of the remolded
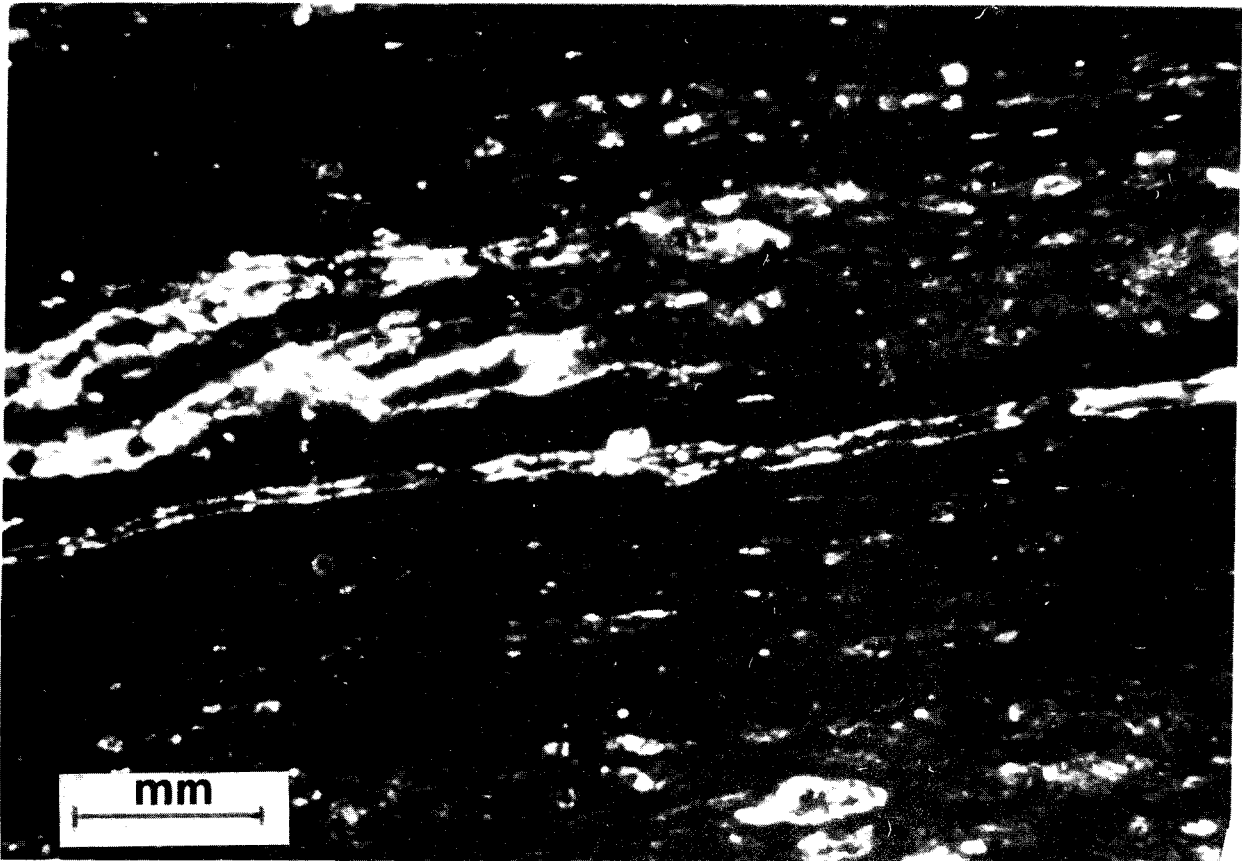
Fig 44.   Optical micrograph of 30 μm section of acrylate-embedded Fish clay.
The irregular light areas represent elongated voids while the regu-
lar band is a fissure of long extension

material was determined in connection with the percolation tests and this, less
accurate measurement showed that the pressure was less than 100 kPa. We are
thus led to the same conclusion as in the preceding discussions of the Forsmark
and Ignaberga clay, namely that the orientation of the smectite minerals and the
continuity of this mineral phase has a strong impact not only on the hydraulic
conductivity but also on the swelling pressure.

4.8.2.3   Rheology

Creep tests were made of an undisturbed clay sample under an effective normal
pressure of 500 kPa, i.e. slightly more than the swelling pressure. The diagrams
in Fig 44 illustrate the general creep properties of this rather smectite-rich,
calcium-saturated clay, which was sheared along the stratification. Creep
parameter data are given in Table 16.

Fig 45. TEM micrograph of ultramicrotomed section of Fish clay showing
the characteristic network of oriented interwoven stacks of smectite
flakes. The dense particles are calcite crystals

The facts that the lowest load, which corresponded to about 25 % of the failure load, gave no time-dependent creep at all and that the second load-corresponding to about 50 % of that yielding failure - produced insignificant strain, suggest that the clay is cemented. Weak cementation is also indicated by the slightly negative t_o-value obtained for the third load step, which also gave the jerky time/strain curve that is concluded to be characteristic of the phase in which cementation bonds are being broken down.

It is concluded from these tests as well as from the fact that the natural clay material is easily disintegrated by rubbing it with the fingers in water, that the cementation is very weak. This would also fit the results of the swelling pressure measurements.

Table 16.   Creep parameters of Fish clay with 1.85 t/m^3
bulk density

Shear stress kPa	A*	B*	t_o s
47	1.52	-1	725
96	2.69	1.4	1462
140	-37	19.2	-9

*The values in the table must be multiplied by 10^{-4} to yield the actual figures

The influence of shear stresses on the creep cannot be estimated with any accuracy because of the small number of load steps. Failure took place at the shear stress 187 kPa, i.e. well in the interval that was back-calculated from the slope stability analyses.

The total axial strain was about 0.5 %o, indicating the creep took place under constant volume conditions.
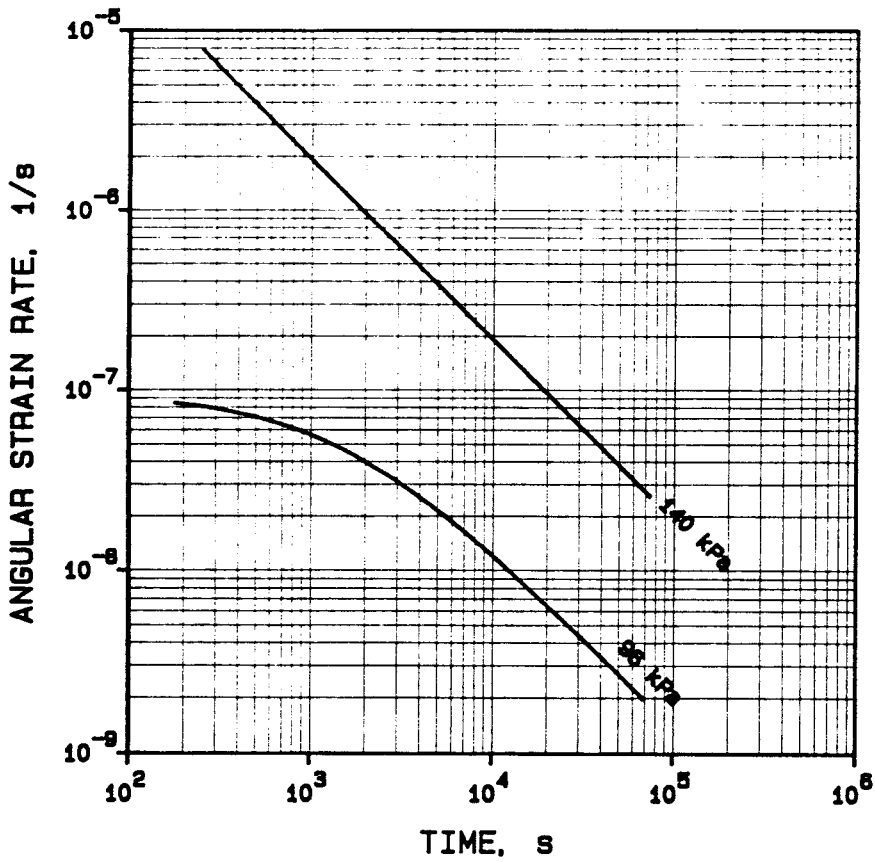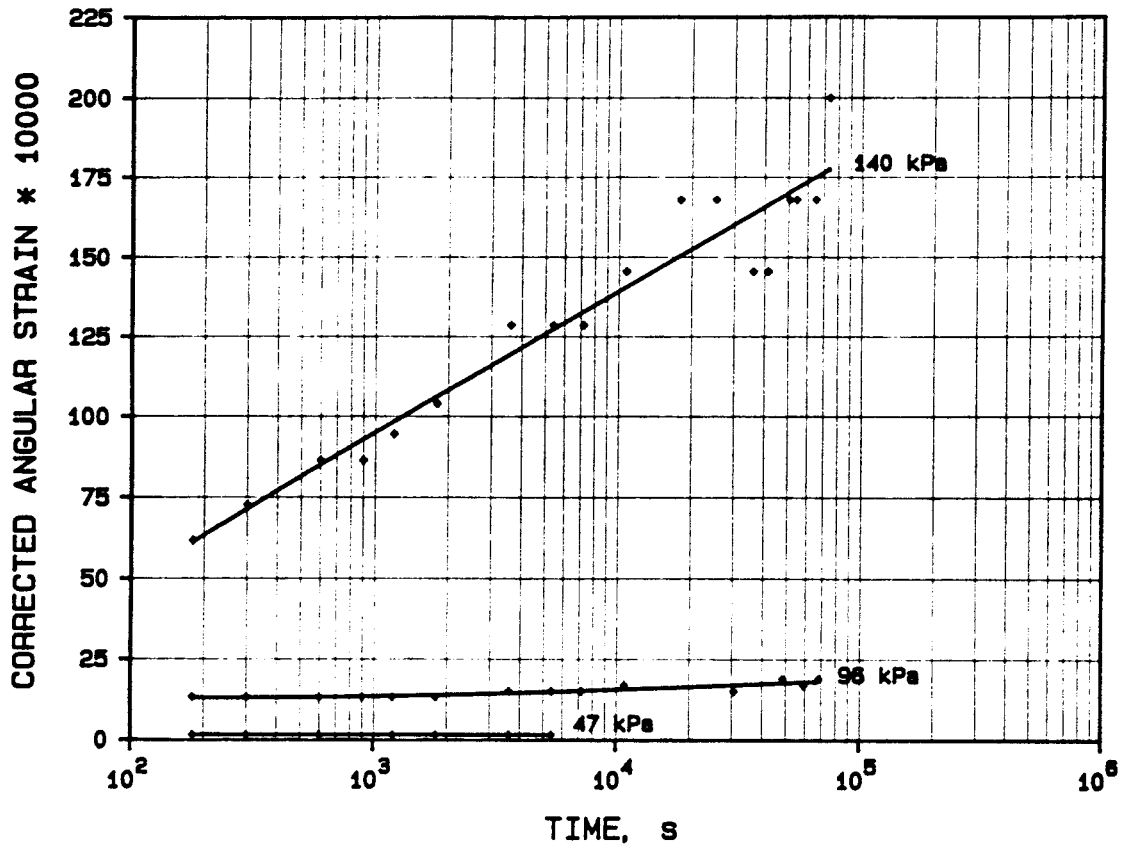
Fig 46.   Creep strain versus time (upper), and strain rate versus time (lower) of Fish clay

5   <u>DISCUSSION</u>

5.1   GENERAL ASPECTS

It is quite clear that the individual representatives of the broad spectrum of pre-Quaternary clays, all of them being several tens or hundred million years old, have physical properties that make them qualify as potential barrier candidates. Thus, even extensive alteration of the originally dominant Na-montmorillonite to illite, feldspars etc may well yield reaction products with good isolating properties in a repository. However, the key factor appears to be the smectite content that remains after the various transformation processes in repository environment, because it largely determines the hydraulic conductivity and the swelling potential. The latter governs the self-healing ability and the rheological properties which determine how well the sealing ability will be retained in the course of the thermo-mechanical processes that the clay barriers will undergo. We will consider these properties in particular in the subsequent discussion.

5.2   HYDRAULIC CONDUCTIVITY

5.2.1   <u>Importance of the clay content</u>

Assuming, in the first place, that the swelling potential is sufficient to make the buffer mass fill up the space which it is supposed to seal off, its average hydraulic conductivity is of course the most essential property. It is mainly controlled by the clay mineral content and the bulk density, the significant sealing ability of the smectite mineral montmorillonite being demonstrated by Fig 47. The diagram indicates that the average hydraulic conductivity of kaolinitic clay is at least two orders of magnitude higher than that of illite, which is in turn more than two orders of magnitude higher than the conductivity of montmorillonite (11). This would suggest that the investigated clays have conductivities that are related to the smectite content and this is also verified by the diagram in Fig 48. We see that the clays termed I, III, IV, V, VI and VII represent a rather well defined band even down to the lowest smectite contents. The anomality of clay VIII (Fish) is explained by its low bulk density. The interesting fact that clay II (Gotland) had a conductivity that would suggest a smectite content of 5-10 %, but which contained no smectite at all, can be explained by its homogeneous microstructure.It is characterized by an interwoven particle network much like that of smectite-rich bentonites.
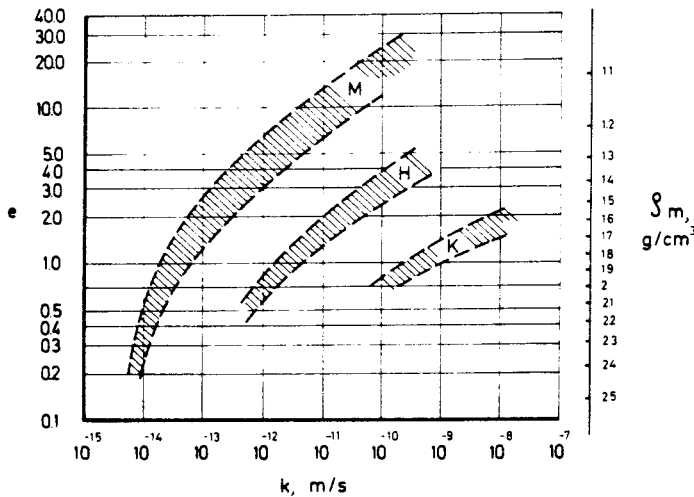
Fig 47. Hydraulic conductivity of clays rich in the respective minerals
montmorillonite (M), illite (H), and kaolinite (K)

BULK DENSITY RANGE		
I	1.90-2.10	t/m3
II	2.11-2.20	"
III	2.05-2.15	"
IV	2.10-2.25	"
V	2.05	"
VI	2.05-2.30	"
VII	2.00-2.10	"
VIII	1.83-1.85	"
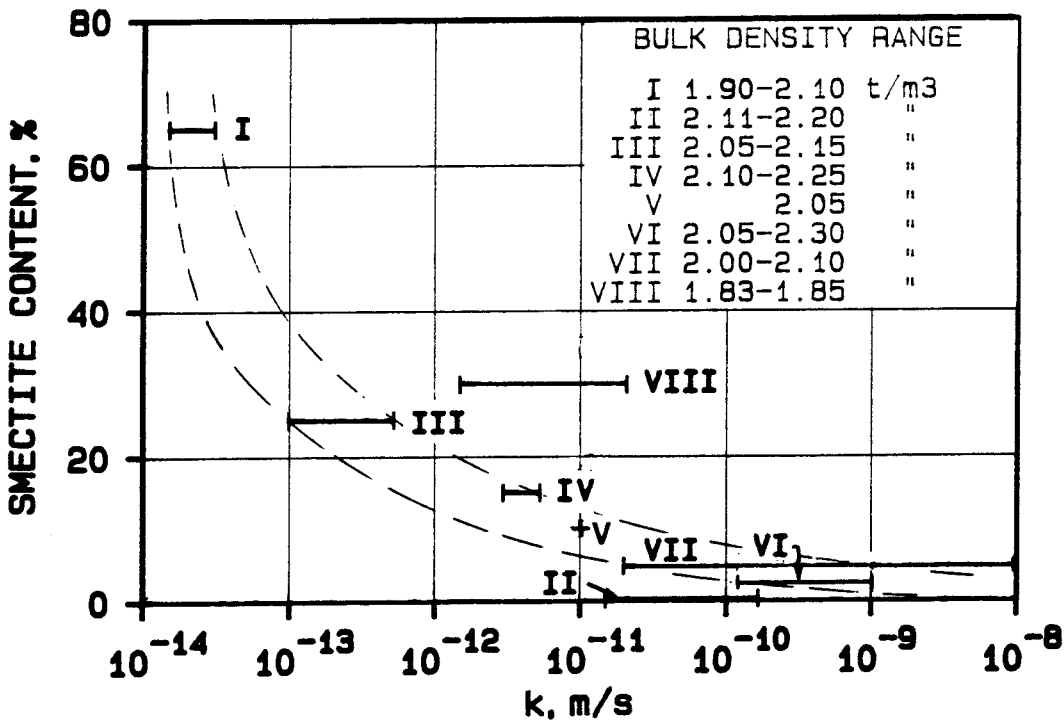
Fig 48. Hydraulic conductivity versus smectite content of the eight clays.
This content is expressed in percent of the total mineral mass. The
band width is taken to represent the average spread in hydraulic
conductivity of the smectitic clays with a bulk density (ρ_m) of at least
2.0 t/m3

Logically, the content of clay-sized particles should also have an influence on the
hydraulic conductivity since for most of the clays the smectite content is related to
the clay content. Fig 49 verifies this but it is clear that the preceding diagram

gives a much more defined relationship, which specifically demonstrates the excellent sealing ability of the smectite component.
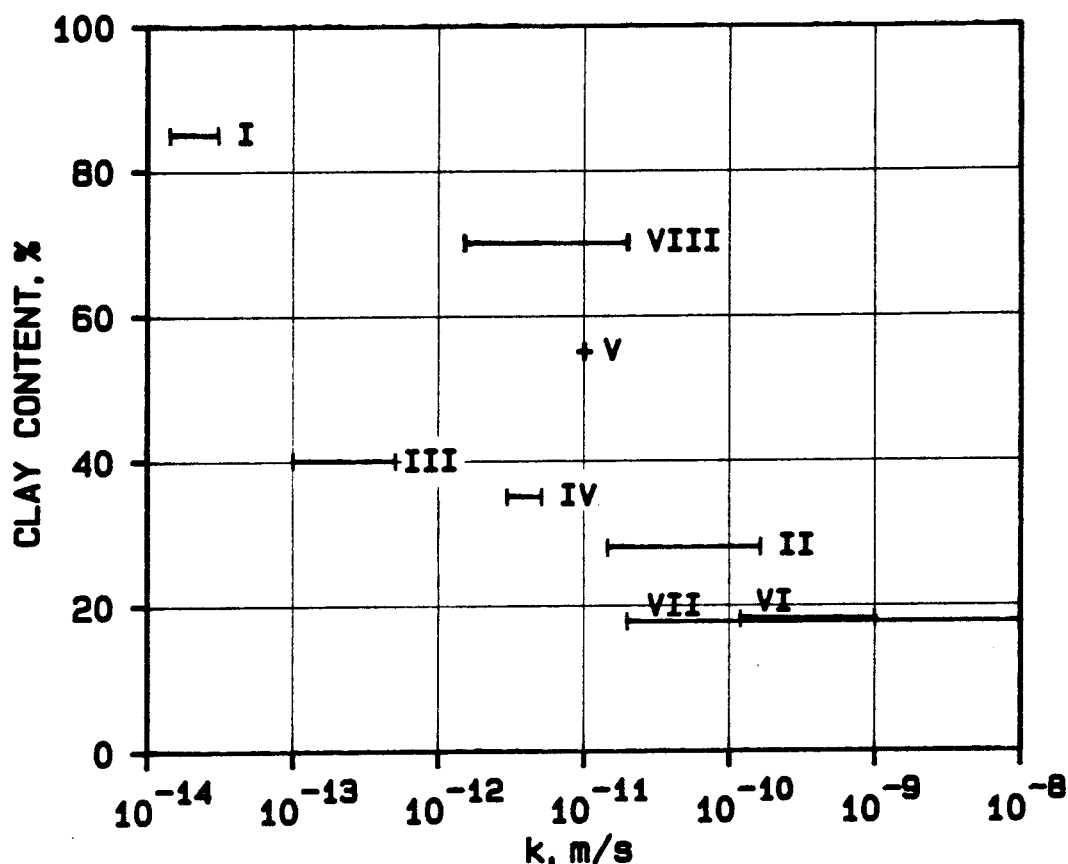
Fig 49.   Hydraulic conductivity versus clay content, i.e. the amount of particles with a Stoke diameter smaller than 2 μm. Bulk density data are given in Fig 48

Finally, the spatial distribution of the clay minerals is concluded to be of great importance with respect to mechanical disturbance caused by shear or expansion. This is illustrated by the diagram in Fig 50 which quantifies the increase in hydraulic conductivity on reducing the bulk density. The change in conductivity is expressed by the factor G defined as $k_{alt} = G \cdot k_i$, where k_i is the hydraulic conductivity of the undisturbed clay and k_{alt} the value obtained after expansion or remolding and reconsolidation to approximately the density of the undisturbed clay. The small number of experiments and the limited accuracy in the determination of the hydraulic conductivity do not allow for any detailed analysis, but it is concluded that even significant microstructural distortion through remolding will generally not increase the hydraulic conductivity by more than one order of magnitude at smectite contents exceeding about 10 %. It is provided, however, that the smectite constituents do not form very thin, mechanically sensitive

layers as in the Ignaberga clay, which appeared to become very pervious on remolding. The distribution of mineral attack and reaction products in the transformation of originally smectite-rich clay barriers depends on the initial pore space distribution, and the microstructure is therefore a determinant of its rate and comprehension. This matter is being considered in the ongoing SKB research on the chemical stability of smectite barriers.
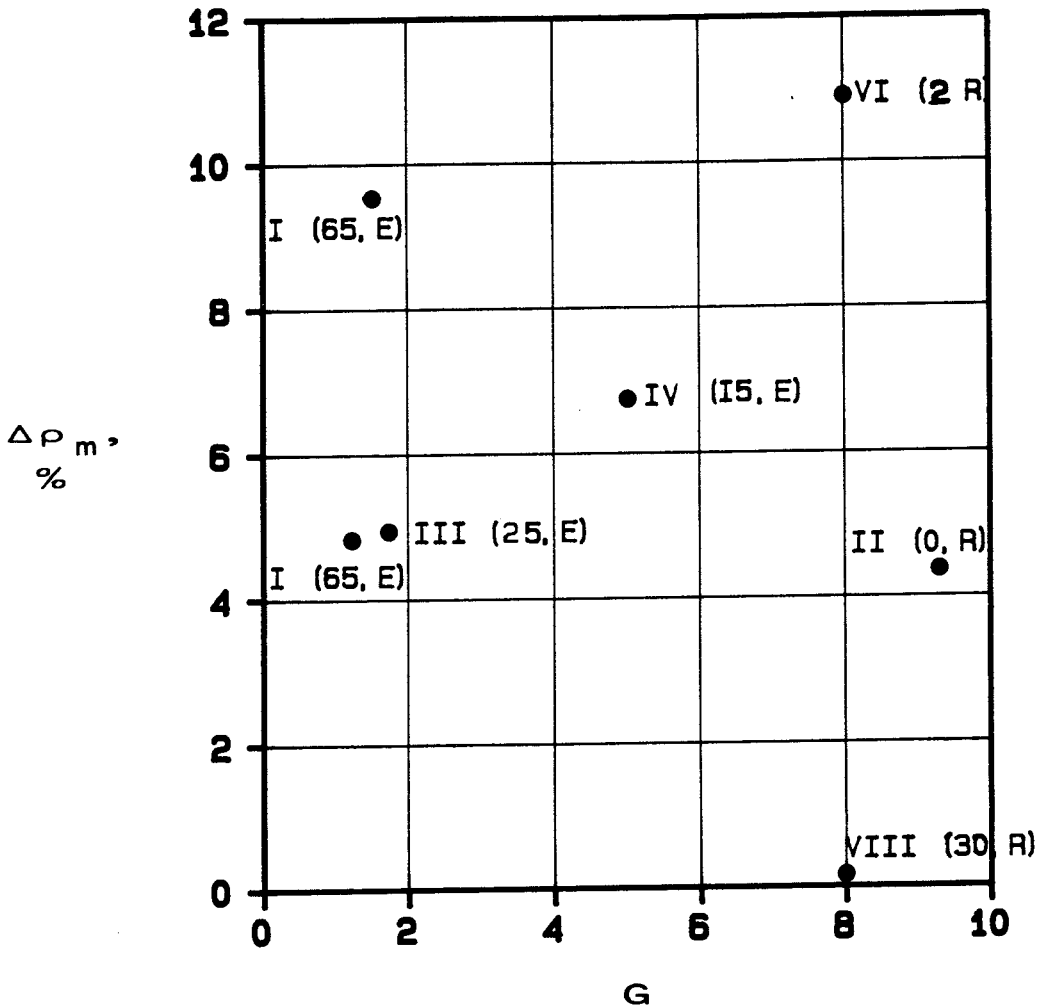
Fig 50.   Change in hydraulic conductivity on reducing the bulk density. For clay VII (Ignaberga) remolding gave G = 500. R denotes remolding while E refers to expansion. Figures given within brackets give the smectite content

In principle, there is general agreement between the diagram in Fig 48 and the results from earlier systematic percolation tests with dense mixtures of a sandy ballast and MX-80 bentonite as compiled in Fig 51. It is obvious, however, that the latter diagram consistently yields higher k-values of the mixtures, which is

due to the difficulty in obtaining a high degree of clay filling in the pores between larger grains and a uniform distribution of the smectite component. As a matter of fact this points to the use of homogeneous natural geological materials rather than artificial mixtures when smectite-poor backfills are required.
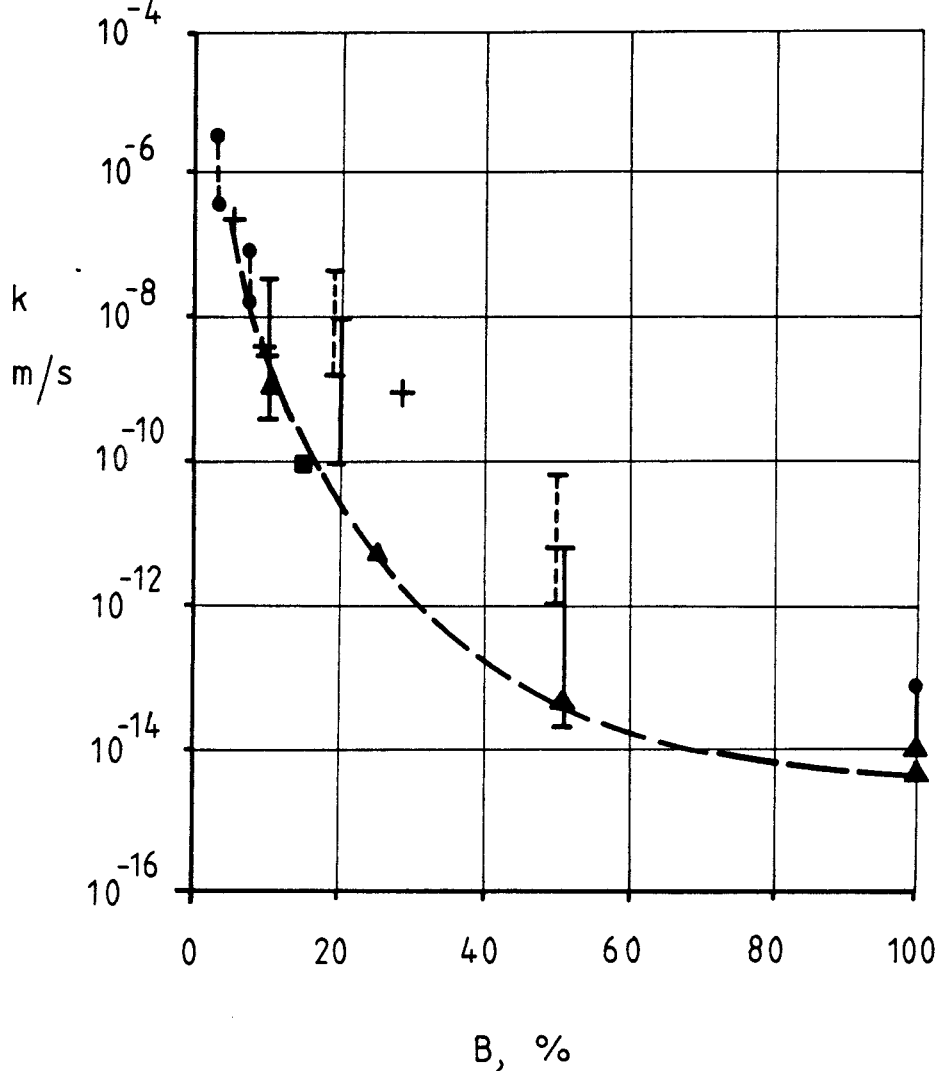
Fig 51.   Hydraulic conductivity of mixtures of Na bentonite and sand with dry densities ranging between 1.5 and 2.1 t/m3 (21). + represent tests with large permeameters, full lines show results from tests in swelling pressure oedometers with very weakly brackish water. Broken curves represent tests with strongly brackish (Forsmark) water

In conclusion, we find that the hydraulic conductivity is very sensitive to changes in the amount of smectite when the content of such minerals is low, and that the increase in conductivity on reducing the bulk density becomes substantial in smectite-poor backfills. It is estimated that a residual smectite content of 15-25 % is required to keep the alteration-related increase in hydraulic conductivity within reasonable limits.

5.2.2 Influence of porewater chemistry

While the chemical composition and concentration of the porewater varied widely
in the natural state of the investigated smectitic clays as documented by the XRD
spectra and liquid limits, they were all largely saturated with rather strongly
brackish water with Na as sole cation in the percolation and rheology tests. This
condition was almost equivalent to the natural state of the Forsmark clay and not
very different from that of the Boom and Kinnekulle clays but it may have
involved some ion exchange from calcium to sodium in the case of the Fish clay.
As to the Ignaberga clay, it is probable that the high calcite content of the silty
matrix did not allow for a significant exchange to sodium of the minor smectite
content, and this may partly explain the insignificant sealing power of this
mineral constituent. Thus, the limited expansion capacity of calcium montmo-
rillonite, together with the strong aggregating power of the strongly brackish
water, must have led to a low void-filling capacity of the smectite gel when the
Ignaberga clay was tested in a remolded state. This accounts for its high perme-
ability.

5.2.3 Influence of mineral density changes

Substantial mineral alteration through processes like those which can be
assumed to transform MX-80 type clay to one consisting largely of illite, is
expected to be associated with an increase in porosity, since illite is generally
assumed to have a slightly higher density than montmorillonite. More important
is, however, the previously mentioned effect that the pore size distribution is
largely altered so that the fraction of larger voids that hold "external", free water
increases while the interlamellar space with internal water collapses. The net
effect of these changes is clearly seen by comparing the permeabilities of the MX-
80 (I) and Gotland (II) clays in undisturbed condition ($\rho_d \approx 1.76$ t/m^3). At this high
density the k-value is about three orders of magnitude higher for the illitic clay.
Alteration of smectite that results in the formation of rock-forming minerals like
quartz and albite, which have densities that are approximately equal to that of
montmorillonite, would yield the same effect on the pore system and permeability
as illitization, while the formation of cristobalite and amorphous silica compounds
having substantially lower densities would tend to reduce the porosity and perme-
ability. The present study does not offer a clear picture of the influence of such
changes but taking the Boom and Ignaberga clays to be representative of altera-
tion products that are rich in rock-forming minerals, we find, in accordance with

the prediction, that, for $\rho_d \approx 1.58$ t/m3, both clays have k-values that are about three orders of magnitude higher than that of MX-80.

5.2.4 Comments on the testing technique

The applied technique for trimming the samples to a conical form and filling the wedge-shaped gap between the confining oedometer ring and the sample with compacted MX-80 clay powder appeared to eliminate flow along the interface. This sample preparation method is therefore recommended for general use.

No systematic variation of the hydraulic gradient was made, nor was the direction of permeation varied, which means that the hydraulic anisotropy of most of the samples was not revealed. Full characterization of the clays would require such testing, and future investigations should comprise percolation along the stratification of sedimentary clays for a proper correlation between microstructure and physical properties.

5.3 SWELLING PRESSURE

5.3.1 Techniques

The accuracy of determinations of the swelling pressure by applying the oedometer technique is on the order of ± 10 % when the recorded pressure exceeds about 1 MPa, the present opinion being that the pressure usually tends to be overestimated. For lower pressures the recorded values are uncertain and they may deviate from the true ones by as much as 50 %. It is therefore hardly relevant to make any detailed analysis of the pressures obtained from the tests with smectite-poor clays.

5.3.2 Conclusions

For the clays with a smectite content of more than about 10 % we find an approximately linear relationship between this content and the swelling pressure (Fig 52). This is different from the one that was derived from comprehensive investigations of mixtures of MX-80 bentonite and sandy ballast materials (22), which indicated a much stronger increase in pressure at increasing smectite content. The discrepancy is at least partly explained by microstructural effects. Thus, it is probable that the very well developed alignment of particles in the investigated

natural clays gave a higher (anisotropic) swelling power at lower smectite concentrations than the random particle orientation of the artificial clay mixtures.
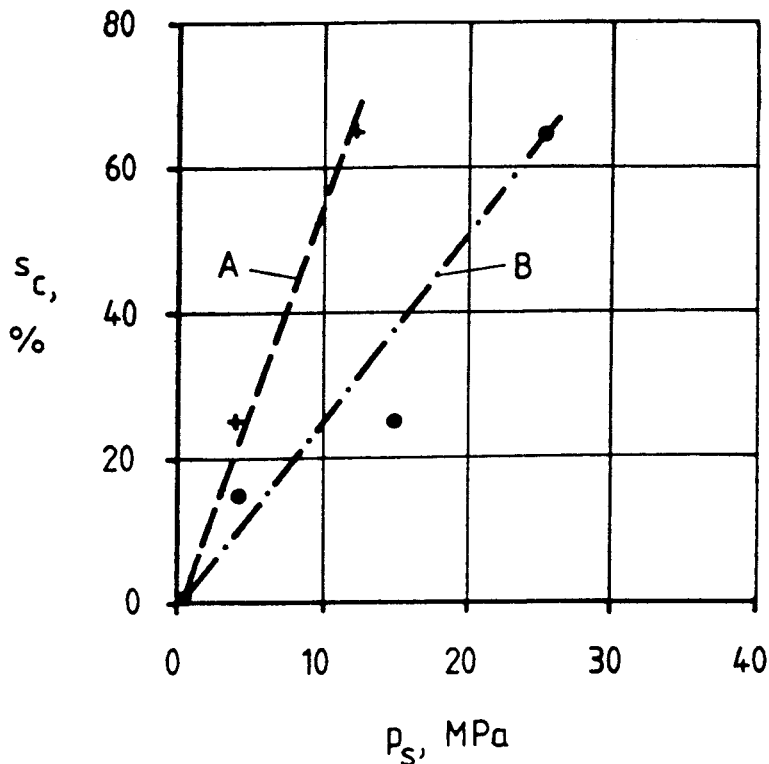
Fig 52.   Smectite content (s_c) versus swelling pressure (p_s). A represents ρ_m
~2.05 t/m³ and B ~2.10 t/m³

5.4   RHEOLOGICAL PROPERTIES

5.4.1   Shear box technique

The preparation of samples for shearing specific, relevant layers turned out to be an easy matter and so was the procedure to arrive at a proper starting point with an effective pressure equal to the swelling pressure, although it took considerable time in certain instances.

A good qualitative picture of the creep behavior was obtained, and the accuracy of the strain measurements appeared to be sufficient to yield a high resolution of the time-dependent strain. This made it worth evaluating the creep curves quantitatively, although the whole curve fitting procedure and selection of creep parameters as well as the loading program may not have been at optimum. We will

consider these things in some detail here, the issue being to work out a proper, simple testing technique that can be taken as a standard procedure in future work.

5.4.2 Predicted and actual time dependence of the creep

5.4.2.1 General

The log time creep law was found to be approximately valid for all the clays at low and intermediate stresses in the relatively short testing time that was applied for the individual load steps. As we will se in this chapter there is also reasonable qualitative as well as quantitative agreement between certain basic physical properties of clays and the evaluated creep parameters B and t_0, which supports the validity of the general constitutive equation, i.e. Eq. (9). We will discuss this matter here with special reference to the microstructural response of non-cemented and cemented clays at creep.

5.4.2.2 Phenomenology of creep of clays

The basic idea of the stochastic creep theory that yields the log time creep law is that heterogeneity in stress and structure on the microscale will jointly result in a distribution of heights of the energy barriers, and that structural changes imply that the energy spectrum will vary in the course of the creep. As in other materials where the creep is known to result from thermally activated glide, it is governed by a stress- and time-dependent spectrum of energy barriers which controls the unit slip events on the molecular scale.

As long as the number of slip units that can be activated in the course of the creep is sufficiently large to allow for redistribution of loads from overstressed to pre-viously not mobilized structural units, various microstructural recovery processes take place, like thixotropy-type formation of new bonds, microdilatancy and mechanical interlocking, by which the creep will be retarded. This is the case for low and intermediate stresses, the stress history and level of stress being deter-minants of the t_0-term of the creep equation. A positive t_0-value is logically arrived at in the general case of non-cemented clays, as can be illustrated by the use of simple rheological models.

In principle, the process of strain- or time-dependent microstructural changes can be visualized by rheological models with successively increased numbers of flow units, like the Blizard-Cauer ladder structure, which is a generalization of the simple Kelvin model. The former is shown in Fig 53, in which a schematic microstructural model is also depicted. The adder structure operates in principle as that suggested by Eyring, in which the successively increased resistance to flow is manifested by a non-linear viscous element (Fig 54). Definition and quantification of the non-linearity have not been deduced on a physical basis for structurally heterogeneous systems like clay and there is no need for this in getting a general picture of the microstructural response to applied shear stresses leading to creep. We will make the simple assumption here that the viscosity increases linearly with time in Eyring's model and, for the sake of simplicity, we will also remove one of the elastic elements so that the model considered will be that in Fig 55.
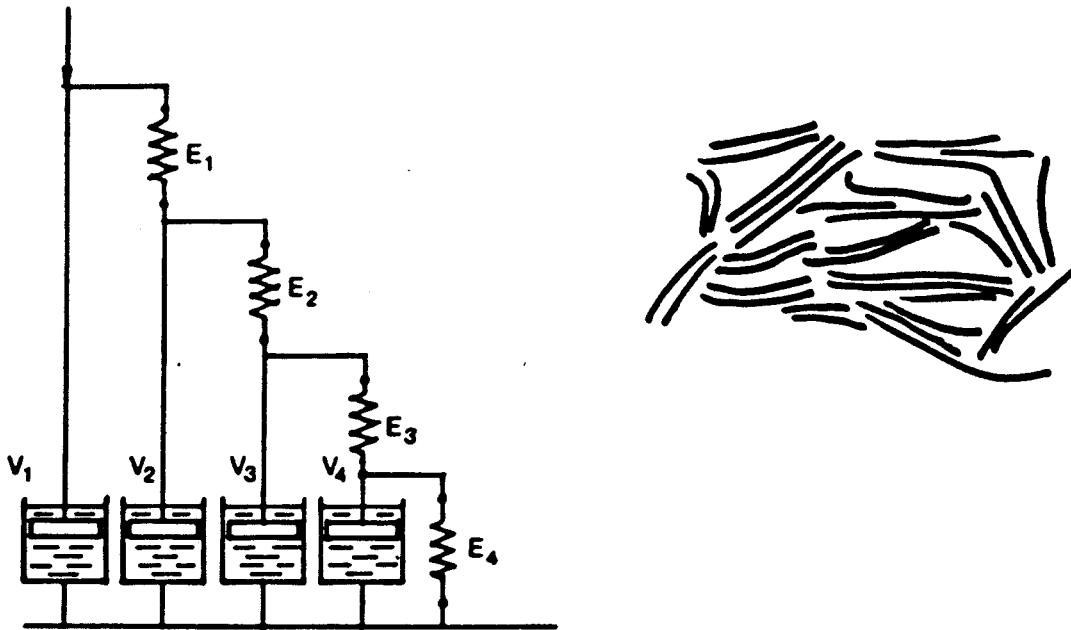
Fig 53.   Blizard-Cauer finite ladder structure with elastic elements E and viscous elements V. The number of elements, with lumped parameters, can be increased to infinity. The schematic microstructural model shows an element of a heterogeneous, non-cemented clay network consisting of components of different strength, yielding at different strain
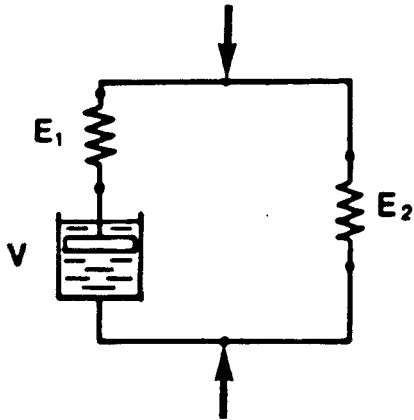
Fig 54. Eyring's model with a non-linear viscous element
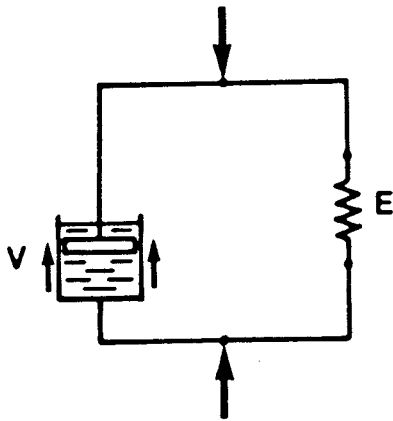
Fig 55. Kelvin model with parallel elastic element and element with non-
linear viscosity

5.4.2.3 Rheology of the simplified Eyring/Kelvin model for non-
cemented clay

The constitutive equation of the model are the following:

$$\sigma_E + \sigma_n = \sigma_o \tag{10}$$

$$\varepsilon_E = \varepsilon_n \tag{11}$$

where σ_o is the instantly applied external stress yielding the stress σ_E in the
elastic element and σ_n in the viscous element. ε_E is the elastic strain and ε_n the
strain of the viscous element.

We get the differential equation:

$$\eta(t)\dot{\varepsilon} + E\varepsilon = \sigma_o \tag{12}$$

with the condition $\varepsilon = 0$ for $t = 0$. The increase of the initial viscosity η_0 is set at:

$$\eta(t) = at + \eta_o \tag{13}$$

which yields the expression:

$$(at + \eta_o)\dot{\varepsilon} + E\varepsilon = \sigma_o \tag{14}$$

with the general solution:

$$\varepsilon = C(at + \eta_o)^{-\frac{E}{a}} + \frac{\sigma_o}{E} \tag{15}$$

where $\quad C = -\dfrac{\sigma_o}{E}\eta_o^{\frac{E}{a}}\quad$ from the condition that $\varepsilon = 0$ for $t = 0$

We obtain:

$$\dot{\varepsilon} = (t + \frac{\eta_o}{a})^{-(1+\frac{E}{a})} \cdot \sigma_o \eta_o^{\frac{E}{a}} \cdot^{-(1+\frac{E}{a})} \tag{16}$$

and

$$\log \varepsilon = -(1 + \frac{E}{a})\log(t + \frac{\eta_o}{a}) + \log\left[\sigma_o \eta_o^{\frac{E}{a}} a^{-(1+\frac{E}{a})}\right] \tag{17}$$

Provided that $a >> E$, for which $a \geq 10^2 E$ is a sufficient criterion, Eq. (17) can be put as:

$$\log \varepsilon = -\log(t + \frac{\eta_o}{a}) + \log(\frac{\sigma_o}{a}) \tag{18}$$

Eq. 18 corresponds to the creep equation, i.e.

$$\dot{\varepsilon} = \frac{B}{t+t_o} \qquad (19)$$

the logarithm of which has the form:

$$\log \dot{\varepsilon} = - \log (t+t_o) + \log B \qquad (20)$$

We find, by comparing Eqs. (18) and (20), that the following identifications can be made

$$t_o = \frac{\eta_o}{a}$$

and

$$B = \sigma_o \eta_o^{\frac{E}{a}} \cdot a^{-(1+\frac{E}{a})}$$

As it is generally assumed that the relationship between B and σ_0 is of the type $B = K\sigma_0^r$, where K is a temperature dependent material parameter, we expect σ_0 to be related to the coefficient a as $a = K^{-1}\sigma^{1-r}$. This yields a stress dependence of to that can be expressed as:

$$t_o = K\eta_o \sigma_o^{r-1} \qquad (21)$$

from which we conclude that t_0 may increase or decrease with σ_0 depending on whether r takes values that are higher or lower than 2. For a series of load steps, the increase in viscosity is expected to depend also on the stress and η_0 is therefore not a constant.

The dependence of a on B and the way in which t_0 is related to η_0/a, are illustrated in Fig 56. E and η_0 are in the range of experimentally determined data of dense smectite clays (23) and σ_0 is taken as 1 MPa. The creep curves are similar to those obtained in tests of non-cemented montmorillonite-rich clay as demonstrated by Fig 18.

5.4.2.4   Rheology of cemented clay structure model

Precipitation of cementing substances, like calcite or silica compounds, increases the number of bonds and therefore the ultimate shear strength of the material. If the cementation is sufficiently extensive, the particle system will become stiff and brittle and insignificant creep will take place at stresses lower than a critical
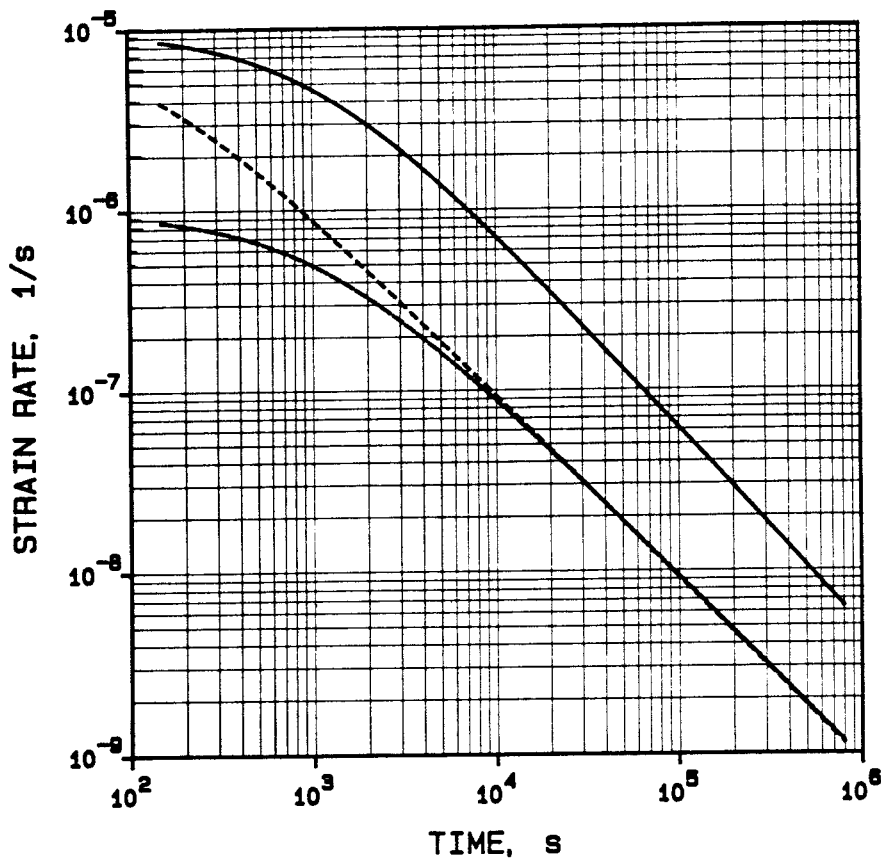
Fig 56. Examples of the appearance of creep curves according to the simpli-
fied Eyring/Kelvin model,Fig 55. The three curves are characterized
by the following sets of data:

Upper: $E = 10^7\,Pa$, $\eta_0 = 10^{11}\,Pas$, $a = 10^8\,Pa$, $t_0 = 10^3\,s$
Central: $E = 10^7\,Pa$, $\eta_0 = 10^{11}\,Pas$, $a = 10^9\,Pa$, $t_0 = 10^2\,s$
Lower: $E = 10^7\,Pa$, $\eta_0 = 10^{12}\,Pas$, $a = 10^9\,Pa$, $t_0 = 10^3\,s$

σ_0 is taken as 1 MPa in all the cases

stress region at which the bonds start to break. At this stage the creep properties
of the virgin particle system become dominant and the creep is less strongly
retarded. The behavior can be illustrated by adding a second set of elements to the
basic rheological model in the way shown in Fig 57. Here, V, and E, represent the
network of cemented structural units that is partially or wholly broken down in
the course of the strain, while V_2 and E_2 characterize the flow properties of the
basic non-cemented system, which determines the overall behavior after a suffi-
ciently long time. A generalized picture of cementing agents is also shown in the
figure.
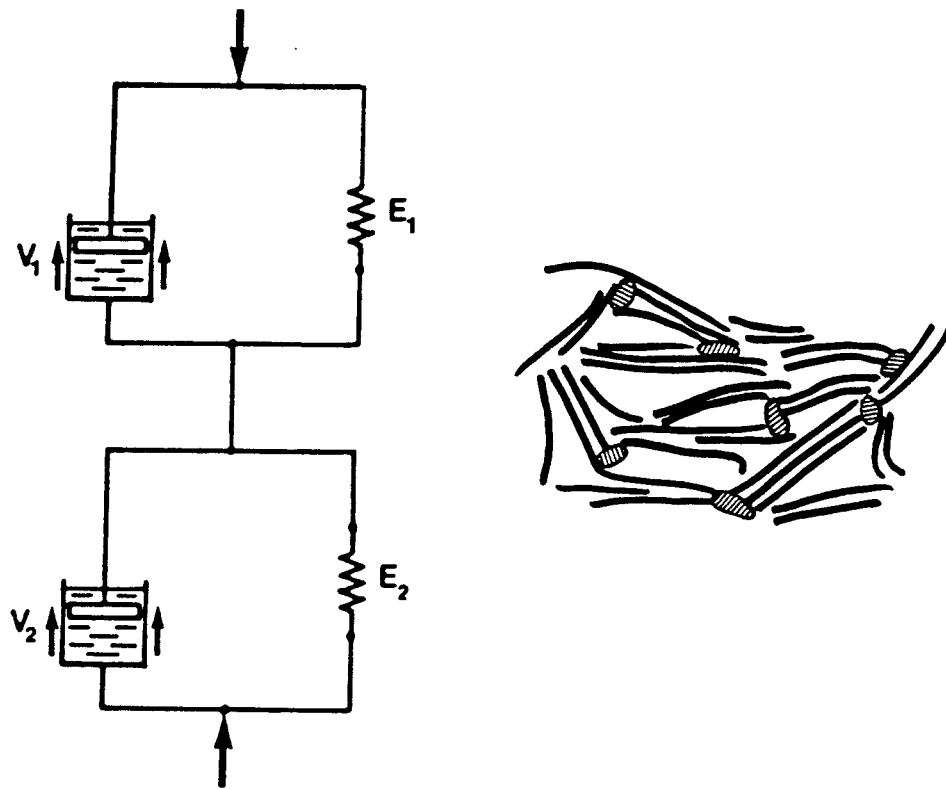
Fig 57.   Rheological model of two sets in series of elements of the
Eyring/Kelvin type. The upper part represents the framework of
cemented units, while the lower is the basic system of non-cemented
units

The constitutive equations of the respective part of the model are those given in
the preceding text with the following additional criteria:

$$\varepsilon_1 + \varepsilon_2 = \varepsilon \tag{22}$$

and

$$\sigma_1 = \sigma_2 = \sigma_o \tag{33}$$

where ε_1, ε_2, σ_1 and σ_2 are the respective strain and stress of the upper and lower parts, and ε and σ the total strain under the stress σ. If the cementation is significant the associated stiffness suggests that $E_1 > E_2$ while the viscous resistance would be lower for the cemented framework. Taking E_1 to be larger than a and $\eta_0/a \sim 10$, which would imply η_0 to be about 1 % of that of the non-cemented system, we find the contribution to ε of the cemented framework to be major in the first few hundred seconds but to be insignificant after about 10^3 s. This would yield the rapidly retarding strain rate, characterized by $t_0 < 0$ shown in Fig 58.
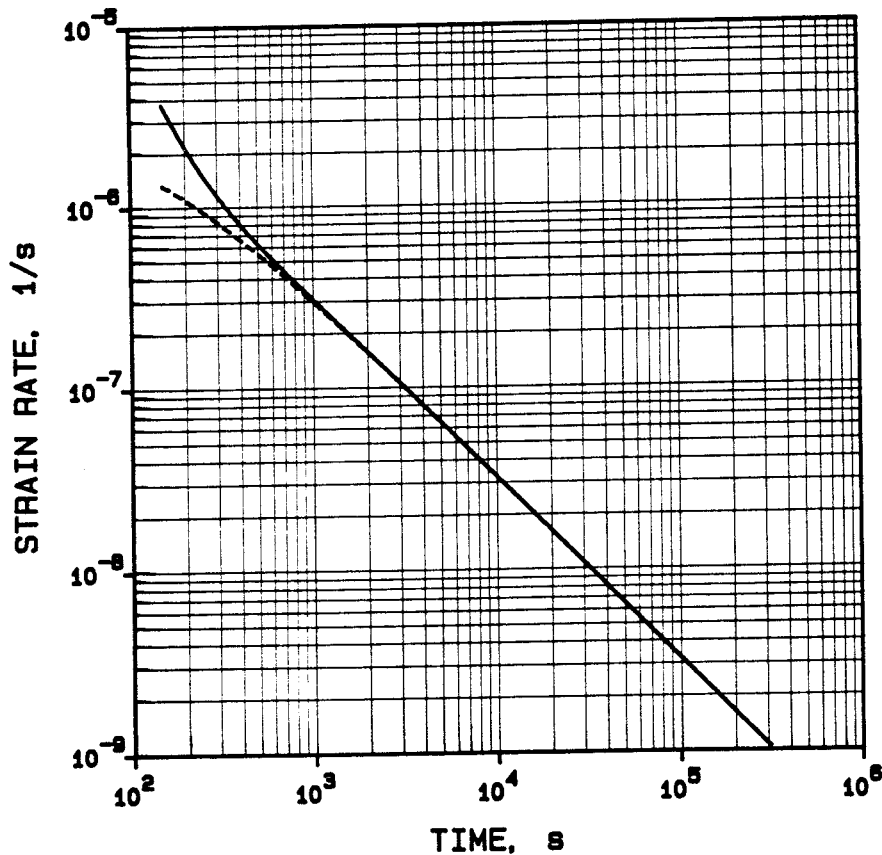
Fig 58.   Negative t_0 resulting from breakdown of cementation bonds in clay particle network. The lower curve originates from the lower part of the model in Fig 56 with the characteristic data:

$E = 10^7$ Pa, $\eta_0 = 3 \times 10^{11}$ Pas, a = 3×10^9 Pa, $t_0 = 10^2$ s
The upper curve is obtained by adding the upper part of the model, giving this part the following properties:

$E = 2 \times 10^7$ Pa, $\eta_0 = 10^8$ Pas, a = 10^7 Pa

Pilot creep tests of sand, cemented by mixing it with a few percent of Portland cement and letting it mature for about one week, aptly illustrate this behavior. The diagram in Fig 59 illustrates the sudden, large increase in angular strain about 10 minutes after increasing the shear stress to 120 kPa, the normal pressure being 106 kPa. The majority of the cementation bonds stayed intact for a couple of minutes but were then progressively broken down, which gave the very strong increase in creep rate before retardation finally took place. Subsequent loading to a shear stress of 140 kPa gave instantaneous failure. The passage from the stage of very rapid shear to the subsequent condition of retarded creep is equivalent to a negative t_0.

Fig 59.   Example of the effect of breakage of cementation bonds on the creep rate as implied by the rheological model in Fig 57. Fine-grained sand with 2 % (dry weight) of Portland cement

It should be pointed out that all types of soils exhibit negative t_0:s if the creep is recorded for the initial 20-50 seconds because the load cannot be applied instantly

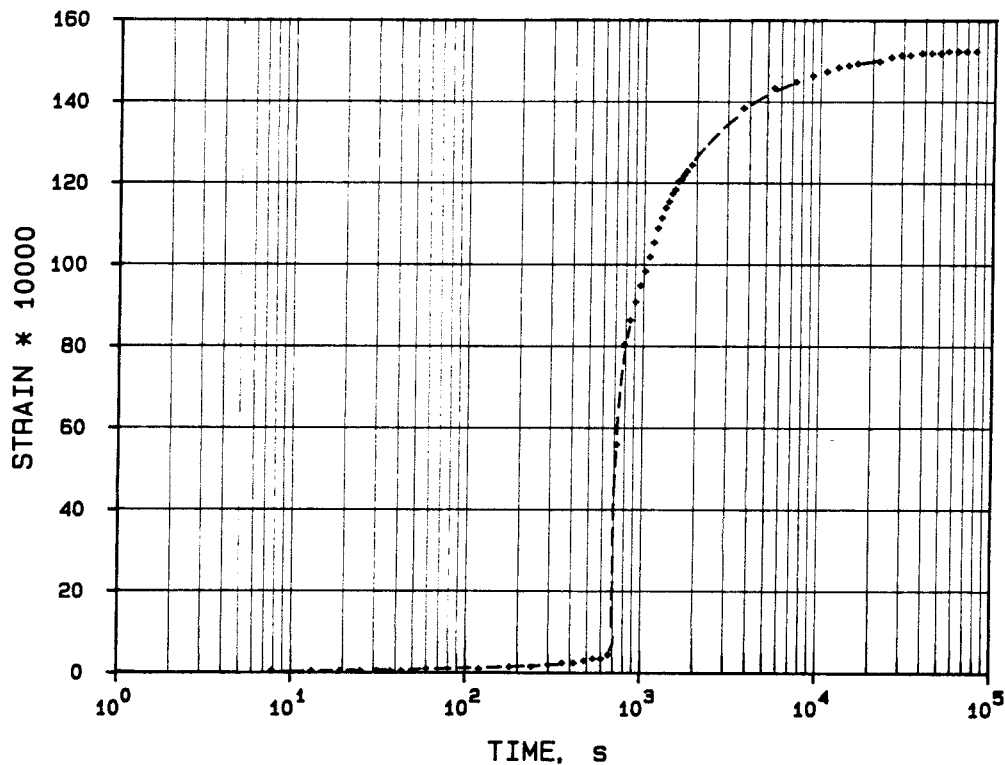and also because friction and machine deformation combine to retard the transfer of the full load to the specimen. The true creep behavior should therefore be evaluated for t-values exceeding about 10^2 s.

5.4.2.5 Comments

As is generally the case in soil and rock mechanics, rheological models for describing the macroscopic creep behavior that results from the involved usually very complex physical processes cannot be taken as a proof of the validity of the applied creep theories. However, the models used in this study are in general agreement with the basic assumptions of microstructural response to shear and they are relevant in the sense that, using separately determined soil data as an input, they yield creep data on the right order of magnitude. Qualitatively, the models for non-cemented and cemented clays appear to offer an explanation of the influence of cementation bonds on the rheological properties.

5.4.3 Conclusions

5.4.3.1 General

The entire procedure to conduct and evaluate simple creep tests of the applied sort seems to be very helpful in the characterization of clay materials for possible use in repositories. Thus, representative creep parameter values can be obtained from curve fitting of the log time creep law, which is a good approximation at moderate stresses and relatively short duration of the tests. However, validation of the applicability of this law for loading of long duration requires a detailed study of the physical processes that govern the development of strain in each respective clay material.

It is quite obvious that a test program of the presently applied type with subsequent load steps yields transient conditions and successively altered clay properties, such that the parameter values derived from any of the load steps are determined by the stress history and the time that has elapsed under previous loads. They can therefore hardly be used for accurate practical prediction of long term creep strain. However, even in its present simple form the test procedure with stepwise, short-term loading is of considerable value, especially for identifying

cementation effects. This finding is innovative and is expected to be of importance also in general soil and rock mechanics.

5.4.3.2   Creep parameters

We will disregard here from the integration constant A and confine ourselves to consider parameters B and t_0 in the basic creep expression Eq. (9). The evaluated data are compiled in Table 17, omitting the values for the first load steps since they may largely mirror machine properties and effects like those mentioned in Chapter 4.3.2.3. Also the values obtained from the last steps are left out because of the reasons given in Chapter 3.2.3.2.

Table 17. Compilation of creep parameter values*

Clay	Smec-tite content	B		t_0, s		Φ^1 degrees
		$\tau<2\tau_f/3$	$\tau>2\tau_f/3$	$\tau<2\tau_f/3$	$\tau>2\tau_f/3$	
MX-80 (I)	65	4.7	17.8-36.2	1615	1641-2492	10.9
Gotland (II)	0	1.5-2.8	16.1	-33 to -107	>0	46.6
Kinnekulle (III)	25	5.4- 5.8	11.6	-154	112-2118	18.4
Boom (V)	10	4.1	15.8	194	465	19.0
Forsmark (VI)	2	-	-	-	-	25.8
Fish (VIII)	30	1.4	19.2	1462	-9	20.5

* Data refer to undisturbed samples saturated with Forsmark water

Significant cohesion resulting from cementation logically yields low B-values for the low stress region (clays II and VIII). The Kinnekulle clay appears to be an exception of this rule but its B-value for the lowest load step, i.e. the one that preceded the initiation of breakage of cementation bonds, was actually only 2.8. For the high stress region B seems to be on the same order of magnitude for all the clays, but the highest values are those recorded for the most smectite-rich clay,

which mirrors the tough character of such clays and their ability to sustain large strain at sub-failure stresses.

As to the parameter t_0 we clearly see the effect of breakdown of cementation bonds, yielding negative t_0:s, and high positive t_0:s for subsequent loads steps. Although there is only very limited experimental background, it can be assumed that smectite-rich clays saturated with Na or K, undergo more microstructural reorganization before "steady" log t-type creep is arrived at than smectite-poor or Ca-saturated smectitic clays. This accounts for the much higher t_0:s of clays I and III at high stresses than of the other clays.

5.4.3.3 Shear strength

The shear strength, i.e. the shear stress τ_f at failure, was evaluated in terms of the angle of internal friction ϕ^1, disregarding from the cohesion that the clays may have (Table 17). This yields a much too high and irrelevant friction angle for the significantly cemented Gotland clay and some minor overestimation for the slightly cemented Kinnekulle (III) and Fish (VIII) clays. The calcium saturation of the latter clay and the assumed partial Ca-adsorption in the Kinnekulle clay are expected to yield a higher friction angle than at sodium saturation, which would thus at least partly explain the deviation of clays III and VIII from the generalized curve in Fig 60, which is based only on the non-cemented, Na-smectite clays. The results are compatible with those reported by Olson (24), who found that very pure sodium montmorillonite clay has a ϕ^1-value that ranges between 4 and 10°, while calcium saturation gives values in the interval of 8-12°. Very pure illite clay was found to yield ϕ^1-values between 16 and 26, according to this investigator.
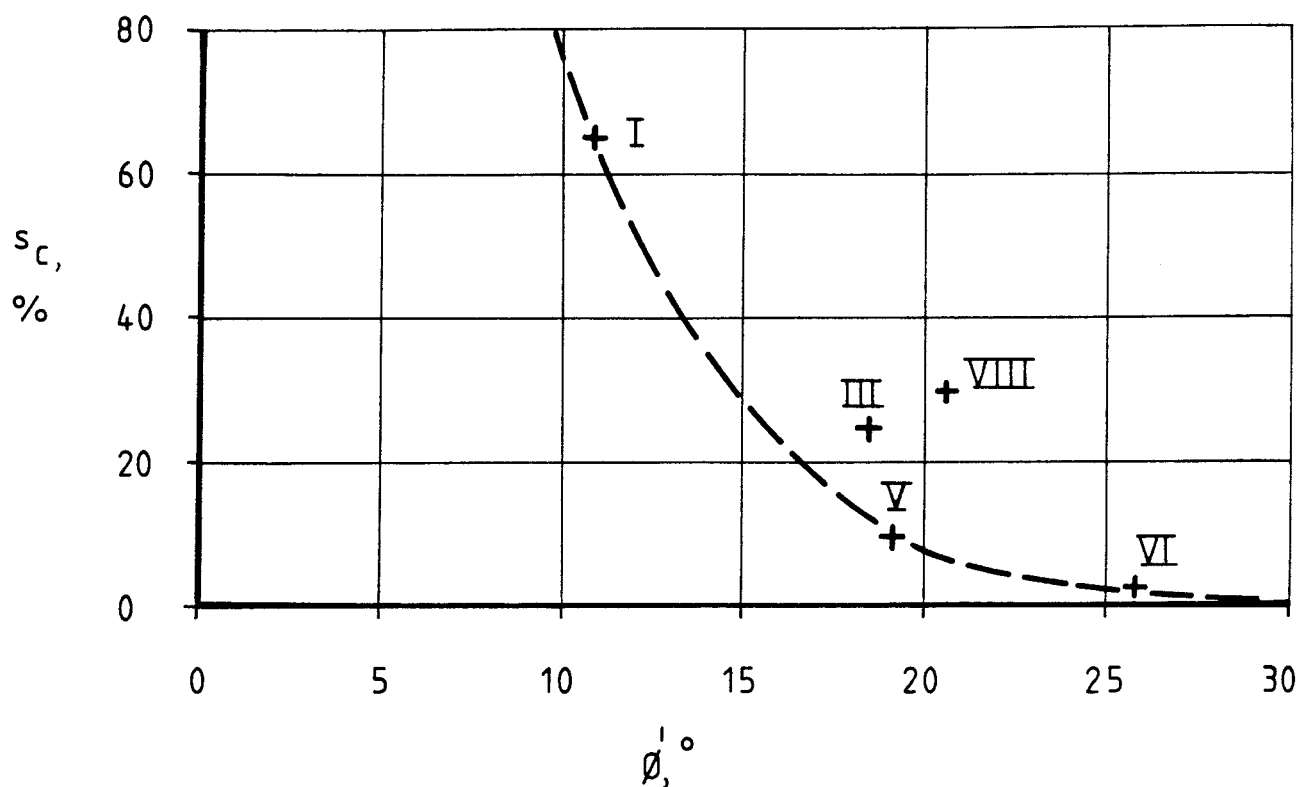
Fig 60.   Relationship between smectite content (s_c) and angle of internal friction (ϕ^1)

6   CONCLUSIONS

6.1   GENERAL

A few important, general conclusions can be drawn from this study, the major ones being:

*   While none of the natural clays came close to the "artificial" MX-80 clay with respect to the hydraulic conductivity, they were all substantially less permeable in an undisturbed state than a typical large granitic rock mass. They would therefore serve as flow barriers in a repository and this clearly demonstrates that even rather extreme chemical attack under repository conditions will not eliminate the most important barrier function of Na bentonite used as canister envelopes or as plug material. It is required, however, that the initial high bulk density is largely preserved

* The two smectite-rich natural clays and also the illite clay - which may have originated from smectite - were found to be cemented, and this property may be common among ancient smectites. Identification of the nature of the cementing agents and their formation is an urgent issue for the understanding of cementing processes in general and their possible development in repository environment in particular

* Even relatively significant but not yet quantified cementation may not be a severe problem, since it is indicated by the tests that hydration and self-healing of reasonably smectite-rich clay will take place after a mechanically induced breakage of the cementation

* Even slight thermo-mechanically or tectonically induced displacements will increase the hydraulic conductivity very significantly at low smectite contents, particularly when calcium is in the exchange positions. The minimum amount of smectite minerals that is required to preserve a reasonable, but not yet quantified self-healing ability appears to be about 15-25 %

* The applied way of characterizing clays for candidature as repository barriers appears to be suitable, with the exception that the creep tests should be conducted in a more defined and systematic way and that their evaluation needs to be looked into much more. This is because the creep properties appear to be of importance not only for the definition of their rheological properties but also for understanding of the microstructural response to stresses.

6.2 RECOMMENDATIONS

A number of essential practical problems remain to be solved before the applied test program can be accepted and suitable candidate materials selected for barrier purposes. The most essential ones are:

1 A rational way of quantitative clay mineral analysis using XRD needs to be worked out. Reynold's method appears to offer a sound basis for this work.

2   Quantitative microstructural analysis is required for proper evalua-
tion of stress-induced changes of major physical properties like the
hydraulic conductivity, creep and self-healing. The earlier derived
microstructural parameter P/T and the way of quantifying particle
orientation that was introduced in this report offer a basis for such
work.

3   Identification should be made of cementing precipitates in the Silurian
clay from Gotland, the Ordovician Kinnekulle clay, and the Cretaceous
Fish clay since their nature may shed light on the possible formation of
cementing agents in repository environment. This requires element
mapping and STEM or SEM microscopy.

4   Long term creep tests need to be made of one of the ancient smectite-
rich clays, preferably natural Wyoming or Canadian bentonites
because this would give an opportunity to investigate the validity of
the log t creep law at long term loading. Tests of this sort on non-
cemented as well as virtually cemented samples would contribute to
the understanding of the influence of cementation on the rheological
properties.

5   A program for rational, routine creep tests need to be worked out to
yield relevant creep parameter values. It calls for the following
detailed studies:

1   Systematic creep tests with different load steps and load dura-
tion, using a well defined reference clay

2   Detailed analysis of the physical processes on a molecular scale
which yield macroscopic strain. The basis of this work is a much
deepened understanding of the clay/water interaction through
MAS/NMR and thermodynamics.

7   <u>REFERENCES</u>

1   Pusch, R. Final Report of The Buffer Mass Test. Volume III: Chemical and Physical Stability of the Buffer Materials. Stripa Project, Technical Report 85-14, 1985

2   Meyer, D.C., Howard, J.J. (Eds.) Evaluation of Clays and Clay Minerals for Application to Repository Sealing. Technical Report, Office of Nuclear Waste Isolation, Battelle Memorial Institute, Columbus, OH 43201, 1983

3   Sposito, G. The Surface Chemistry of Soils. Oxford University Press, New York/Clarendon Press, Oxford, 1984

4   Pusch, R., Karnland, O. Aspects of the Physical State of Smectite-adsorbed Water. SKB Technical Report 86-25, 1986

5   Pusch, R. Chemical Interaction of Clay Buffer Materials and Concrete. Arbetsrapport SFR 82-01, SKBF/SFR, 1982

6   Erlström, M. Complex Fracture-filling Material from the Singö Fault Zone at Forsmark, Central Sweden. Geolog F¦ren Stockh F¦rh 109:1, 1987

7   Pusch, R. Stability of Deep-sited Smectite Minerals in Crystalline Rock - Chemical Aspects. SKBF Technical Report 83-16, 1983

8   Mitchell, J.K., Campanella, R.G., & Singh, A. Soil Creep as a Rate Process. J. Soil Mech Found Div Proc ASCE, SM1, Jan 1968 (pp 236-243)

9   Pusch, R. & Feltham, P. A Stochastic Model of the Creep of Soils. Geotechnique, Vol 30, No 4 (pp 497-506), 1980

10   Pusch, R. Börgesson, L., Hökmark, H. A Simple Technique for Creep Testing of Highly Expansive Clays (In press)

11   Pusch, R., Hökmark, H. & Börgesson, L. Outline of Models of Water and Gas Flow through Smectite Clay Buffers. SKB Technical Report 87-10, 1987

12   Pusch, R. Geotechnical Aspects of the Interpretation of Distorted Strata in Silurian Deposits. Stockholm Contributions in Geology, Vol XXI:2, 1969 (pp 21-42)

13   Pusch, R. Microstructural Features of Pre-Quaternary Clays. Stockholm Contributions in Geology, Vol. XXIV:1, 1971 (pp 1-43)

14   Brusewitz, A-M. Chemical and Physical Properties of Paleozoic Potassium Bentonites from Kinnekulle, Sweden. Clays and Clay Minerals, Vol. 34, No 4, 1986 (pp 442-454)

15   Müller-Vonmoos, M. & Kahr, G. Langzeitstabilität von Bentonit Unter Endlagerbedingungen. Technischer Bericht 85-25. NAGRA, Switzerland, 5401 Baden 1985

16   Lundegren, A. Kristianstadsområdets Kritbilddningar. Sveriges Geologiska Undersökning, Bd 56,H.2

17   Pusch, R., Börgesson, L., Knutsson, I. On the Origin of Silty Fracture Fillings in the Bedrock. (In press)

18   Rosenkrantz, A. Die Senon/Dan Grenz in Dänemark. Ber. Deutsch. Ges. Geol. Wiss. A, Geol. Paläont. Vol. 11, No 6, Berlin, 1966, (pp 721-727

19   Kastner, M., Asaro, F., Michel, W., Alvarez, L.W. The Precursor of the Cretaceous-Tertiary Boundary Clays at Stevns Klint, Denmark, and DSDP Hole 465 A. Science, Vol. 226, Oct 1984 (pp 137-143)

20   Pytte, A.M. The Kinetics of the Smectite to Illite Reaction in Contact Metamorphic Shales. M.A. Theses, Dartmouth College, Hanover, N.H., 1982

21   Börgesson, L. & Stenman, U. Laboratory determined Properties of
        Sand/Bentonite Mixtures for WP-Cave. SGAB Internal Report, IRAP
        85511

22   Börgesson, L., & Pusch, R. Basic Properties of Bentonite-based Buffer
        Materials and Their Function in WP-Cave Repositories. SGAB Int Rep.
        IRAP 86501, 1986

23   Pusch, R. Stability of Bentonite Gels in Crystalline Rock - Physical
        aspects. SKBF/KBS Technical Report 83-04, 1983

24   Olson, R.E. Shearing Strengths of Kaolinite, Illite, and Montmo-
        rillonite. J. Geot. Eng. Division, ASCE Proc. GT II, Nov 1974

List of SKB reports

Annual Reports

1977-78
TR 121
KBS Technical Reports 1 – 120.
Summaries. Stockholm, May 1979.

1979
TR 79-28
The KBS Annual Report 1979.
KBS Technical Reports 79-01 – 79-27.
Summaries. Stockholm, March 1980.

1980
TR 80-26
The KBS Annual Report 1980.
KBS Technical Reports 80-01 – 80-25.
Summaries. Stockholm, March 1981.

1981
TR 81-17
The KBS Annual Report 1981.
KBS Technical Reports 81-01 – 81-16.
Summaries. Stockholm, April 1982.

1982
TR 82-28
The KBS Annual Report 1982.
KBS Technical Reports 82-01 – 82-27.
Summaries. Stockholm, July 1983.

1983
TR 83-77
The KBS Annual Report 1983.
KBS Technical Reports 83-01 – 83-76
Summaries. Stockholm, June 1984.

1984

TR 85-01
Annual Research and Development Report 1984
Including Summaries of Technical Reports Issued during 1984. (Technical Reports 84-01–84-19)
Stockholm June 1985.

1985
TR 85-20
Annual Research and Development Report 1985
Including Summaries of Technical Reports Issued during 1985. (Technical Reports 85-01-85-19)
Stockholm May 1986.

1986

TR 86-31
SKB Annual Report 1986
Including Summaries of Technical Reports Issued during 1986
Stockholm, May 1987

Technical Reports

1987

TR 87-01
Radar measurements performed at the Klipperås study site
Seje Carlsten, Olle Olsson, Stefan Sehlstedt,
Leif Stenberg
Swedish Geological Co, Uppsala/Luleå
February 1987

TR 87-02
**Fuel rod D07/B15 from Ringhals 2 PWR:
Source material for corrosion/leach tests in groundwater
Fuel rod/pellet characterization program part one**
Roy Forsyth, Editor
Studsvik Energiteknik AB, Nyköping
March 1987

TR 87-03
**Calculations on HYDROCOIN level 1 using the GWHRT flow model
Case 1 Transient flow of water from a borehole penetrating a confined aquifer
Case 3 Saturated-unsaturated flow through a layered sequence of sedimentary rocks
Case 4 Transient thermal convection in a saturated medium**
Roger Thunvik, Royal Institute of Technology, Stockholm
March 1987

TR 87-04
**Calculations on HYDROCOIN level 2, case 1 using the GWHRT flow model
Thermal convection and conduction around a field heat transfer experiment**
Roger Thunvik
Royal Institute of Technology, Stockholm
March 1987

TR 87-05
Applications of stochastic models to solute transport in fractured rocks
Lynn W Gelhar
Massachusetts Institute of Technology
January 1987

TR 87-06
Some properties of a channeling model of fracture flow
Y W Tsang, C F Tsang, I Neretnieks
Royal Institute of Technology, Stockholm
December 1986

TR 87-07
Deep groundwater chemistry
Peter Wikberg, Karin Axelsen, Folke Fredlund
Royal Institute of Technology, Stockholm
June 1987

TR 87-08
An approach for evaluating the general and localized corrosion of carbon steel containers for nuclear waste disposal
GP March, KJ Taylor, SM Sharland, PW Tasker
Harwell Laboratory, Oxfordshire
June 1987

TR 87-09
Piping and erosion phenomena in soft clay gels
Roland Pusch, Mikael Erlström,
Lennart Börgesson
Swedish Geological Co, Lund
May 1987

TR 87-10
Outline of models of water and gas flow through smectite clay buffers
Roland Pusch, Harald Hökmark,
Lennart Börgesson
Swedish Geological Co, Lund
June 1987

TR 87-11
Modelling of crustal rock mechanics for radioactive waste storage in Fennoscandia—Problem definition
Ove Stephansson
University of Luleå
May 1987

TR 87-12
Study of groundwater colloids and their ability to transport radionuclides
Kåre Tjus* and Peter Wikberg**
 *Institute for Surface Chemistry, Stockholm
**Royal Institute of Technology, Inorganic
   Chemistry Stockholm
March 1987

TR 87-13
Shallow reflection seismic investigation of fracture zones in the Finnsjö area method evaluation
Trine Dahl-Jensen
Jonas Lindgren
University of Uppsala, Department of Geophysics
June 1987

TR 87-14
Combined interpretation of geophysical, geological, hydrological and radar investigations in the boreholes ST1 and ST2 at the Saltsjötunnel
Jan-Erik Andersson
Per Andersson
Seje Carlsten
Lars Falk
Olle Olsson
Allan Stråhle
Swedish Geological Co, Uppsala
1987-06-30

TR 87-15
Geochemical interpretation of groundwaters from Finnsjön, Sweden
Ignasi Puigdomènech[1]
Kirk Nordstrom[2]
[1]Royal Institute of Technology, Stockholm
[2]U S Geological Survey, Menlo Park, California
August 23, 1987

TR 87-16
Corrosion tests on spent PWR fuel in synthetic groundwater
R S Forsyth[1] and L O Werme[2]
[1]Studsvik Energiteknik AB, Nyköping, Sweden
[2]The Swedish Nuclear Fuel and Waste Management Co (SKB), Stockholm, Sweden
Stockholm, September 1987

TR 87-17
The July — September 1986 Skövde aftershock sequence
Conny Holmqvist
Rutger Wahlström
Seismological Department, Uppsala University
August 1987

TR 87-18
Calculation of gas migration in fractured rock
Roger Thunvik[1] and Carol Braester[2]
[1]Royal Institute of Technology
Stockholm, Sweden
[2]Israel Institute of Technology
Haifa, Israel
September 1987

TR 87-19
Calculation of gas migration in fractured rock — a continuum approach

Carol Braester[1] and Roger Thunvik[2]
[1]Israel Institute of Technology
Haifa, Israel
[2]Royal Institute of Technology
Stockholm, Sweden
September 1987

TR 87-20
Stability fields of smectites and illites as a function of temperature and chemical composition

Y Tardy, J Duplay and B Fritz
Centre de Sédimentologie et de Géochimie de la Surface (CNRS)
Institut de Géologie Université Louis Pasteur (ULP)
1 rue Blessig, F-67084 Strasbourg, France
April 1987

TR 87-21
Hydrochemical investigations in crystalline bedrock in relation to exesting hydraulic conditions: Klipperås test-site, Småland, Southern Sweden

John Smellie[1]
Nils-Åke Larsson[1]
Peter Wikberg[3]
Ignasi Puigdomènech[4]
Eva-Lena Tullborg[2]
[1]Swedisch Geological Company, Uppsala
[2]Swedisch Geological Company, Göteborg
[3]Royal Institute of Technology, Stockholm
[4]Studsvik Energiteknik AB, Nyköping
September 1987

TR 87-22
Radionuclide sorption on granitic drill core material

Trygve E Eriksen and Birgitta Locklund
The Royal Institute of Technology
Department of Nuclear Chemistry
Stockholm
November 1987

TR 87-23
Radionuclide co-precipitation

Jordi Bruno and Amaia Sandino
The Royal Institute of Technology
Department of Inorganic Chemistry
Stockholm
December 1987

TR 87-24
Geological maps and cross-sections of Southern Sweden

Karl-Axel Kornfält[1] and Kent Larsson[2]
[1]SGU, Lund
[2]Softrock Consulting, Genarp
December 1987

TR 87-25
**The Bolmen tunnel project
Evaluation of geophysical site investigation methods**

Roy Stanfors
December 1987

TR 87-26
**The Kymmen power station
TBM tunnel
Hydrogeological mapping and analysis**

Kai Palmqvist[1] and Roy Stanfors[2]
[1]BERGAB-Berggeologiska Undersökningar AB
[2]Lunds University
December 1987

TR 87-27
**Earthquake measurements in southern Sweden
Oct 1, 1986 — Mar 31, 198**

Ragnar Slunga
Leif Nordgren
Swedish Defence Research Establishment
Department 2
Stockholm
December 1987

TR 87-28
Radionuclide deposition and migration within the Gideå and Finnsjö study sites, Sweden

A study of the fallout after the Chernobyl accident
Erik Gustafsson[1], Mats Skålberg[2], Björn Sundblad[3], Olle Karlberg[3], Eva-Lena Tullborg[4], Thomas Ittner[2], Paul Carbol[2], Niklas Eriksson[2], Svante Lampe[3]
[1]Swedish Geological Company, Uppsala
[2]Chalmers University of Technology, Göteborg
[3]Studsvik Energiteknik AB, Nyköping
[4]Swedish Geological Company, Göteborg
December 1987